University of Zagreb
Faculty of Pharmacy and Biochemistry

Gabrijel Zubčić

STABILITY AND REARRANGEMENTS OF *N*-CENTERED RADICALS RELEVANT FOR SYNTHESES OF BIOACTIVE COMPOUNDS

DOCTORAL DISSERTATION

Zagreb, 2025

University of Zagreb
Faculty of Pharmacy and Biochemistry

Gabrijel Zubčić

STABILITY AND REARRANGEMENTS OF *N*-CENTERED RADICALS RELEVANT FOR SYNTHESES OF BIOACTIVE COMPOUNDS

DOCTORAL DISSERTATION

Supervisors
Associate Professor Davor Šakić, PhD
Professor Valerije Vrček, PhD

Zagreb, 2025

Sveučilište u Zagrebu
Farmaceutsko-biokemijski fakultet

Gabrijel Zubčić

STABILNOST I PREGRAĐIVANJE *N*-RADIKALA RELEVANTNIH ZA SINTEZE BIOAKTIVNIH SPOJEVA

DOKTORSKI RAD

Mentori
Izv. prof. dr. sc. Davor Šakić
Prof. dr. sc. Valerije Vrček

Zagreb, 2025

The doctoral thesis was submitted to the Faculty Council of the Faculty of Pharmacy and Biochemistry, University of Zagreb in order to acquire a PhD degree in the area of Biomedicine and Health, the field of Pharmacy, the branch of Pharmacy.

The doctoral thesis was prepared at the Department of Analytical Chemistry of the University of Zagreb, Faculty of Pharmacy and Biochemistry, under the dual mentorship of Prof. Valerije Vrček, PhD and Assoc. Prof. Davor Šakić, PhD. The work was financed by the Croatian Science Foundation project "Light-driven functionalization of non-reactive positions using oxidative amination" (HRZZ UIP 2020-02-4857, LIGHT-N-RING) led by Assoc. prof. Davor Šakić, PhD as PI and was carried out as part of the PhD program in Pharmaceutical-Biochemical Sciences at the University of Zagreb, Faculty of Pharmacy and Biochemistry.

ACKNOWLEDGEMENTS

I would like to thank my first mentor, Assoc. Prof. Davor Šakić, PhD for giving me the opportunity to write my doctoral thesis and enabling the development of my scientific career. I am grateful for the introduction to the world of computational chemistry, which has broadened my horizons and allowed my creativity to shine. He has given me his time, patience and understanding, and offered his help and guidance. He gladly shared with me his knowledge and expertise. I am most thankful for the sincere and selfless effort he invested in my scientific and personal growth and advancement.

I would like to thank my second mentor, Prof. Valerije Vrček, PhD for the knowledge, experience and help I have received in my work and for the time and effort he has devoted to the advancement of my scientific career.

I would like to thank Assoc. Prof. Erim Bešić, PhD for the knowledge and experience he selflessly shared with me. Thank you for the help, support and for selflesly providing us with key instruments with which crucial experiments have been done and without which this doctoral thesis wouldn't have been written.

I would like to thank Research Assoc. Tomislav Portada, PhD from the Institute Rudjer Bošković for the guidance and help during my stay at the Institute.

I would like to thank Research Assoc. Iva Džeba, PhD and Research Assoc. Jiangjang You, PhD from the Institute Rudjer Bošković for their collaboration as well as advice and guidance.

I would like to thank Asocc. Prof. Maria Kolympadi Marković, PhD and Prof. Dean Marković, PhD from Faculty of Biotechnology, University of Rijeka, Rijeka, Croatia, for their knowledge and experience they have so selflessly shared with me and for their hospitality during my stay in Rijeka.

I would like to thank Boris Maryasin, PhD from the Institute of Theoretical Chemistry, University of Vienna, Austria, for being such a great host and for the selfless advice and knowledge he has shared with me.

I would like to thank Prof. Hendrik Zipse, PhD from the Department of Chemistry, Ludwig-Maximilian University Munich, Munich, Germany, for his hospitality and collaboration.

I would like to thank all members of the Department of Analytical Chemistry of the FBF for the pleasant working atmosphere.

I would like to thank all colleagues from the Faculty for the socializing, discussions and nice moments.

To my parents, Silva and Frane, for your love and support.
To my sister Klara, for being such a great sister and friend.

To Senka, my gorgeous girlfriend, for her love and support.
To all of my friends and relatives, thank you.

SUMMARY

The main goal of this doctoral thesis was to investigate the rearrangement reactions in which nitrogen centered radicals participate. Specific goals of this thesis were to investigate nitrogen centered radicals in the context of the Hofmann–Löffler–Freytag (HLF) reaction, namely, to explain the regioselectivity, investigate the propagation cycle, determine the rate limiting step, utilize the reaction for the generation of pharmaceutically relevant compounds, and compute stabilities of nitrogen centered radical. In this thesis, *N*-chloro derivatives as radical precursors were synthesized using existing methods, and new method was developed for the synthesis of *N*-bromo derivatives. A methodology was developed for the *in-situ* generation and trapping of nitrogen centered radicals and its carbon counterparts using the phenylbutylnitrone (PBN) spin trap and subsequent investigation of the resulting adducts *via* electron paramagnetic resonance (EPR) spectroscopy. Laser flash photolysis (LFP) method was used to directly detect the transient species generated after laser excitation. Nuclear magnetic resonance (NMR) methods were employed in order to analyze complex product mixtures. Quantum-chemical methodology was developed and employed to obtain a quantitative description of the thermodynamic and kinetic properties of the HLF reaction. Additionaly, kinetic modelling was done.

Using LFP, NMR, and EPR spectroscopy, in combination with density functional theory (DFT) calculations and kinetic modelling, the HLF reaction profile was monitored, and all significant intermediate radicals and products were identified in this light-induced radical generation and subsequent chain reaction. It is claimed that major regioselective product of the HLF reaction is kinetically controlled in the hydrogen atom transfer (HAT) step as the thermodynamic preference for the formation of one product over the other is lost due to the second step of the cycle being highly exothermic. When both radical intermediates have similar stability, the observed regioselectivity can be attributed to a rearrangement reaction exclusive to the C_6-radical where it rearranges to a more stable C_2-radical. When positions are non-equal, NMR analysis of the product mixture revealed the presence of four major products. These four products are amine, imine, C_6- and C_5-chlorinated products. Amine and imine are products of a "self-reaction" of nitrogen radicals (termination) and is the probable reason why many synthetic chemists block the C_2-position in their synthetic works and why the HLF reaction proceeds only in certain solvents in high yields. Kinetic modelling of the HLF reaction showed that its kinetics are pseudo first order with respect to the second step. Thus, it is proposed that the rate limiting step of the HLF reaction is the halogen atom transfer (XAT) step. Additionally, it was proposed that by adding halogen sources, typically used as chlorinating agents the propagation cycle can be interrupted and terminated. Finally, it was demonstrated that the HLF reaction is a viable method for late-stage functionalization (LSF) in the synthesis of pharmaceuticals. We used HLF reaction as a route for preparing bicyclic rings from *N*-chlorinated macrocyclic lactams. Interplay of different experimental and theoretical techniques have provided a deeper insight into the fundamental aspects of the HLF reaction, and results will be used for better utilization in future synthesis.

Keywords: Nitrogen centered radicals, chain reaction, Hofmann–Löffler–Freytag (HLF) reaction, regioselectivity, rate limiting step, self-reaction.

SAŽETAK

Uvod

Dušikovi radikali su izrazito reaktivne vrste i kao takvi u tragovima sudjeluju u lančanim reakcijama. Pokazuju visok stupanj kemoselektivnosti i sudjeluju u različitim vrstama reakcija kao što su intra/intermolekulska odcjepljenja vodikovog atoma, intra/intermolekulske supstitucijske reakcije i intra/intermolekulske adicije na dvostruke veze. Pored toga, poznato je da dušikovi radikali sudjeluju u samoreakcijama koje daju produkte dimerizacije i/ili disproporcioniranja. Stabilnost dušikovih radikala može se opisati izodezmičkim reakcijama u kojima sudjeluju dušikovi radikali s amonijakom te mjerenjem reakcijske entalpije, tj. radikalske stabilizacijske energije (eng. *radical stabilisation energies*, RSE) takve reakcije. Korištenjem tih reakcija mogu se izraditi RSE ljestvice koje pružaju praktičan način dobivanja informacija o njihovoj stabilnosti i procjeni reaktivnosti u odnosu na druge radikale. Postoje mnoge metode za generiranje dušikovih radikala, među kojima se njihovo fotokemijsko ili toplinsko generiranje iz *N*-haloamina koristi za sintezu pirolidina. Ova reakcija, poznata kao Hofmann–Löffler–Freytagova reakcija, prva je otkrivena sintetska metodologija koja uključuje dušikove radikale, a otkrio ju je Hofmann 1879 (1). Lančani radikalski mehanizam HLF reakcije sastoji se od intramolekulskog prijenosa atoma vodika (HAT) kao prvog koraka propagacijskog ciklusa i prijenosa atoma halogena (XAT) kao drugog koraka. Regioselektivnost i definiranje najsporijeg koraka HLF reakcije nedovoljno su istraženi. Nejasno je zašto HLF reakcija u pojedinim otapalima stvara produkte u visokim prinosima, dok je u drugim otapalima iskorištenje reakcije vrlo nisko te je potrebno blokirati C_2-poziciju supstrata kako bi reakcija dala pirolidinske produkte. Konačno, ostaje neistraženo može li se HLF reakcija iskoristiti za sintezu bickličkih sustava iz makrocikličkih sustava.

Materijali i metode

Modelni sustavi su sintetizirani iz komercijalno dostupnih spojeva nakon čega je uslijedilo pročišćavanje produkata kromatografijom na stupcu. Tankoslojna kromatografija (TLC) u odgovarajućem sustavu otapala služila je za praćenje tijeka reakcije. TLC mrlje promatrane su osvjetljavanjem ultraljubičastim (UV) svjetlom na valnoj duljini od 254 nm. Ukoliko TLC mrlje nisu bile vidljive nakon osvjetljavanja UV svjetlom, detektirane su uporabom komore s jodom. NMR spektri reakcijske smjese dobiveni su na NMR spektrometru Varian Inova 400 nakon čega su podaci uneseni i obrađeni u programu MestreNova 11.0.4.

Elektronska paramagnetska rezonancija (EPR) je provedena korištenjem EPR spektrometra Bruker ELEXSYS E500 sa šupljim rezonatorom ER4122SHQE. Budući da ovaj rezonator sa šupljinom nema optički prozor za osvjetljenje, izvor svjetla je montiran ispod šupljine, a svjetlost je dolazila kroz dno EPR cjevčice. Dekonvolucija EPR spektara i simulacija pojedinačnih spektara radikalskih specija rađene su pomoću modula EasySpin u programskom paketu MATLAB. Vizualizacija EPR spektara i preliminarna obrada odrađena je korištenjem web stranice VisualEPR.

Mjerenja tranzijentne apsorpcijske spektroskopije (TAS) provedena su laserskom pulsnom fotolizom (LPF). Apsorpcijski spektri otopina mjereni su UV-Vis spektrofotometrom (Varian UV/VIS spektrofotometar Cary 4000) u području valnih duljina od 200 do 500 nm. Apsorpcijski spektri otopina uzoraka su snimani prije i nakon propuhivanja dušikom te tijekom i nakon mjerenja laserskom pulsnom fotolizom kako bi se pratila fotostabilnost spojeva te izbjeglo pobuđivanje laserom nastalih fotoprodukata.

Instrumentacija za LFP uključivala je niz vremenski usklađenih uređaja, a mjerenje se odvijalo pomoću računala. Kao izvor pobude uzorka koristio se nanosekundni pulsni Nd:YAG laser

(Quantel, Q-smart 450, trajanje pulsa 6 ns, pulsiranje 10 Hz, maksimalne energije do 450 mJ na 1064 nm) uz ostale valne duljine pobude od 532 nm, 355 nm i 266 nm. Detekcija se odvijala pomoću spektrometra (LP980, Edinburgh Instruments) koji kao izvore zračenja koristi ksenonsku lampu (mogućnost pulsnog rada) i halogenu lampu (pogodniju za veće vremenske skale od ms do s u spektralnom području > 300 nm), monokromator i detektor fotomultiplikator. Konformacijski prostor za sve lokalne minimume i sedlaste točke prvog reda na plohi potencijalne energije istražen je korištenjem Conformer–Rotamer Ensemble Sampling Tool─CREST, uz optimizaciju na semiempirijskoj XTB-gfn2 razini. Dobivene strukture ponovno su optimizirane metodom teorije funkcionala gustoće (DFT) korištenjem B3LYP/6-31G(d) metode. Za svaku strukturu sa stabilnom valnom funkcijom izvršen je izračun frekvencije kako bi se identificirali strukturni minimumi i sedlaste točke prvog reda na plohi potencijalne energije. Sedlaste točke prvog reda imaju jednu imaginarnu frekvenciju. Iz svih struktura konformera koje su sedlaste točke prvog reda provedeno je pretraživanje intrinzične reakcijske koordinate (IRC) te su posljednje točke optimizirane dajući tako predreakcijski intermedijarni kompleks i postreakcijski intermedijarni kompleks. Time se definira struktura sedlaste točke prvog reda kao struktura prijelaznog stanja koja povezuje minimume na strani reaktanata i produkata. „*Single point*“ energije dobivene su korištenjem dvostruko hibridne metode RO-B2PLYP na G3MP2 baznom skupu uz D3 disperzijsku korekciju i univerzalnim kontinuiranim modelom solvatacije (SMD) s acetonitrilom kao otapalom. Toplinske korekcije slobodne energije izvedene su iz izračuna frekvencije pod uvjetima od 298,15 K i 1 atm.
Izračuni EPR parametara napravljeni su korištenjem B3LYP funkcionala i mješovitog baznog skupa: EPR-III za atome ugljika, vodika i kisika, def2-QZVP za atom sumpora i 6-31G(d) za atom dušika. Za točne izračune *g*-faktora i hiperfinih konstanti (*hfc*) potreban je mali bazni set na *N*-atomu. Kada se koristi veći bazni set za atom dušika, npr. EPR-III ili def2-QZVP, dobiveni rezultati sustavno podcjenjuju *hfc*. Svi proračuni su obavljeni na Gaussian verziji 16.C01 korištenjem servisa naprednog računanja (klasteri Isabella i Supek). Spektri elektronskih prijelaza izračunati su u plinovitoj fazi i u otapalu s vremenski ovisnom CAM-B3LYP/TZVP/PCM metodom na molekularnoj geometriji optimiziranoj na B3LYP/TZVP razini teorije. Kako bi se objasnio entropijski učinak prisutnosti molekula otapala oko otopljene tvari, korišten je "stanični model“ (2). Ovaj model je predložen kako bi se eksplicitno procijenio učinak gubitka translacijskih stupnjeva slobode u otopini na Gibbsovu aktivacijsku energiju u bimolekulskoj reakciji (ili reakciji višeg reda molekularnosti).
Provedeno je kinetičko modeliranje reakcijskih puteva. Kompletan matematički model, koji je uključivao sve moguće korake reakcije, rezultirao je sustavom nelinearnih diferencijalnih jednadžbi koji je bio izuzetno složen, te su uvedene aproksimacije za analitičko rješavanje.

Rezultati

Uspješno su primijenjene postojeće sintetske procedure te su razvijene nove za sintezu odabranih sustava. To je dokazano dobivenim iskorištenjima i NMR analizom. Prilagodba metode otplinjavanja ciklusima zamrzavanje-otplinjavanje-odmrzavanje na vakuum liniji je uspješno uspostavljena. Naime, učinkovitost uklanjanja kisika korištenjem ciklusa zamrzavanje-otplinjavanje-odmrzavanje dokazana je širinama linija izmjerenih EPR-om. Eksperimentalne širine linija manje od 0,4 Gaussa dokazale su da je u otopinama bilo prisutno vrlo malo kisika, što je važno za sprječavanje reakcija oksidacija u radikalskom ciklusu. Za detekciju radikalskih specija koristi se EPR spektroskopija uz metodu *in situ* generiranja tih specija i stvaranje stabilnih adukata uz pomoć *N*-*tert*-butil-α-fenilnitronske spinske stupice. Dobiveni spektri su dekonvoluirani na spektre individualnih specija, te je postignuta dobra reproducibilnost mjerenja u smislu podudaranja *g*-faktora i *hfc* vrijednosti sličnih radikalskih adukata detektiranih u različitim mjerenjima na različitim sustavima (*N*-kloro i *N*-bromo

derivati) i u različitim otapalima. Rezultati su potvrdili radikalski put, detektiran je novi radikalski adukt (C_2-radikal) čime je prošireno razumijevanje postojećih EPR istraživanja HLF reakcije. NMR mjerenja su provedena uspješno budući da se analiza pokazala u skladu s literaturno dostupnim podacima. LFP metoda se pokazala prikladnom za direktnu detekciju radikalskih intermedijera nakon ekscitacije laserom. Naime, vremena poluživota detektiranih dušikovih i ugljikovih radikala odgovaraju literaturnim podacima. Kvantno-kemijskom računima objašnjeni su svi ekperimentalni rezultati.

Zaključci

Korištenjem NMR, LFP i EPR spektroskopije u kombinaciji s DFT izračunima, proučavan je profil HLF reakcije i identificirani su radikalski intermedijeri i produkti. Primarna hipoteza je da je uočena regioselektivnost pod kinetičkom kontrolom budući da ne postoji termodinamička pokretačka sila za stvaranje C_6-funkcionaliziranog produkta u odnosu na C_5-funkcionalizirani produkt. Alternativna hipoteza tvrdi da se uočena regioselektivnost može pripisati dodatnoj reakciji pregradnje koja je vezana isključivo uz C_6 radikal. Kroz dodatni 1,5-HAT korak, C_6 radikal se transformira u stabilniji C_2-radikal. Postojanje C_2-radikala eksperimentalno je dokazano ne samo pomoću EPR spektroskopije, već analizom nusprodukata u sintetskim reakcijama, gdje su pronađeni imini i aldehidi kao razgradni produkti reakcija kojima podliježe C_2-radikal. NMR analiza smjese produkata ukazuje na prisutnost četiri glavna produkta. Utvrđeno je da su ova četiri produkta amin, imin, C_6- i C_5-klorirani produkti. Amin je produkt samoreakcije dušikovih radikala, dok imin može nastati i samoreakcijom i daljnjim pregrađivanjima C_2-radikala. Reaktivnost C_2-pozicije je razlog zašto neke istraživačke skupine u svojim sintetskim postupcima blokiraju C_2-poziciju sterički ili funkcionalizacijom.
Kinetičko modeliranje HLF reakcije daje snažne dokaze u prilog tome da postoje dvije različite i dobro definirane radikalsko-lančane reakcije na koje se primjenjuje Bodensteinova aproksimacija zajedno s aproksimacijom dugog lanca i aproksimacijom koja se odnosi na koncentracije nositelja lanca. Ove dvije radikalsko-lančane reakcije vode do dva različita produkta te imaju zajedničku ravnotežnu koncentraciju dušikovih radikala. Nadalje, dobiven je matematički izraz na temelju kojeg se tvrdi da HLF reakcija slijedi kinetiku pseudo prvog reda s obzirom na drugi korak te da je brzina propagacijskog ciklusa određena drugim korakom. Na temelju ovog se tvrdi da je drugi korak najsporiji korak u reakciji. Dodatno, predloženo je da dodavanje izvora halogena, koji se obično koriste kao sredstva za kloriranje može interferirati s XAT korakom propagacijskog ciklusa, terminirajući sam ciklus.
Konačno, pokazalo se da je HLF reakcija dobra metoda za kasnu funkcionalizaciju laurolaktama. U ovakvim konformacijski ograničenim makrocikličkim sustavima dušikovi radikali su pokazali smanjenu stabilnost. S druge strane, ugljikovi radikali, posebno oni koji su susjedni karbonilnim ili aminskim skupinama, pokazali su povećanu radikalsku stabilnost, uz značajne iznimke u visoko konformacijski ograničenim strukturama poput 2-azetidinona. Računalno modeliranje pokazuje da su barijere za 1,5- i 1,6-HAT *egzo* procese s karbonilnom skupinom izvan manjeg prstena najpovoljnije. Izračunato je da se reakcije 1,4-HAT *endo*-tipa odvijaju uz nižu barijeru u usporedbi s egzo-tipom.

Ključne riječi: Dušikovi radikali, lančana reakcija, Hofmann–Löffler–Freytag (HLF) reakcija, regioselektivnost, korak koji određuje brzinu reakcije, samoreakcija

Table of Contents:

LIST OF ABBREVIATIONS AND SYMBOLS

AIBN	azobisisobutyronitrile
Boc	*tert*-butyloxycarbonyl
Bu_3SnH	tributyltin hydride
DFT	density functional theory
DMF	dimethylformamide
EPR	electron paramagnetic resonance
HFIP	hexafluoroprop-2-ol
HAT	hydrogen atom transfer
hfc	hyperfine constant
HLF	Hofmann–Löffler–Freytag
k	rate coefficient
LFP	laser flash photolysis
LSF	late-stage functionalization
MD	molecular dynamics
NIS	*N*-iodosuccinimide
NMR	nuclear magnetic resonance
PTOC	*N*-hydroxypyridine-2-thione
PIDA	(diacetoxyiodo)benzene
PBN	phenylbutylnitrone
RSE	radical stabilization energy
rt	room temperature
SMD	universal continuum solvation model
SOMO	singly occupied molecular orbital
t-BuSH	*tert*-buthylthiol
THF	tetrahydrofuran
t-BuOH	*tert*-butanol
t-BuOI	*tert*-butyl hypoiodite
TLC	thin-layer chromatography
TAS	transient absorption spectroscopy
XAT	halogen atom transfer
UV	ultraviolet

UV-Vis	ultraviolet-visible

1. INTRODUCTION

1.1. Brief history and background

In chemistry, a radical is an atom, molecule, or ion with at least one unpaired valence electron (3,4). It is generally accepted that the first free radical was identified by Gomberg (5) in 1900, in the form of a trivalent compound, triphenyl methyl radical. This experimental observation was due to the radical's exceptional stability, where both steric and thermodynamic effects play a significant role. The first nitrogen free radical was identified a decade later, in 1911, by Wieland (6) who discovered that tetraphenylhydrazine **1** thermally dissociates at about 100 °C to form green diphenylaminyl radicals **2** (Scheme 1).

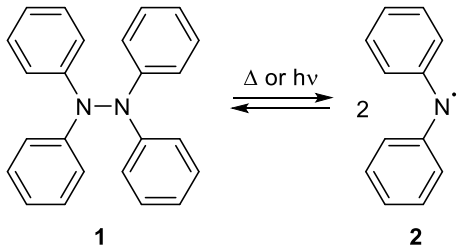

Scheme 1. Thermal dissociation of tetraphenylhydrazine (6).

Almost 20 years later, a much more reactive free radical, the methyl radical was prepared by Paneth and Hofeditz (7) by heating lead tetramethyl in a rapid current of hydrogen at a pressure of 1 to 2 mmHg. From 1940 onwards, deeper insights into the formation, structure and reactions of free radicals showed that these reactive species could be tamed (8). The first synthetic methodologies involving carbon free radicals were done in the 1960s by Lamb (9) and Julia (10) and first synthetic methodology involving nitrogen free radicals was discovered much earlier in 1879, by Hofmann (1), but was not recognized as such, until mechanistic insights were provided by Wawzonek and Helen (11) and Corey and Hertler (12). Information on various kinds of radicals, their properties, chemistry and uses in organic chemistry have culminated in a wealth of literature in recent decades (13–20). The radical cyclisation continues to receive a lot of attention due to its synthetic value in the design and synthesis of many natural products containing heterocyclic rings, as one of the most useful transformations of radicals. The majority of this work will discuss the use of nitrogen radicals and their chemistry involved in synthetic applications, with a focus on cyclization reactions as a strategy in the late-stage functionalization (LSF) toolbox for derivatization of parent compounds in drug development.

1.2. Characteristics of free radicals

Free radicals have several important features. First, due to one free electron in the system, they belong to a class of very reactive species, with stability provided either by the means of steric interference, delocalization through multiple bonds, and/or inductive effects (21,22). Free radicals can be generated via several pathways, including photochemically, thermally, Lewis acid activation, and (single electron) redox reactions (electrochemically) (23). Due to their high reactivity, only trace amounts can be found, and their detection is done using either spin-trapping or detection at low temperatures directly via electron paramagnetic resonance (EPR) spectroscopy or laser flash photolysis (LFP).

Compared to carbanions and carbocations, free radicals are neutral species. Carbanions and carbocations suffer from solvent and aggregation phenomena, hence being more bulky intermediates. This is both a negative and a positive characteristic since carbanions and carbocations are solvated, *i.e.* stabilized by the solvent. A consequence of this is that the energy required for heterolytic cleavage of a bond in a solution is less than the homolytic cleavage needed for the generation of free radical species. Furthermore, a non-ionic fission of a covalent bond will be improbable if the dipole moment of that bond is large. A general rule of thumb is that reactions in solvents containing ions or dipoles, or of high dielectric constant, are unlikely to proceed via neutral radicals, whilst reactions in non-polar solvents of low dielectric constant, such as benzene, carbon tetrachloride (CCl_4), or carbon disulfide, may do so (24). Chemistry of free radical reactions differs from the chemistry of ionic organic reaction as the latter specifically occur at functional or otherwise activated positions in organic compounds compared to free radical reactions in which even inert methylene groups can be targeted in preference to activated positions due to kinetically favored product. Alas, this property is responsible for mixtures of polysubtituted products, and expert control over radical reactions is needed (25).

1.3. Nitrogen-centered radicals

The chemistry of nitrogen-centered radicals has received considerable attention and their use as intermediates in organic chemistry has long been appreciated (26–28). In comparison to carbon-centered radicals, the potential of nitrogen radicals in the area of alkaloid and heterocyclic synthesis of the pyrrolidine ring is high and has been reviewed (29,30).

1.4. Electronic states of nitrogen radicals

In aminyl free radicals, the central nitrogen must accommodate both an unpaired electron and a lone pair of electrons, this yields two electronic ground states, *i.e.* a π or a σ state (Figure 1) (21,31).

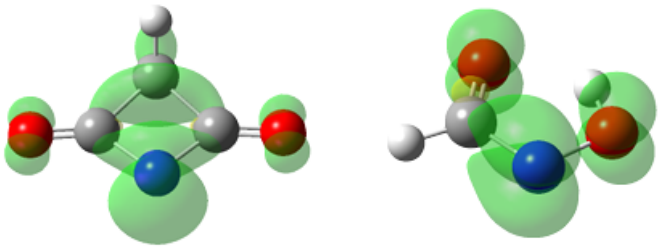

Figure 1. Singly occupied molecular orbitals (SOMO) of a π and a σ aminyl radical.

1.5. Characteristic reactions of neutral nitrogen radicals and their reactivity

The type of reaction favored by aminyl radicals depends to a significant degree upon the extent to which the electron pair in the aminyl radical is associated with electron-withdrawing or donating groups or with a proton or other acids (including transition metal ions). When both groups attached to nitrogen are small alkyl groups, aminyl radicals tend to engage in self-reactions, *i.e.* dimerize to hydrazines and disproportionate to Schiff bases and amines (32,33). In the presence of olefins, they show a strong tendency to abstract hydrogen (34–36) in preference to addition reactions, although addition of the dimethylamino radical to ethylene has been reported, but no yield was given (37). Aminyl radicals add to styrene and to α-methylstyrene (38) as well as to arenes (39). They engage in intramolecular abstractions of hydrogen of the Hofmann–Loffler–Freytag (HLF) type only when they are activated via the direct incorporation of an activating group (40,41).

1.6. Generation of aminyl radicals

There are many methods for the generation of aminyl radicals. This part of the introduction is intended as a brief summary of the main methods that have been used by chemists.

1.6.1. Tetrazenes

Gassman *et al*. (42) have demonstrated that under photolytic conditions the aminyl radical **4** can be readily formed from tetrazene **3** to afford parent amine **5** in 63 % yield and imine **6** in 34 % yields (Scheme 2). Depending on the conditions, they generate either aminyl radicals or

nitrenium ions. These two species differ in a sense that they follow different reaction paths. Specifically, they have shown that, while the imine **6** was completely absent in the methanolysis of **7**, it was a major product of all of the reactions, which should proceed via the nitrogen radical **4**. This was an indication that both the silver ion promoted and noncatalyzed methanolysis of **7** proceed via heterolytic cleavage of the N-Cl bond (42).

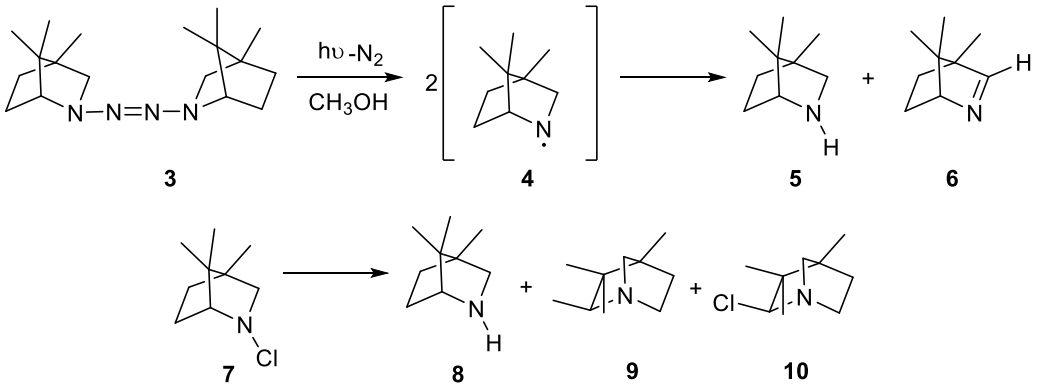

Scheme 2. Methanolysis of a tetrazene (42).

Newcomb and co-workers (43) studied the feasibility of using tetrazenes for cyclization and found that thermal decomposition of tetrazene **11** gave the aminyl radical **12** which rearranged to the 5-*exo* cyclised product **13** and the uncyclized reduced product **14** in a 1 : 1 ratio from the aminyl radical (Scheme 3).

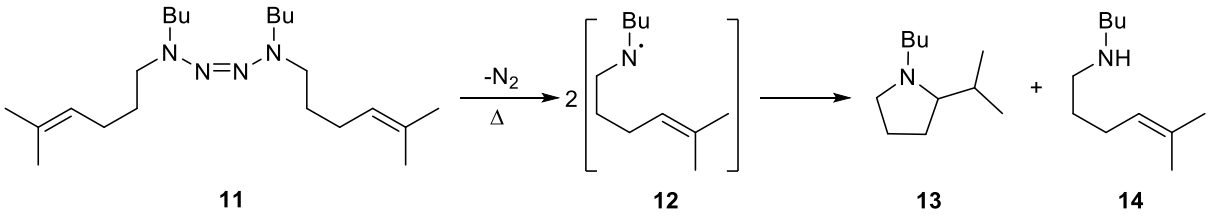

Scheme 3. Thermal decomposition of a tetrazene (43).

1.6.2. *N*-haloamines

N-chloroamines are readily synthesized in high yield and under mild condition by treatment of primary and secondary amines with trichloroisocyanuric acid (44). The use of *N*-chloramines allows the facile generation of aminyl radicals upon ultraviolet (UV) photolysis or thermolysis in neutral media. The use of *N*-bromo and *N*-iodo amines for the generation of aminyl radicals will be described in subsequent chapters. Ogata and co-workers (45) have shown that aminyl radicals generated from monochloramine **15** add to cyclohexene **16** by means of radical

intermediates, to give *trans*-2-chlorocyclohexylamine **17** (Scheme 4). The yield of the desired product was, however, below 10 %, as multiple products were obtained.

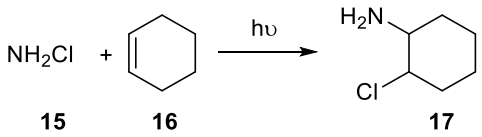

Scheme 4. Addition of a monochloroamine to cyclohexene (44).

F. M. Robinson *et al*. (46) report on photolysis of the *N*-chloroamine **18** in concentrated sulfuric acid yielding the *N*-methyltetrahydrocyclopentaquinoline **20** in 90 % yield. *δ*-hydrogen abstraction by the protonated aminyl radical **19** could have led to a hexahydroindenopyrrole. However, the preference of this intermediate for intramolecular aromatic substitution dominated the reaction (Scheme 5).

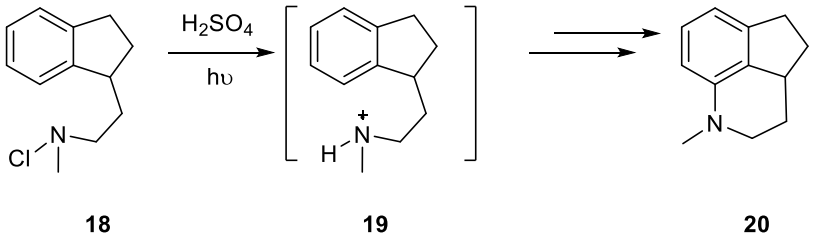

Scheme 5. Photolysis of an *N*-chloroamine followed by intramolecular aromatic substitution (46).

Surzur *et al*. report (47) on the synthesis of methylbenzomorphan **26**, utilizing as a key step an intramolecular addition of a Lewis acid complexed aminyl radical to an olefinic double bond. This 8-step sequence from benzaldehyde proceeds with an an overall yield of 18 %. The key step, homolytic scission of the nitrogen-chlorine bond in **21** yields the aminyl radical-titanium complex **22** which underwent 6-*exo* cyclisation by intramolecular addition to the double bond yielding cyclized radical **23**. The cyclized radical **23** abstracted a chlorine atom from **21**, in a chain reaction, furnishing 2-chloromethyl-1-methyl-4-phenylpiperidine as a mixture of *trans* **27** and *cis* **24** stereoisomers, in overall yield of 92 %. Inversion of to the 2,4-diaxial piperidine **25**, a favorable conformer for cyclisation, took place in the presence of aluminium trichloride in boiling cyclohexane and produced the benzomorphan **26** in 60 % yield (Scheme 6).

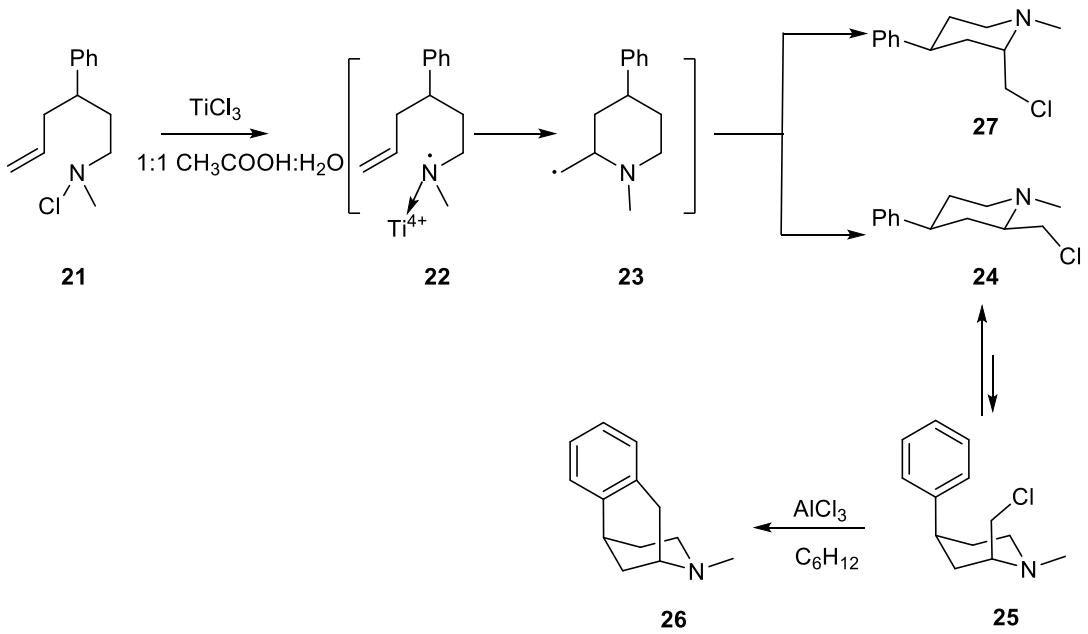

Scheme 6. Synthesis of methlynezomorphan (47).

1.6.3. *N*-nitrosoamines

Lavanish and Burger (48) report on the generation of nitrogen radicals **29** from *N*-dibenzylnitrosamine **28** in hydrocarbon solvents wlth ultraviolet UV light, which then undergo bimolecular disproportionation reaction yielding a 1 : 1 mixture of *N*-phenyl-1-phenylmethaneimine **30** and *N*-benzylaniline **31** (Scheme 7). The mixture was isolated by gas chromatography and identified by comparison with authentic samples. *N*-Nitrosoamines are carcinogenic and hence not suitable substrates. The use of these compounds has largely been replaced by safer methods of generation of nitrogen radicals.

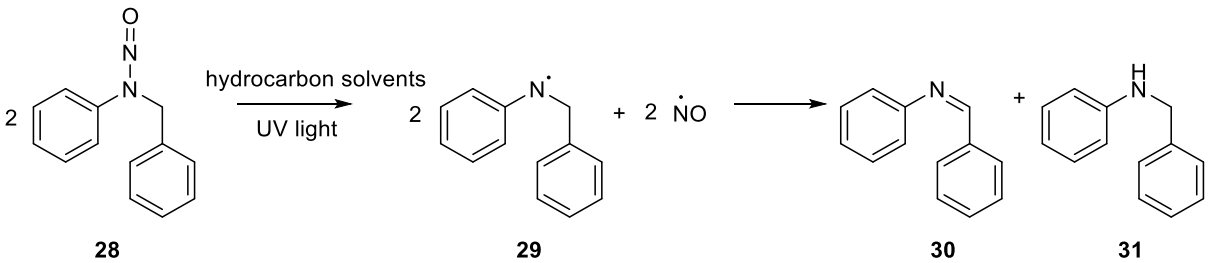

Scheme 7. Generation of aminyl radicals from *N*-nitrosoamines (48).

1.6.4. *N*-Hydroxypyridine-2-thione carbamates

Newcomb and Ha (49) disclosed the generation of Lewis acid complexed aminyl radicals 3**4** from *N*-hydroxypyridine-2-thione carbamates (PTOC carbamates) **32**, which then cyclize to pyrrolidine products **36** in high yields (Scheme 8). These carbamates are related to Barton's

(50) PTOC esters which are used for the controlled generation of carbon radicals from carboxylic acids. The procedure employes a wide variety of Lewis acids to activate aminyl radicals from PTOC carbamates with several of the Lewis acids demonstrating true catalytic behavior as the yields of the pyrrolidine products exceeded the amounts of Lewis acid present. The Lewis acids also exhibited and inhibitory effect, at a certain concentration, as it was able to bind to the PTOC carbamate precursor, producing a species that failed to react in the chain propagation sequence thus terminating the radicals chain reaction and lowering the yield. The method is mild, permitting production of radicals at temperatures as low as –78 °C.

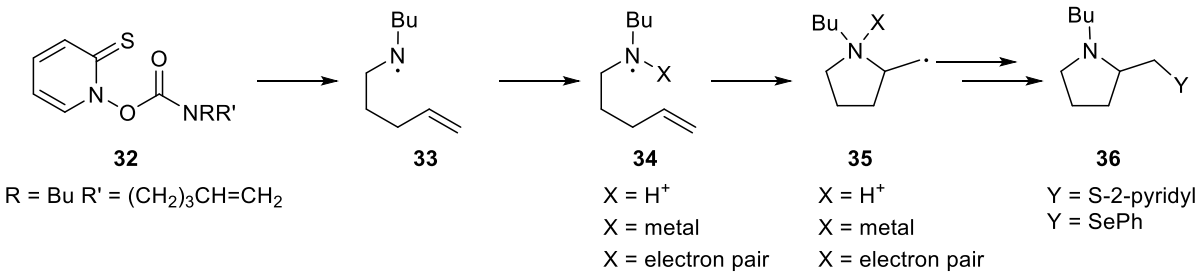

Scheme 8. Generation of aminyl radicals from *N*-hydroxypyridine-2-thione carbamates (49).

Deeb and Newcomb (51) have demonstrated that *N*-hydroxypyridine-2-thione carbamates **37** are convenient sources for both aminyl radicals and aminium radical cation generation under mild conditions which are then involved in intramolecular N–C bond forming reactions. They have shown that the neutral aminyl radical **38** is in dynamic equilibrium with its cyclic radical **39** as a mixture of cyclic **40** and acyclic products **41**, in the presence of hydrogen atom donor, was obtained (Scheme 9). The yield of the pyrrolidine product increased to 100 % in the presence od acetic acid and suitable hydrogen atom donor. This was an indication that the cyclization of the aminium cation radical was much faster when compared to its neutral counterpart or/and the attained equilibrium is larger than that of the neutral pair.

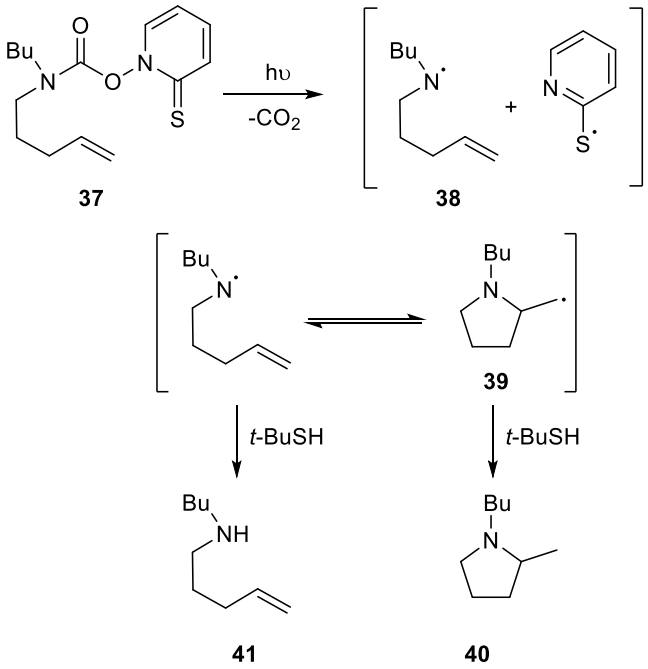

Scheme 9. Dynamic equilibirum of an aminyl radical and it's cyclic counterpart (51).

Marquardt *et al*. (52) report on the formation of dialkyl aminyl radicals from *N*-hydroxypyridine-2-thione carbamates. These dialkyl radicals **44** are formed from carbamates **42** by homolytic cleavage of the O–N bond to give carbamoyloxy radicals **43** which then decarboxylate (Scheme 10). Various methods of inducing O–N cleavage are possible, including thermal or photochemical decomposition of the PTOC carbamate precursor or reaction of the precursor in a radical chain reaction with a hydrogen atom donor as a chain carrier. In the case of *N*-propylcyclobutaneamine radical, the relative rates of the reduction by hydrogen atom donors and the ring opening reaction were measured. Rate constant for the ring opening reaction of the similar but smaller cyclopropane ring in cyclopropylaminyl radicals has been measured to be 50 times greater. In the case of dipropylaminyl radical, when no hydrogen atom source was available, the radicals disproportionated to amine **45** and imine **46** (Scheme 10).

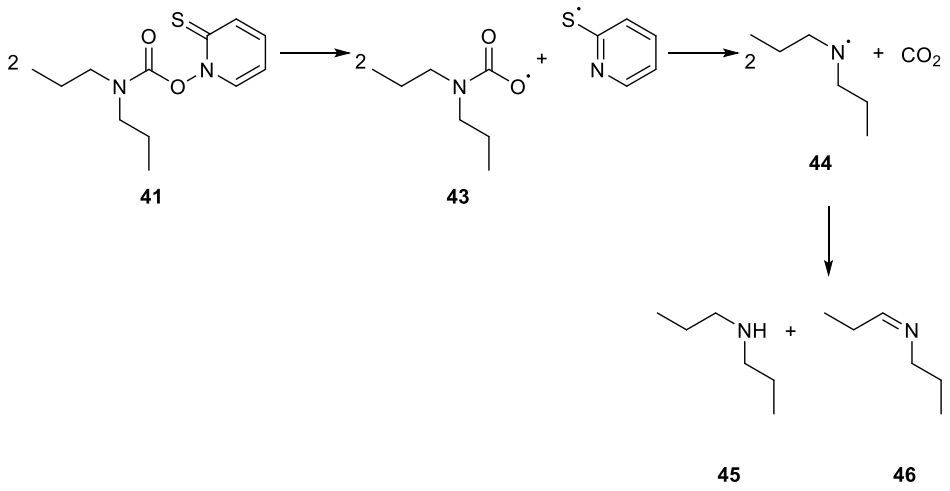

Scheme 10. Generation of an aminyl radical from an intermediary carbamoyloxy radical (52).

Newcomb and Esker (53) report on the formation of lactam, pyrrolidine and benzoindolizidinone ring systems via intramolecular addition of amidyl radicals to olefinic double bonds and quenching of the cyclic radicals formed with hydrogen bond donors. In a specific case of benzoindolizidinone ring formation, the reaction sequence involved decomposition of **47** and subsequent cyclization of the amidyl radical **48** in a 5-*exo* manner to give radical **49** that subsequently cyclized to radical **50**. The highly delocalized radical apparently was too stable to react with *tert*-buthylthiol (*t*-BuSH), and it accumulated and eventually reacted only by hydrogen atom donation to an amidyl radical, an oxidation step that regenerated the aromatic ring in benzoindolizidinone product **51** at the expense of half of the acyclic radical (Scheme 11).

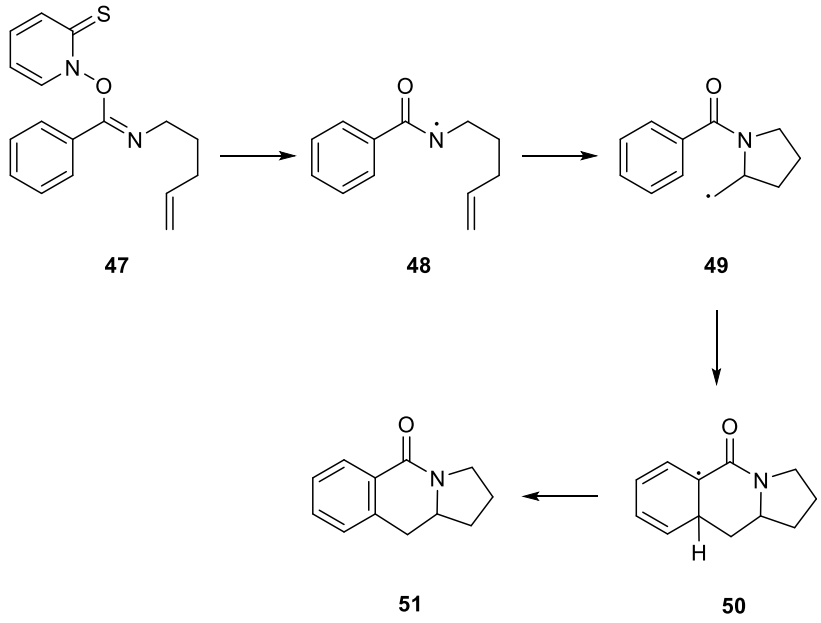

Scheme 11. Intramolecular addition of amidyl radicals to olefinic double bonds (53).

1.6.5. Se-phenyl benzoselenohydroximate derivatives

Kim and Lee (54) report on an alternative approach of generation of aminyl radicals via Se-phenyl benzoselenohydroximate derivatives. Utilizing aminyl radical precursors **52** with tributyltin hydride (Bu_3SnH)/azobisisobutyronitrile (AIBN) in refluxing tetrahydrofurane under a high dilution conditions, they obtained cyclized pyrrolizidines **55** in 50 % yield along with the reduction product **56** in 30 % yield. Such product distribution is an indication that the aminyl radical **53** is in equilibrium with its cyclized product **54** (Scheme 12). These pyrrolizidine rings are obtained via two succesive 5-*exo* radical cyclization reactions. Authors also report that the reaction carried out in refluxing tetrahydrofurane was cleaner than in refluxing benzene and that poor cyclization to pyrrolizidine rings was observed in refluxing cyclohexane (55).

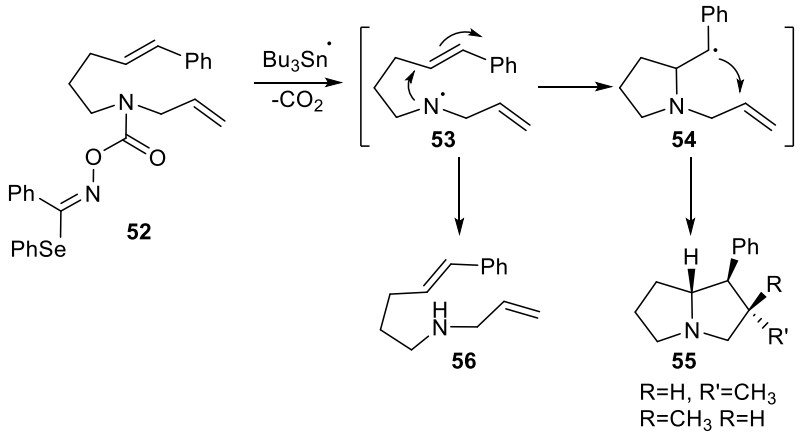

Scheme 12. Generation of aminyl radicals from Se-phenyl benzoselenohydroximate derivatives (54).

1.6.6. Sulfenamides

Bowman and co-workers (56) report on the generation of aminyl radicals from sulfenamides and Bu_3SnH. Evidence for the formation of the aminyl radicals was provided by carefully designed experiments of ring-opening reactions of *N*-popylcyclobutylaminyl and *N*-butylcyclopropylaminyl radicals.

In subsequent work by Bowman *et al*. (57), cyclization of aminyl radicals using sulfenamide precursors with Bu_3SnH was achieved. To obtain products in sufficiently high yields, *endo*-2-(bicyclo[2.2.1]hept-2-en-5-yl)ethyl radicals **59** were deployed as the rate for such radicals is one of the fastest reported (1×10^7 s^{-1}) because of the strained alkene and close orientation of

the carbon-radical to the alkene. With the implementation of an *N*-allyl substitutent, *i.e.*, an intramolecular trap to prevent equilibrium back to aminyl radical **58**, quadracyclic pyrrolizidine **61** was obtained in the high yield (90 %) (Scheme 13).

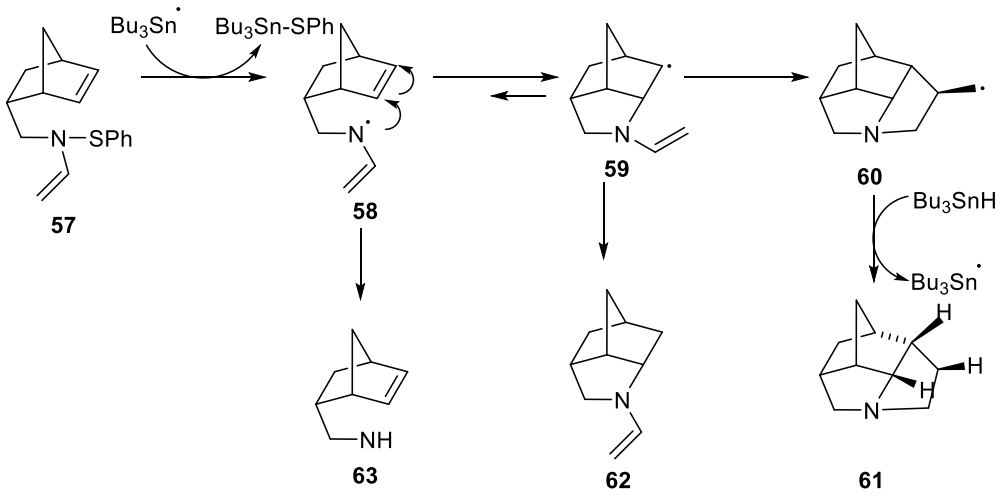

Scheme 13. Generation of aminyl radicals from sulfenamides and Bu_3SnH (57).

1.7. Chain reactions

Chain reactions rely on the presence of highly reactive intermediates, known as chain carriers, which participate in a cycle of consumption and production (Scheme 14). Radicals are usually such chain carriers and a typical sequence of this type with two chain carriers, *i.e.* radicals X and Y converting reactants A and B to products P and Q, is

$$X + A \longrightarrow P + Y$$

$$Y + B \longrightarrow Q + X$$

Scheme 14 Chain carriers participate in a cycle of consumption and production.

Radical X, consumed in the first step, re-appears as a product in the second. Similarly, Y, consumed in the second step, re-appears as a product in the first. These chains are started by reactions that serve as a source of radicals and terminated by reactions that consume radicals without generating others. Radicals are similar to catalysts in that they are regenerated after having been consumed, but differ in that they have extremely short lifespans and do not survive the overall reaction. As highly reactive species with very short lifespans, radicals remain at

trace levels. Thus, the Bodenstein approximation (58,59) of quasi-stationary behavior which states: „The net rate of formation of an intermediate that is and remains at trace level is negligible compared with its contributing formation and decay rates", applies to them.

The simplest chain reactions are those with two radical species (Scheme 15), one or both generated by initiation, and with termination by recombination of the radicals. The propagation steps may or may not be reversible.

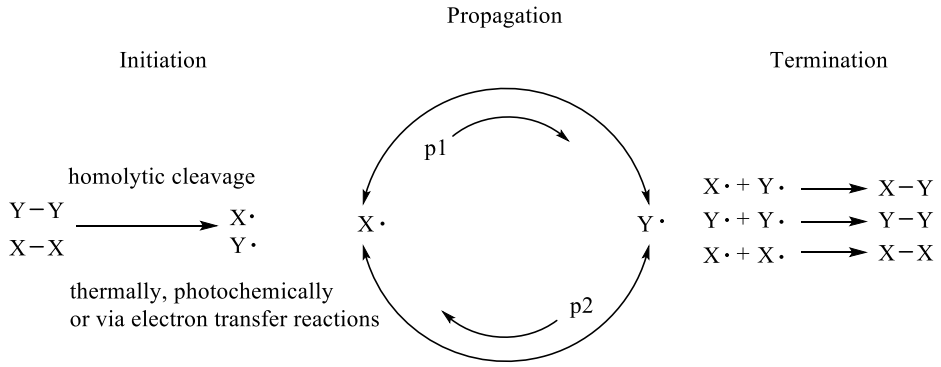

Scheme 15. Model of the simplest chain reaction. The two headed arrows represent reversible steps, indices p1 and p2 represent the rates of the steps

In such a network, the rates of the two propagation steps are

$$r_{p1} = \lambda_{p1} C_X - \lambda_{-p1} C_Y \qquad \text{eqn 1.}$$

$$r_{p2} = \lambda_{p2} C_Y - \lambda_{-p2} C_X \qquad \text{eqn 2.}$$

(indices p1 and p2 are used to avoid ambiguity; minus signs in indices indicate reverse steps; λ stands for pseudo-first order rate coefficient). The Bodenstein approximation for X gives

$$r_X = (r_X)_{init} + C_Y(\lambda_{-p1} + \lambda_{p2}) - C_X(\lambda_{p1} + \lambda_{-p2}) + (r_X)_{trm} \cong 0 \qquad \text{eqn 3.}$$

Here, $(r_X)_{init}$ and $(r_X)_{trm}$ are the rates of production and elimination of X by initiation and termination, respectively (the termination rate is negative) (60).

Characteristic of most chain reactions is that the propagation cycle is repeated many times between initiation and termination. If so, the initiation and termination terms (eqn 3) are small compared to the propagation terms. The so-called long-chain approximation ignores them. Equation 3. can then be used to express the concentration of one chain carrier as a function of that of the other:

$$C_Y \cong C_X \left[\frac{\lambda_{p1} + \lambda_{-p2}}{\lambda_{-p1} + \lambda_{p2}}\right] \qquad \text{eqn 4.}$$

With this substitution, eqns 1. and 2. yield

$$r_{p1} \cong r_{p2} \cong C_X \left[\frac{\lambda_{p1}\lambda_{p2} - \lambda_{-p1}\lambda_{-p2}}{\lambda_{-p1} + \lambda_{p2}}\right] \quad \text{eqn 5.}$$

Equation 5, derived with the long-chain approximation, shows the rates of the two propagation steps under quasi-stationary conditions to be equal, *i.e.* each of the two steps consumes as many chain carriers as the other produces. Since the total number of chain carriers is not altered by the propagation steps, the overall rates of chain carrier production and consumption (of X plus Y) must be equal in magnitude:

$$r_{init} + r_{trm} \cong 0 \quad \text{eqn 6.}$$

The equality applies to the total chain-carrier population, X + Y, but by no means necessarily to each chain carrier separately (60).

1.8. Hofmann–Löffler–Freytag reaction

In the previous sections, we have discussed what radicals are, their stability, and typical reactions for generating them. Also, we have described necessary theory for kinetic considerations of chain reactions. As stated, one of the first *N*-centered radical was generated and was involved as an intermediate in the HLF chain-reaction.

1.8.1. HLF reaction from a historical perspective and its modern versions.

In 1879, Hofmann (1) discovered that treating *N*-bromo-2-propylpiperidine, an *N*-halodialkylamine, with hot sulfuric acid produced a tertiary amine, eventually identified as octahydroindolizine (61,62). Löffler and Freytag (63) extended the Hofmann reaction to simple secondary amines and discovered it to be a general approach for synthesizing pyrrolidines (25). Upon the activation of *N*-chloroamine **64** with sulfuric acid (Scheme 16), the protonated *N*-chloroamine **65** undergoes homolytic cleavage in the presence of heat, light, or initiators. The formed protonated aminyl radical **66** takes part in an intramolecular HAT abstracting a hydrogen atom to afford, regioselectively, an alkyl radical **67**, which in turn abstracts a chlorine atom, through intermolecular halogen atom transfer (XAT) to form a chloroalkylammonium ion **68**, which then cyclizes in the presence of a base providing cyclic tertiary amine **69**.

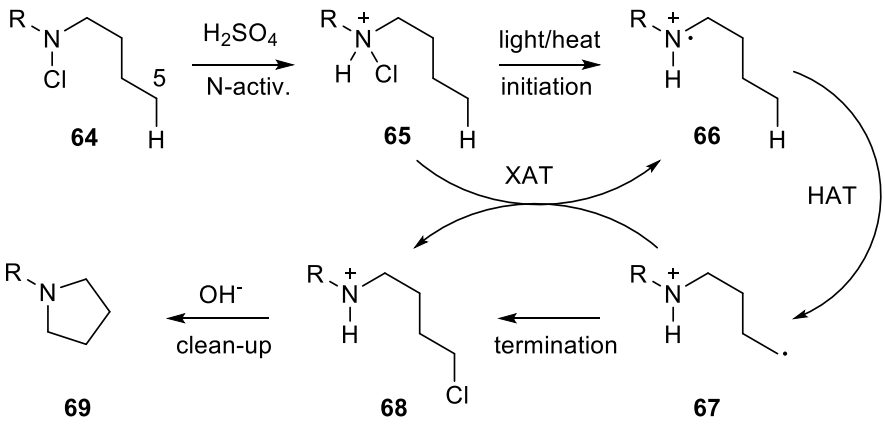

Scheme 16. Cyclization of *N*-halogenated amines (HLF reaction) (63).

Suarez and co-workers (64–68) have modified the HLF reaction by starting with the synthesis of the *N*-iodamide precursor, while reducing the photochemical C –H bond activation and cyclization to one synthetic step. Furthermore, hypervalent iodine-containing oxidants such as (diacetoxyiodo)benzene (PIDA) were used in combination with I_2.

The next step in the development of the HLF reaction was made by Corey *et al*. (69). These methods involve the preparation of the appropriate bromamide precursor using acetyl hypobromite. Irradiation of the precursor **71** in CCl_4 at room temperature produced the C_5-bromo derivative **74** in 90 % yield. The obtained derivative can be cyclized to pyrrolidine **75** by reaction with a sterically hindered amine base (Scheme 17).

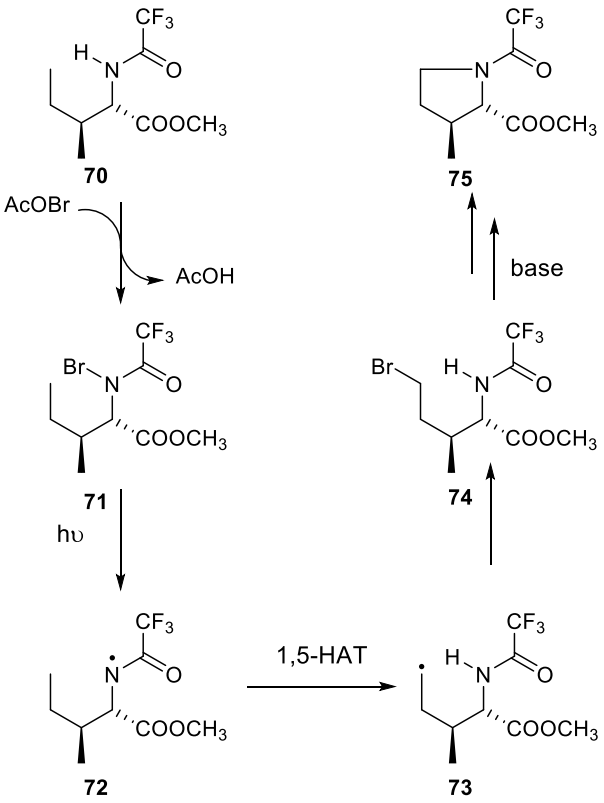

Scheme 17. Corey's modification of the HLF reaction (69).

Löffler and Kober have utilized the HLF reaction in their nicotine synthesis (63). More than a hundred years later, Muñiz *et al*. (70) developed an enantioselective total synthesis of nicotine utilizing the HLF reaction. The HLF reaction was followed by the removal of methoxy and tosyl groups in an acidic medium with heating. The resulting cyclic imine was converted into pyrrolidine by reduction with $NaBH_4$ in ethanol at 0 °C. Finally, Eschweiler-Clarke *N*-methylation produced the desired nicotine product **83**.

Šakić et al. (40) have calculated that Löffler and Kober's synthesis of nicotine, but also Muñiz's synthesis could have been carried out under milder conditions by using appropriate activating substituents on the nitrogen atom (Scheme 18).

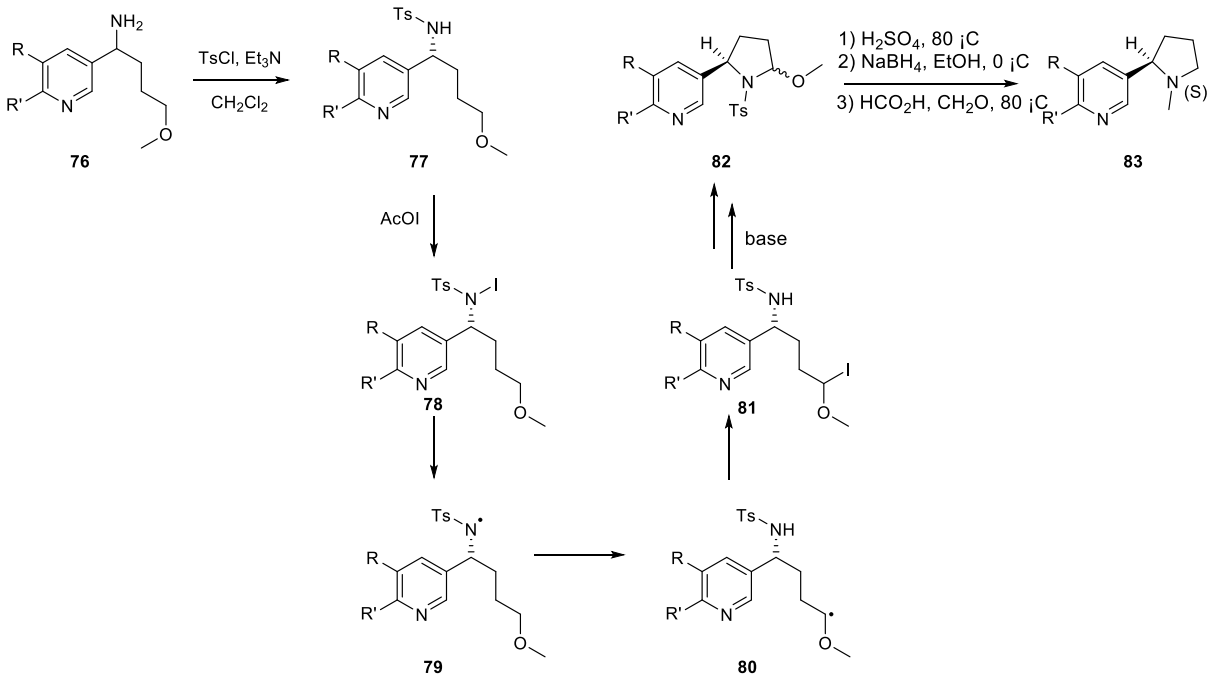

Scheme 18. Enantioselective total synthesis of nicotine utilizing the HLF reaction (70).

Fan *et al*. (71) developed a method for pyrrolidine synthesis using iodo-benzene diacetate ($PhI(OAc)_2$) and I_2. They report that the reaction proceeds in high yield in dichloroethane, in moderate yields in dichloromethane and ethyl acetate, and fails completely in tetrahydrofuran (THF), dimethylformamide (DMF), *tert*-butanol (*t*-BuOH) and toluene (Scheme 19).

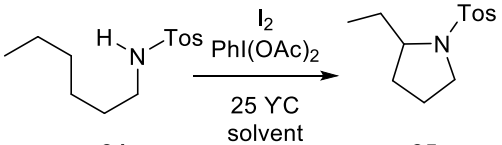

solvent	yield [%]
ClCH2CH2Cl	82
CH_2Cl_2	42
THF	–
toluene	–

Scheme 19. Synthesis and yields of pyrrolidine in different solvents (71).

Zipse and Šakić (41) proposed a hypothesis as to why the HLF reaction does not occur in solvents Fan *et al*. (71) have worked with. They propose that intermolecular HAT steps between substrate molecules and some organic solvents suppress the HLF. They found that there is a competing HAT reaction between solute radicals and solvent molecules of THF and toluene. They have also calculated the reaction enthalpy and the barrier of the HAT for the classical, Suarez and Corey versions of the HLF reaction. Calculations show that the thermochemical profiles differ significantly despite the fact that the key step in all three versions is 1,5-HAT. For the original HLF reaction, it was shown that the protonated aminium radical participates in a thermodynamically and kinetically much more favorable 1,5-HAT process compared to the aminyl radical. Therefore, highly acidic conditions are necessary for the original HLF reaction in order to obtain the products in satisfactory yields. On the other hand, the 1,5-HAT step in Corey's modification of the HLF reaction takes place in a neutral medium with excellent yields. This was achieved by incorporation of the trifluoroacetyl group on the nitrogen atom, as this provides the necessary driving force for the HAT step by destabilizing *N*-centered radical. It was also calculated for the Suarez modification, which uses sulfonamide radicals in the 1,5-HAT step, a favorable driving force was obtained by the stabilization of the carbon radical and activation of the aminyl radical. In the case when the C_6-radical is more stable than the C_5-radical, the 1,6-HAT process can occur.

1.8.2. HLF regioselectivity: 1,5-HAT *vs* 1,6-HAT

Muñiz *et al*. (72) developed an iodine-catalyzed HLF reaction where 1,6-HAT step is closely followed by the Ritter's amination, which prevents the usual cyclization and enables the intermolecular nucleophilic regeneration of iodine as a catalyst and the final formation of 1,3-α-tertiary diamines **88** (Scheme 20).

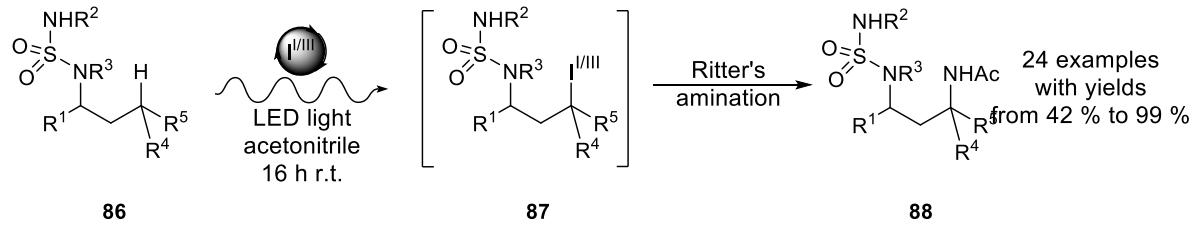

Scheme 20. An iodine-catalyzed HLF reaction combined with Ritter's amination yielding 1,3-α-tertiary diamines (72).

Minakata *et al*. (73) developed a procedure for intramolecular C-H amination of sulfamate esters using *tert*-butyl hypoiodite (*t*-BuOI) or *N*-iodosuccinimide (NIS) with iodine, whereby cyclic oxathiazinan derivatives **90** are formed that can be converted into 1,3-diamines **91** (Scheme 21).

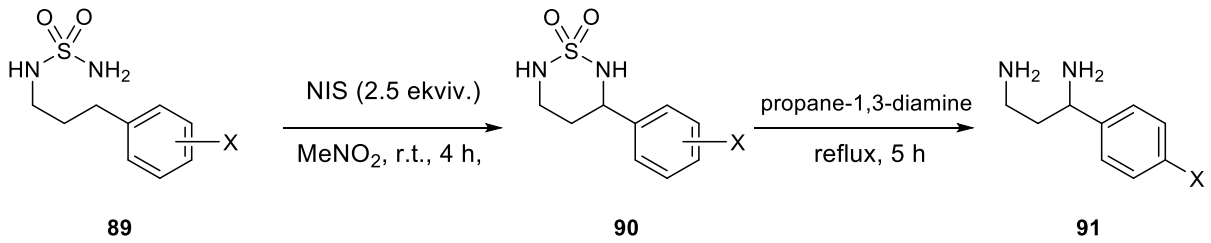

Scheme 21. Intramolecular C–H amination of sulfamate esters and conversion of the cyclic products to 1,3-diamine (73).

Short *et al*. (74) have used the HLF reaction without the cyclization step to obtain C–H functionalized products. In their method they deploy two structural variants of the aminyl radical precursors. In the case when the external nitrogen of the radical precursor is protected by a *tert*-butyloxycarbonyl (Boc) group **92**, the aminyl radical participates in a 1,5-HAT and yields C_5-functionalized products **93** (Scheme 22). However, when the internal nitrogen is protected by a Boc group **94**, the external nitrogen participates in two competitive processes, 1,6-HAT and 1,7-HAT, and renders a mixture of C_6- and C_7-functionalized products **95** and **96**, respectively (Scheme 22). The ratio of the obtained products is controlled by adjusting the steric and electronic properties of the substituents attached to the nitrogen atom. In a large number of cases, the majority of the product is produced by the 1,6-HAT process.

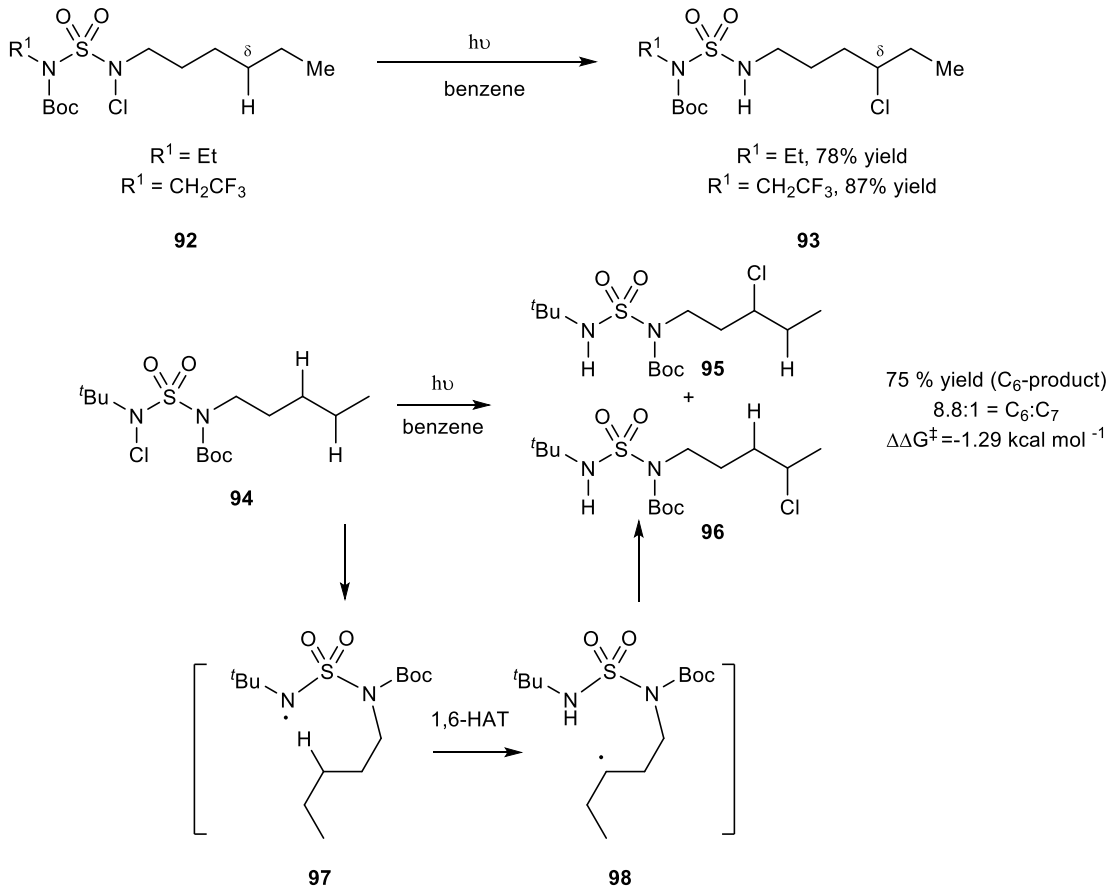

Scheme 22. Chlorination of aliphatic C-H bonds utilizing HLF reaction (74).

Baran *et al*. (75) synthesized 1,3-diols from alcohols using the HLF reaction and brominated carbamates. To prepare the necessary bromide precursor **101**, they used the oxidant acetyl hypobromite. It was shown that carbamyl radical intermediates preferentially abstract H-atoms from tertiary and benzylic positions and participate in the 1,6-HAT process (Scheme 23).

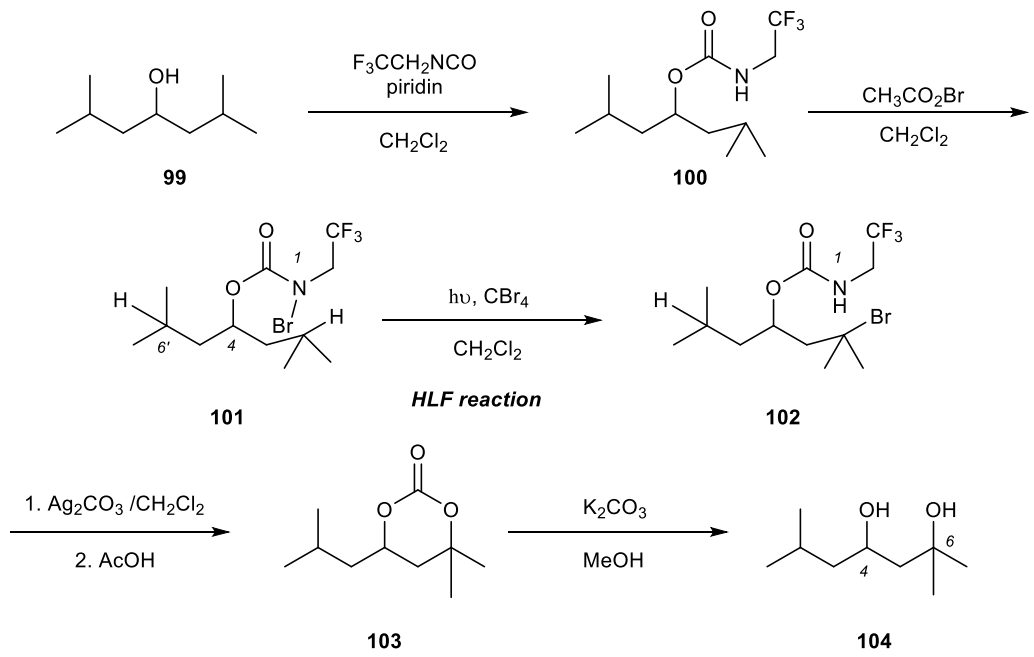

Scheme 23. Formation of 1,3-diols from alcohols using the HLF reaction and brominated carbamates(75).

Muñiz and Zhang (76) developed a synthesis of piperidine under the influence of visible light. Roizen *et al*. (77) developed a procedure for selective chlorination of aliphatic C–H bonds mediated by sulfamate esters. It is assumed that the aminyl radical **106** participates in the 1,6-HAT step, whereby a C_6-functionalized product **108** is formed with excellent regioselectivity (Scheme 24). This method transforms C–H bonds on secondary, tertiary and benzylic centers even when the selected molecule has weaker C–H bonds and in the presence of a number of functional groups incorporated into the substrate. The authors propose why sulfamyl radicals participate in the 1,6-HAT and not in the 1,5-HAT process. Namely, the elongated S–O and S–N bonds and the reduced O–S–N bond angle geometrically affect the selection of the seven-membered transition state for C–H abstraction.

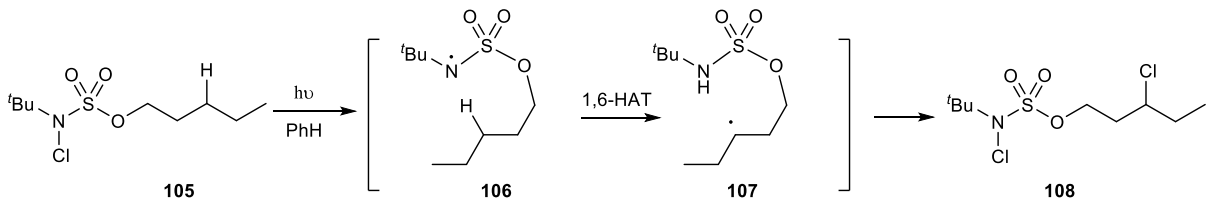

Scheme 24. Selective chlorination of aliphatic C–H bonds mediated by sulfamate esters (77).

Muñiz *et al*. (78) developed a procedure for the synthesis of pyrollidine rings utilizing iodine and photoredox catalyst. It is assumed that iodine serves as the primary catalyst that activates the C–H bond via light-induced homolytic cleavage of the *in situ* generated N–I bond followed by a 1,5-HAT process involving amidyl radicals (Scheme 25). The authors showed that the mixture of 1,2-dichloroethane and hexafluoroprop-2-ol (HFIP) as solvents and the intensity of the radiation source are crucial in order to obtain satisfactory yields of the reaction.

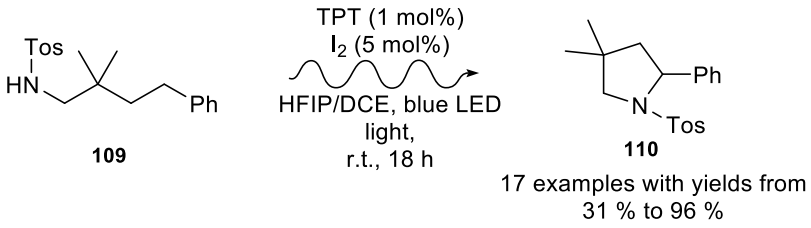

Scheme 25. Iodine/photoredox catalysed amination of C-sp^3-H bonds (78).

Muñiz *et al*.(79) developed a method of multiple halogenation of aliphatic C–H bonds using hydantoin **112**. It is assumed that this halogenation involves HLF reaction with aminyl radicals as intermediates that are involved in 1,5-HAT and 1,6-HAT processes followed by halogenation (Scheme 26).

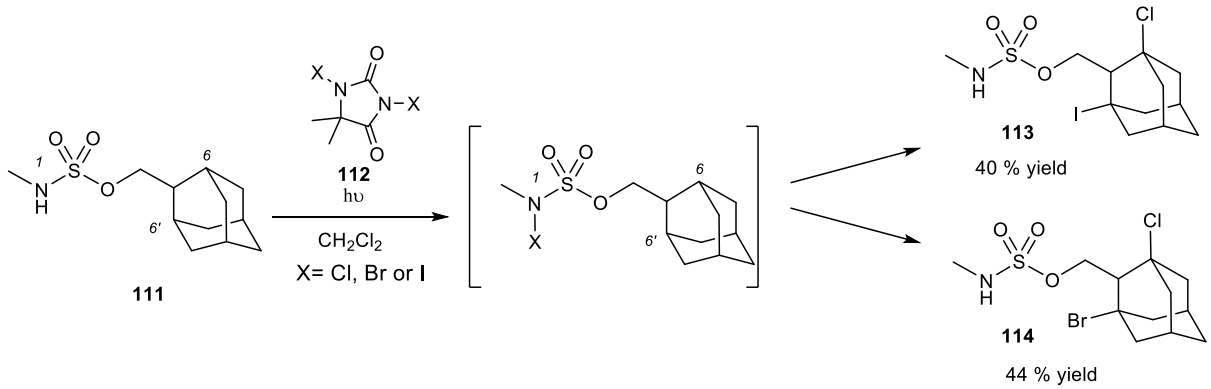

Scheme 26. Multiple halogenations of aliphatic C−H bonds via consecutive HLF reactions (79).

1.8.3. Mechanistic studies of the HLF reaction

Since the discovery of the HLF reaction, mechanistic studies point conclusively to a radical chain mechanism involving intramolecular HAT as the first step of the propagation cycle, with XAT as the second step (11,12,80–82).

Thelen and Wawnozek (11) made the first study of the mechanism of the cyclization of *N*-haloamines (Scheme 27). They found that a solution of *N*-chloro-*N*-methylcyclooctylamine **115** in sulfuric acid when irradiated with ultraviolet light in the presence of chlorine or when treated with hydrogen peroxide in the dark gave up to 24 % yield of *N*-methylgranatinine **120**, much more than is formed in the absence of light and peroxide. It was proposed from this evidence that the reaction proceeds by a free radical chain mechanism.

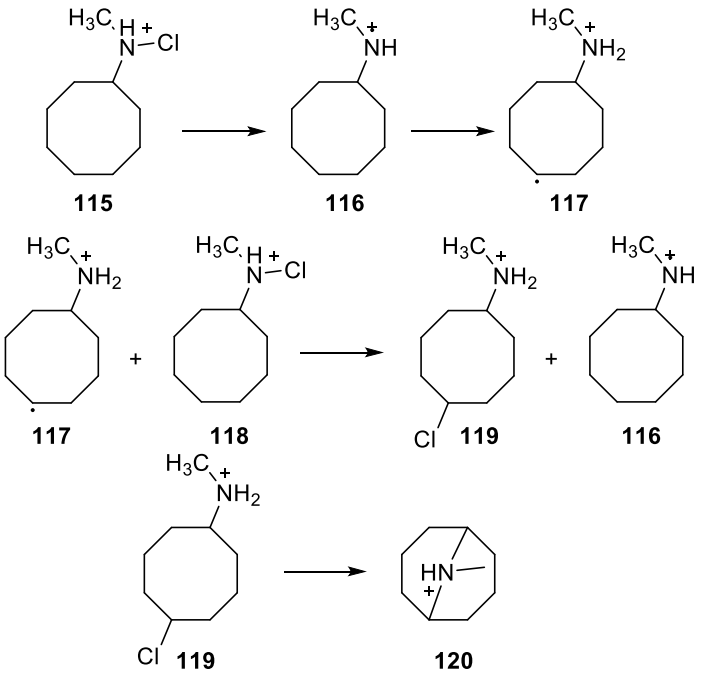

Scheme 27. Preaparation of *N*-methylgranatinine(11).

Wawzonek and Thelen also report (81) on the preparation of quinuclidines in 85 % sulfuric acid with both *N*-chloro and *N*-bromoamines. Best yields were obtained if the solution was irradiated with UV light at room temperature or lower, for 24 hours. This differs a bit from the classical HLF reaction in that high temperatures are not required, when the source of light is used for radical chain initiation. The results indicate that comparable yields are obtained with both the bromoamines and the chloroamines.

In a review by Wolff (25), it was noted that the best evidence for intramolecular hydrogen abstraction by the aminium radical to afford a carbon radical was the loss of stereoselectivity in the cyclization of (−)-*N*-methylpentylamine-4-*d*. Although an isotope effect (k_H/k_D) of 3.54 is observed in this conversion, the 1,2-dimethylpyrrolidine obtained is optically inactive, showing that a trigonal C_6 intermediate capable of inversion is formed. Furthermore, Wolff claims that the initiation of the HLF reaction with small amounts of chemical initiators, as well

as the inhibition of the reaction by radical trapping agents such as oxygen and *N*-chlorodiethylamine, provide good evidence for a chain mechanism. Wolff notes that the majority of HLF reactions that have been conducted in sulfuric acid have the intermediate alkyl halides cyclizing without isolation. In these cases, the acid solution is made alkaline and heated to effect cyclization, and the resulting amines are separated by steam distillation. The desired tertiary amines are frequently contaminated with considerable amounts of secondary amines arising from disproportionation reactions.

Hertler and Corey (12) have studied the mechanism of the HLF reaction and report that chlorination of the deuterated amine followed by thermal decomposition of the *N*-chloro derivative in sulfuric acid at 95 °C gave a 43 % yield of pure 1,2-dimethylpyrrolidine which was optically inactive. This is strong evidence that the decomposition of *N*-chloroamines in acid involves an intermediate in which C_6 is trigonal. It was further found that addition of catalytic amounts of potassium persulfate and ferrous ammonium sulfate or ferrous ammonium sulfate alone to a solution of dibutylchloroainine in sulfuric acid in dark caused disappearance of the chloroamine. Workup of the reaction mixture gave good yields of *N*-butylpyrrolidine. This is evidenced by the decomposition of the chloroamine in a free radical chain process. Indeed, it is likely that under the conditions used in their experiments with UV irradiation, the free chloroamine is responsible for most of the initiation and, hence, the initiation rate was decreased. Acid catalysis must therefore involve acceleration of the propagation process and/or retardation of chain termination.

1.8.4. Detection of nitrogen-centered radicals via EPR and LFP measurements

The majority of known aminyl radicals are short-lived and can only be detected by EPR at low temperatures. Extremely short-lived aminyl radicals, such as diacyl- and monoacylaminyl radicals, could only be detected by trapping them with 2-methyl-2-nitrosopropane or phenyl-*t*-butylnitrone (PBN) (83,84).

Danen and Kensler (85) were the first to have made the discovery that dialkylamino radicals can be observed by EPR spectroscopy on performing photolysis reaction on tetraalkyltetrazenes directly in the EPR cavity in cyclopropane solution. They have reported an EPR spectra of dimethyl-, diethyl-, and diisopropylamino radicals in solution with isotropic nitrogen hyperfine coupling constant on the order of 14 Gauss indicating that the unpaired electron is located predominantly in the nitrogen 2*p* orbital since the nitrogen coupling would be much larger for unpaired electron residence in a sp^3 or another hybrid orbital. In the case of the diisopropylamino radical, a substantially stronger EPR signal was obtained indicating increased

stability of these radicals, and therefore the increased likelihood of it being detected via EPR measurements.

The rather large isotropic nitrogen hyperfine interaction of 32 Gauss reported by Hadley and Volman (86) for both methylamino and dimethylamino free radicals would suggest that the unpaired electron resides in a hybrid orbital with appreciable *s* character. These radicals were, however, generated under different condition with UV irradiation of pure amines.

Danen and Rickard (87) report on the EPR spectra of several dialkylaminium radical cations generated by photolysis of sulfuric acid solutions of the corresponding *N*-chloramines. Their report constitutes direct observation of aminium radicals in conditions in which original HLF reaction was discovered.

Important work on the mechanism of HLF was done by Sutcliffe and Ingold (88). They report on the direct detection of amidyl and alkyl radical traces of the HLF reaction via EPR spectroscopy. Amidyl radicals involved in intramolecular hydrogen atom abstractions were detected at temperatures ranging from 173 – 200 K. The intensities of all signals corresponding to the amidyl radical's spectra diminished rapidly with the increase of temperature. The reason behind this observation is the start of the propagation cycle of the HLF reaction due to the increase of the energy of the radical molecules needed for the kinetic barrier for the intramolecular abstraction. They were able to detect primary alkyl radicals at temperatures 213 – 243 K, although just for half of the systems examined. They were not able to observe the unrearranged amidyl radicals and the rearranged alkyl radicals simultaneously, *i.e.*, in equilibrium, and to measure their absolute concentration under steady-state condition. They claim that the occurrence of a *N*-chloroamide consuming chain reaction rendered the procedure impossible. They also report on the estimated rate constants at 300 K for hydrogen atom abstractions via six-center cyclic transition states and they are $1 \cdot 10^5$ s^{-1} and $4 \cdot 10^4$ s^{-1} for abstraction from a methyl group in the alkyl and acyl moieties, respectively. This corresponds to relative barriers of roughly 46 ± 1 kJ/mol.

Danen and Gellert (89) report on the detection of two simple amidyl radicals generated by photolysis of the corresponding *N*-chloroamides in cyclopropane directly in the cavity of the EPR spectrometer. The derived data are typical of those for a π-electronic ground state rather than a *σ*-electronic ground state. The magnitudes of hyperfine couplings for nitrogen and hydrogen are consistent with other nitrogen-centered π-radicals and suggest that there is not extensive delocalization of the unpaired electron onto the carbonyl group. A σ-radical would be expected to exhibit a much greater *hfc* for nitrogen since the unpaired electron would reside in an orbital of appreciable *s* character. By photolyzing *N*-chloramides in air-saturated toluene

solutions, spectra of the corresponding nitroxides were observed. The identity of these radicals is evidenced by the relatively small a^N and a^H coupling constants, the *g* values characteristic of nitroxides and the enhanced stability as compared to the transient amido radicals. In poorly degassed aminyl samples, nitroxides are frequently observed (90). Roberts and Inglod report (33) that 2,2,6,6-tetramethyl-1-piperidyl reacts rapidly and quantitatively with oxygen to yield the corresponding nitroxide which can be distinguished from its analog 2,2,6,6-tetramethylpiperidyl radical by its higher *g* values and the absence of splitting of the nitrogen nucleus with the hydrogen nucleus. This reaction may also occur with other aminyl radicals. Stable aryl substituted aminyl radicals, such as *N*-phenyl-2-naphthylamino radical are relatively inert (91).

Although there are no LFP studies in the literature on the intramolecular hydrogen atom rearrangements, there are plenty studies regarding intramolecular additions of aminyl radical to double bonds.

Newcomb and coworkers (92) report on unimolecular rate constants for a series of dialklyaminyl radicals and the second order rate constants for reactions of several hydrogen atom donors. PTOC carbamates were used as radical precursors in direct, laser-flash kinetic measurements and in indirect, radical chain kinetic studies. From the comparison in Table 1. of the intramolecular addition reactions of aminyl, carbon and aminium cation radicals, the aminyl radicals have much longer lifetimes when compared to carbon analogs. Aminium cation radicals are the most reactive species in this series and cyclize the fastest, although the kinetics of the aminium cation radicals is solvent dependent. For this series of compounds, 5-*exo* cyclizations **123** are faster than 6-*exo* **121** cyclization (Table 1). All of the dialkylaminyl radicals studied were designed such that unimolecular reactions would produce benzylic or diphenylalkyl radicals that have long wavelength λ_{max} values at approximately 315 and 325 nm, respectively. This feature permits direct LFP kinetic studies using UV detection.

Table 1. Lifetimes of radicals involved in intramolecular addition reactions to olefinic double bonds (92).

Radical structure	Radical lifetime		
	X = N	X = CH	X = HN^+
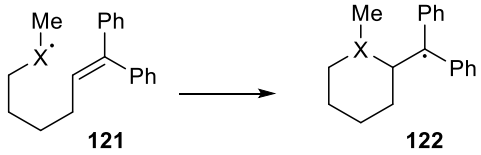 **121** **122**	95 μs	3.5 μs	17 ns
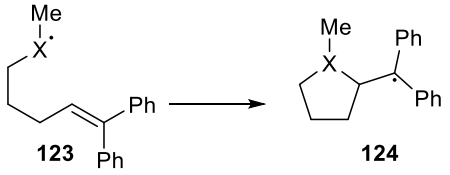 **123** **124**	2.2 μs	35 ns	68 ps

In subsequent work by Newcomb *et al*. (93), an absolute kinetic scale for amidyl radical reactions was established via LFP experiments. Arrhenius parameters were determined for 6-*exo* cyclization and for 1,5-HAT reactions for six distinct amidyl radicals. Radicals **125** and **130** react in 5-*exo* cyclization reactions and react at the kinetic limit of the conducted LFP measurements with their lifetimes surmounting to 3 ns. Radicals **126** and **131** are involved in 6-*exo* cyclization reactions and their lifetimes are 22 ns and 67 ns respectively. Radical **128** is involved in a 1,5-HAT reaction and its lifetime is 125 ns, this HAT is, however, not part of a propagation cycle, usually associated with the HLF reaction.

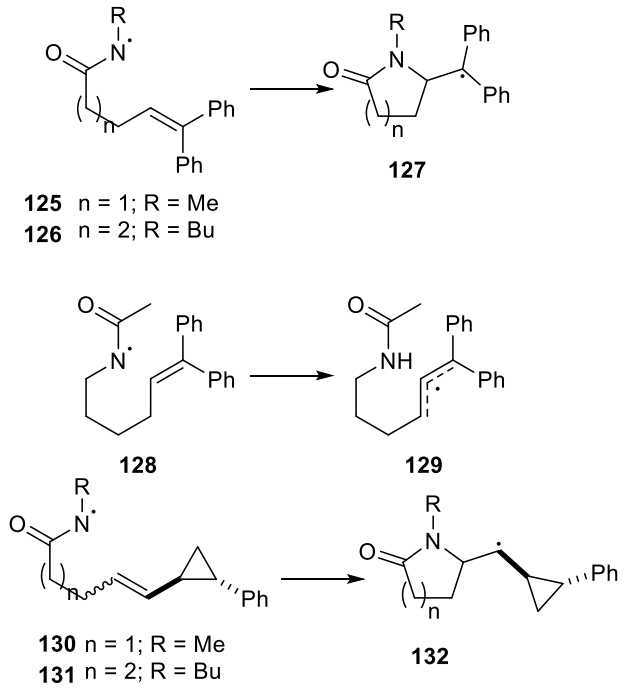

Scheme 28. 5-*exo* and 6-*exo* cyclization reactions of aminyl radicals(93).

The kinetics of cyclization of an iminyl radical were measured by LFP and a lifetime of 315 ns for the iminyl radical was obtained at 25 °C (94).The cyclization of this iminyl radical is slower than the corresponding reactions of alkyl radicals.

2. HYPOTHESES AND RESEARCH GOALS

Hypothesis

HLF reaction is a radical chain reaction and the regioselectivity of this reaction is either governed by thermodynamics, kinetics or both.

Research goals

Main objective of this work was to elucidate parameters governing regioselectivity of HLF reaction, and to determine how to predict the major products of this reaction.

Specific goals:

1. Compute *N*-centered radical stabilities and steric hinderances from multiple conformations and molecular dynamic simulations.
2. Compute thermodynamic and kinetic parameters for all the steps in the propagation cycle.
3. Experimentally detect intermediates and products in the HLF reaction using EPR, LFP, and NMR techniques.
4. Investigate HAT pathways in drug-like systems.

In order to test our hypothesis and achieve research goals set in thesis theme defense, we first picked two similar systems, namely *N*-hexyl-4-methylbenzenesulfonamide and *N*-(hept-2-yl)-4-methylbenzenesulfonamide as model systems to gauge the effect of steric hinderance on the reaction rate and product distribution. Different halogenation reactions and conditions for producing *N*-centered radicals were done. Regioselectivity of the HLF reaction was closely monitored using NMR and EPR techniques, while radical stability was computed. Next, 4-methyl-*N*-(5-phenylpentyl)benzenesulfonamide was reinvestigated. Using LFP, EPR and NMR techniques, elucidation of the role of each step in the propagation cycle was accomplished, as well as characterization of all intermediates and side products that were not sufficiently described in the literature. Finally, collected knowledge on the HLF reaction was used to predict products in the rearrangement reaction of laurolactam, a model macrocycle for the more stable bicyclic moieties with potential pharmaceutical application.

3. REGIOSELECTIVE REARRANGEMENT OF NITROGEN- AND CARBON-CENTERED RADICAL INTERMEDIATES IN HOFMANN–LÖFFLER–FREYTAG REACTION

THE JOURNAL OF PHYSICAL CHEMISTRY A
A JOURNAL OF THE AMERICAN CHEMICAL SOCIETY

pubs.acs.org/JPCA
Article

Regioselective Rearrangement of Nitrogen- and Carbon-Centered Radical Intermediates in the Hofmann−Löffler−Freytag Reaction

Gabrijel Zubčić, Jiangyang You, Fabian L. Zott, Salavat S. Ashirbaev, Maria Kolympadi Marković, Erim Bešić, Valerije Vrček, Hendrik Zipse, and Davor Šakić*

Cite This: J. Phys. Chem. A 2024, 128, 2574−2583
Read Online

ACCESS | Metrics & More | Article Recommendations | Supporting Information

ABSTRACT: The Hofmann−Löffler−Freytag (HLF) reaction serves as a late-stage functionalization technique for generating pyrrolidine heterocyclic ring systems. Contemporary HLF protocols utilize in situ halogenated sulfonamides as precursors in the radical-mediated rearrangement cycle. Despite its well-established reaction mechanism, experiments toward the detection of radical intermediates using EPR techniques have only recently been attempted. However, the obtained spectra lack the distinct features of the N-centered radicals expected for the employed reactants. This paper presents phenyl-butylnitrone spin-trapped C-centered and N-centered radicals, generated via light irradiation from N-halogen-tosyl-sulfonamide derivatives and detected using EPR spectroscopy. NMR spectroscopy and DFT calculations are used to explain the observed regioselectivity of the HLF reaction.

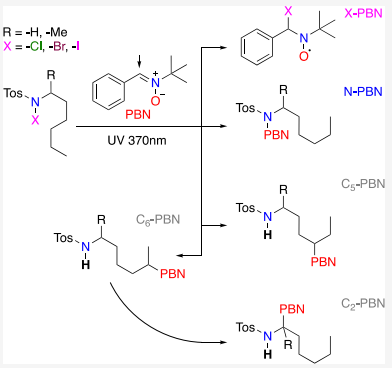

INTRODUCTION

Modern C−H functionalization chemistries have introduced late-stage functionalization (LSF) strategies in medicinal chemistry, targeting drug lead C−H bonds for creating new analogues. This toolbox includes photoredox-mediated and radical reactions and among them, amination reactions for the direct formation of C−N bonds.[1,2] Recently, the focus is shifting from metal to organocatalytic protocols, paving the way to sustainability and adhering to green chemistry principles to minimize waste and improve yield and atom economy.[3] This approach aligns with the EU's sustainable development policy.[4,5] Numerous research groups are exploring new C(sp^3)-H functionalization reactions with high chemo-, regio-, and stereoselectivity. The Hofmann−Löffler−Freytag (HLF) reaction, used for building pyrrolidine (and in some cases, also piperidine) ring systems, is among photo-activated amination reactions without metal catalysis.[6,7] The HLF reaction, first discovered in synthetic studies of N-haloamines,[8−11] is a multistep process involving nitrogen atom activation through halogenation, N-centered radical generation via irradiation, intramolecular hydrogen atom transfer (HAT), and radical termination with cyclization to form the final C−N bond (Scheme 1).

Contemporary adaptations of the HLF reaction employ toluenesulfonyl (tosyl, Tos)-activated amines (**1**), which undergo in situ iodination at the nitrogen atom (**2**) via an iodine source and a co-oxidant. The formation of an N-centered radical (**3**) was recently examined using EPR spectroscopy (Figure 1).[12]

However, the obtained spectra (**I**, in green), while presenting a triplet indicative of the nitrogen hyperfine splitting, raised questions due to issues such as broad line width, a high *g*-factor (2.0064) value for the proposed N-centered radical, and the absence of α-hydrogen splitting. Calculated EPR spectra for a model compound of **3** are shown in Figure 1 (**II**, orange line).[13] The spectra of the ditosylated aminoxyl radical (**III**, in blue) fit with the EPR parameters of **I**, thus suggesting this species to be the correct assignment of the EPR spectra **I**.[14] Neither C-centered radical (**4**) nor C_5-iodo functionalized (**5**) intermediates were observed in the EPR and NMR studies. The only confirmed product in this reaction was the pyrrolidine ring compound (**6**). Experimental attempts for in situ generation of N-centered radicals and detection via time-resolved EPR included *N*-isopropyl-4-methoxybenzene-sulfonamide as a radical precursor under electrochemical conditions.[15] It is, however, likely that the detected radical is not an amidyl radical but a nitroxide radical instead. A reaction of the observed radical with 5,5-dimethyl-1-pyrroline-*N*-oxide (DMPO) did not occur, which is consistent with stable nitroxide radicals. The experimentally observed hyperfine coupling constant (hfc) value for hydrogen at C_2 is

Received: December 1, 2023
Revised: March 6, 2024
Accepted: March 6, 2024
Published: March 22, 2024

https://doi.org/10.1021/acs.jpca.3c07892
J. Phys. Chem. A 2024, 128, 2574−2583

Scheme 1. Modern HLF Reaction Sequence Involving Tosyl-Sulfonamides and In Situ Iodination with Iodine and a Co-Oxidant [$PhI(OAc)_2$]

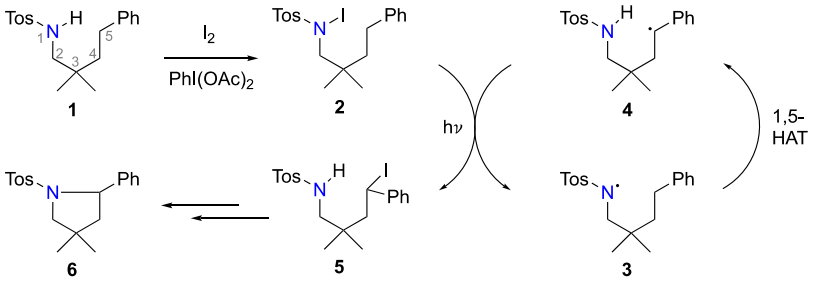

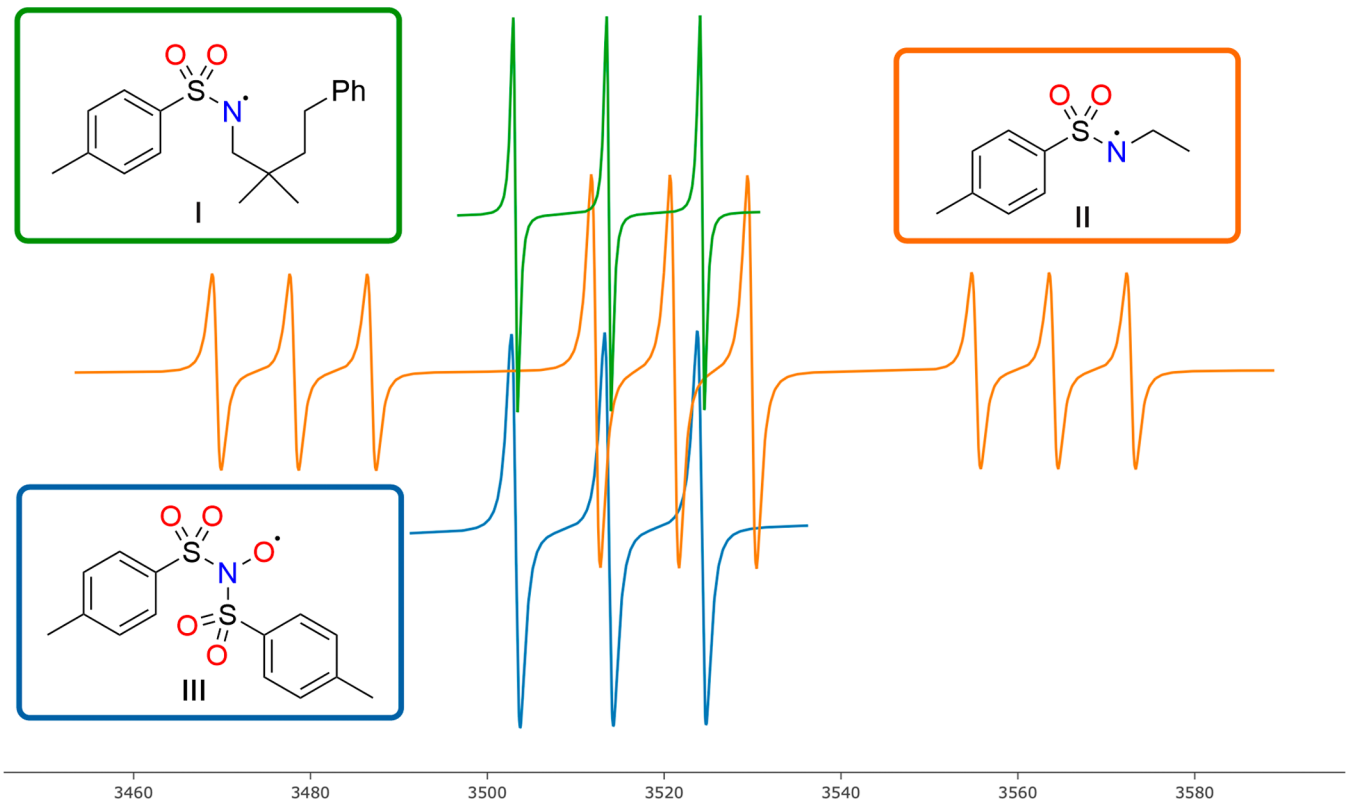

Figure 1. Simulated EPR spectra for tosyl-N-centered and ditosyl-N-centered radicals with the corresponding structures assigned by the authors. The green line is from EPR experiments,[12] the orange line represents calculated EPR parameters,[13] and the blue line is from EPR experiments.[14]

significantly smaller than those in typical amidyl radicals but is similar to the calculated values for the nitroxide radicals.

Numerous synthetic studies utilizing HFL chemistry[16−20] report the regioselective functionalization and subsequent formation of 5-membered pyrrolidine rings. In some especially rigid and/or previously functionalized systems, the formation of piperidines has been reported.[21−24] The observed regioselectivity in HLF reactions occurs during the HAT phase and can result from two different pathways. The intramolecular mechanism, governed by the kinetic preference of 1,5- over 1,6-HAT steps, represents one pathway. Alternatively, an intermolecular route directs the product distribution based on the thermodynamic stability of the resulting C-centered radicals. Muñiz suggested the latter mechanism in the context of selective piperidine formation,[24] where a phenyl-stabilized radical at the C_6 position is formed from an N-centered radical in a bimolecular reaction and a pyrrolidine product was not observed. Between the three distinct pathways, it is unclear which one is dominant for a given set of reaction conditions, and detailed investigations are thus warranted.

MATERIALS AND METHODS

The purchased compounds were sourced from Kefo [sulfuric acid (98%), methanol, petroleum ether, *p*-toluenesulfonyl chloride, silica gel, pyridine, silver acetate, ethyl acetate, cyclohexane, trifluoroacetic anhydride, toluene, and trichloroisocyanuric acid], Ru-Ve [hydrochloric acid (37%), acetone, silicon oil, petroleum ether, and cyclohexane], and Biovit [toluene (anhydrous), acetonitrile (anhydrous), 1,4-dioxane (anhydrous), tetrahydrofuran (anhydrous), *N*,*N*-dimethylformamide (anhydrous), *N*,*N*-dimethylacetamide, 1,2-dichloroethane (anhydrous), and dichloromethane (anhydrous)]. All reagents and chemicals were obtained commercially and used without further purification, unless otherwise noted.

Moisture-sensitive reactions were performed using flame-dried glassware under a nitrogen atmosphere (N_2). Air- and moisture-sensitive liquids and solutions were transferred with a

https://doi.org/10.1021/acs.jpca.3c07892
J. Phys. Chem. A 2024, 128, 2574−2583

Scheme 2. (a) Preparation of Precursors and Possible Intermediates in HLF Reactions of 7-H and 11-H, (b) Observed Products in the Reaction of 7-H with PIDA/I_2 under Dark and Irradiation Conditions, and (c) Investigated Reaction Sequences and Possible Products in Spin-Trapping Experiments

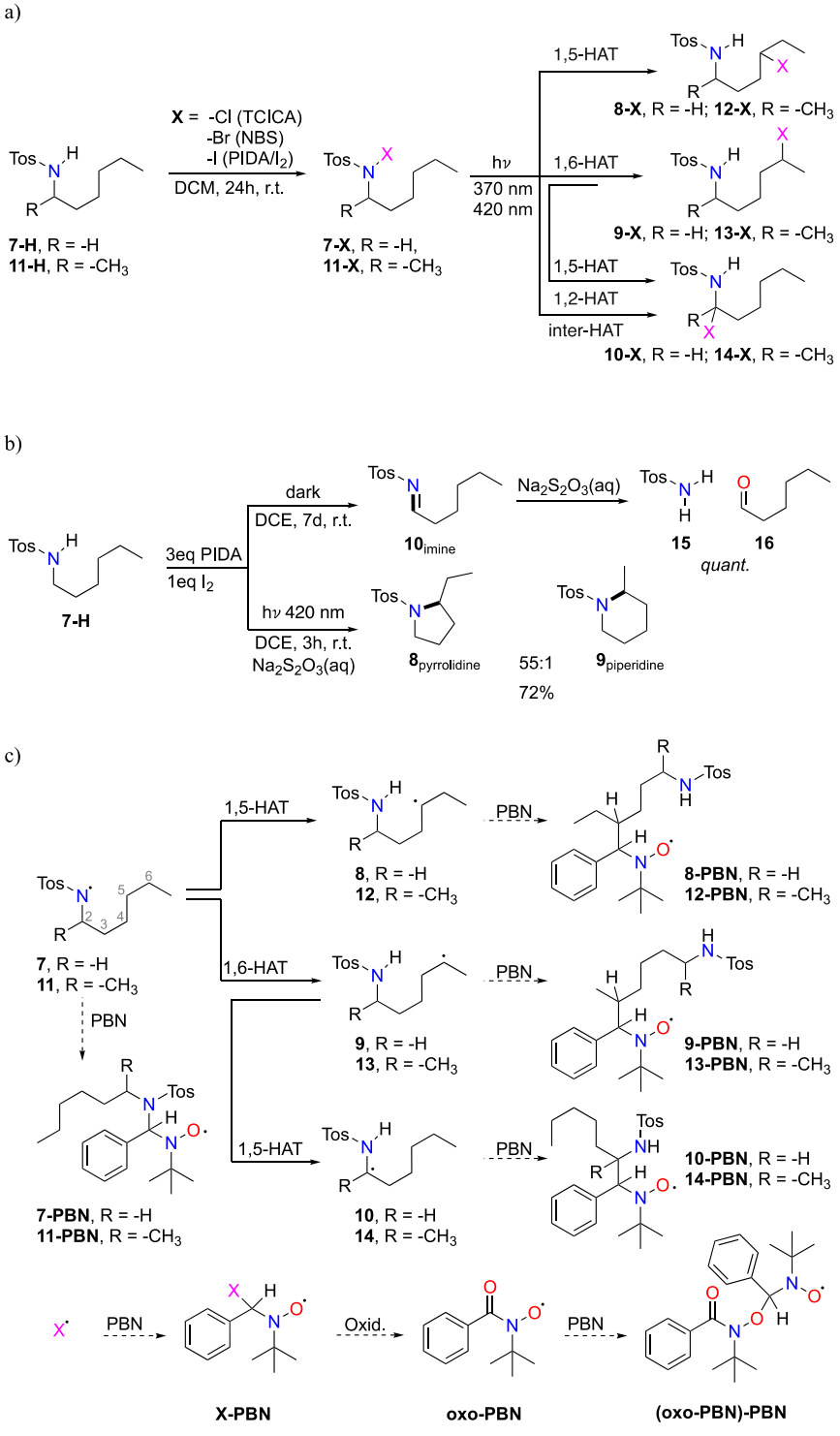

plastic or glass syringe. Chromatographic purification of the products was carried out using column chromatography filled with silica gel (Macherey-Nagel) 0.063−0.2 mm, and appropriate solvent mixtures were used as eluents: petroleum ether/ethyl acetate. Thin-layer chromatography (TLC) was performed on precoated TLC plates ALUGRAM SIL G/UV254, 0.20 mm silica gel 60 with a fluorescent indicator UV254 (Macherey-Nagel) in the appropriate solvent system. TLC spots were observed after illumination with UV light at a wavelength of 254 nm and after immersion in an aqueous solution of $KMnO_4$ (3 g $KMnO_4$, 20 g K_2CO_3, 5 mL aq. NaOH 5%, and 300 mL water) followed by heating. If TLC spots were not visible after illumination with UV light, they were detected utilizing an iodine chamber.

Synthetic photocatalyzed reactions were performed in a custom-built photoreactor with built-in temperature control as

https://doi.org/10.1021/acs.jpca.3c07892
J. Phys. Chem. A 2024, 128, 2574−2583

well as standardized luminous intensity for a certain set of high-power LED light sources. The InGaN-based H2A1-420 LED (420 ± 20 nm) used in this experimental setup was purchased from Roithner Lasertechnik GmbH and mounted on a standard hexagonal aluminum package. Irradiation was performed in situ (EPR) and off-site (NMR) with Kessil PR-160L 370 ± 10 nm gen-2 LED UV, with an average intensity of 137 mW/cm^2 when the sample is 6 cm from the lamp, according to the manufacturer.[25]

The reactant and products were identified using ^{1}H NMR spectra, which were recorded on Varian Inova 400 and 600 machines in $CDCl_3$ at 400 or 600 MHz at room temperature. All ^{13}C NMR spectra were recorded, respectively, at 101 and 151 MHz. The chemical shifts are reported in ppm (δ), relative to the resonance of $CDCl_3$ at δ = 7.27 ppm of ^{1}H and for ^{13}C, relative to the resonance of $CDCl_3$ at δ = 77.16 ppm. NMR spectra of the reaction mixture were obtained on a Varian Inova 400 NMR spectrometer operating at 399.90 MHz for ^{1}H NMR and 100.6 MHz for ^{13}C NMR and are reported as chemical shifts (δ) in ppm. The spectra were imported and processed in the MestreNova 11.0.4 program.[26]

GC measurements were obtained at a Shimadzu GC-2010 Plus gas chromatograph with an AOC-20i autosampler (with a temperature-controlled sample holder) and an Optima 1701−0.25 μm (25 m × 0.25 mm) column.

HR-MS spectra were obtained using a Thermo Finnigan LTQ FT machine of the MAT 95 type with a direct exposure probe and electron impact ionization (70 eV).

EPR spectroscopy was done by using a Bruker E500 ELEXSYS EPR spectrometer with an ER4122SHQE cavity resonator. As this cavity resonator does not have an optical window for illumination, the light source was mounted underneath the cavity, with light coming through the bottom of the EPR 4 mm-inner-diameter tube. EPR deconvolution and simulation was done using an EasySpin module with the MATLAB program package.[27] EPR visualization and spectroscopy were done using the VisualEPR Web page.[28]

The conformational space was sampled and investigated using the Conformer−Rotamer Ensemble Sampling Tool—CREST[29] coupled with the xtb-GFN2 program package and MD simulation using xtb-GFN1[30] and xtb-GFN2.[31] The obtained structures were reoptimized using the B3LYP/6-31G(d) level of theory.[32−34] For each structure with a stable wave function, frequency calculation was performed to identify the minima and transition-state structures. From the transition-state structure, an intrinsic reaction coordinate search was performed to characterize the corresponding reaction and product complexes/reactive conformers. Improved thermodynamics were obtained using RO-B2PLYP[35,36] with a G3MP2 large basis set[37] on geometries obtained at the B3LYP/6-31G(d) level of theory, with additional D3 dispersion correction.[38] Additionally, for smaller and model systems, the G3B3[37] composite method was used, with results matching the RO-B2PLYP-D3/G3MP2 large results.

Calculations of EPR parameters were done using the B3LYP functional and the mixed basis set: EPR-III for C, H, and O atoms, def2-QZVP for the S atom, and 6-31G(d) for the N atom. A small basis set on the N atom is necessary for the correct calculations of the g-factor and hfcs.[39,40] When using a larger basis set for the N atom, e.g., EPR-III or def2-QZVP, the obtained results systematically underestimate the hfc. Calculations were performed on the Gaussian version 16.C01[41] using the advanced computing service (clusters Isabella and Supek) provided by the University of Zagreb University Computing Centre—SRCE[42] and the computational resources of the PharmInova project (sw.pharma.hr) at the University of Zagreb Faculty of Pharmacy and Biochemistry.[43]

RESULTS AND DISCUSSION

Insights into the HAT steps of the HLF reactions can be gained through the simulation of thermodynamic and kinetic parameters. The thermodynamics (driving force) of the reaction can be evaluated by comparing bond dissociation energies (BDEs) or by utilizing the radical stabilization energies (RSEs) of molecular fragments containing radical precursors and products (see below).[44−46] Reaction kinetics are linked to thermodynamics via the Bell−Evans−Polanyi principle, a relationship that has been demonstrated for various HAT reactions for both inter- and intramolecular pathways.[47] When the C_5 and C_6 positions are both unsubstituted as in substrate **7-H**, the regioselectivity toward the C_5 product is experimentally evident even when the kinetic and thermodynamic parameters for 1,5- and 1,6-HAT align closely.[48] There are no notable differences in energies vs the geometrical parameter (N−H−C angle) between 1,5- and 1,6-HAT energy profiles. Both of them resemble those of the intermolecular HAT (see Chart S1 in Supporting Information). There is room for unknown factors governing the regioselectivity of HLF reactions. To determine whether the transient N- and C-centered radicals influence the observed regioselectivity, we attempted in situ generation and trapping of these radical intermediates using the phenylbutylnitrone (PBN) spin trap and investigation of the resulting adducts with EPR. Additionally, the reaction progress was monitored using NMR techniques, with off-site light irradiation.

The same starting conditions reported earlier[12,16] were employed for *N*-hexyl-4-methylbenzenesulfonamide (**7-H**) as the substrate. This reactant was chosen as the simplest model for unsubstituted C_5 and C_6 positions. The corresponding *N*-iodo (**7-I**) derivative was prepared in situ from **7-H** using hypervalent phenyliodine (III) diacetate (PIDA) as an oxidant with elemental I_2 as the iodine source.[12,16] After 3 h of irradiation of a reaction mixture containing 3 equiv of PIDA, 1 equiv of I_2, and 1 equiv of **7-H** with a 420 nm light source, two distinct products could be observed (Scheme 2b). These products were identified through GC−MS and NMR techniques as a 55:1 mixture of the five-membered ring compound $\mathbf{8}_{\text{pyrrolidine}}$ and six-membered ring analogue $\mathbf{9}_{\text{piperidine}}$ in a combined yield of 72% (see Supporting Information). When the same reactant mixture was stored in darkness for 7 days, the crude ^{1}H NMR spectrum revealed the unexpected presence of imine $\mathbf{10}_{\text{imine}}$ together with 4-methylbenzenesulfonamide (**15**) and hexanal (**16**). Subsequent processing with aqueous sodium thiosulfate resulted in near-quantitative recovery of compound **15**.

With these results in hand, an attempt was made to identify transient intermediates by monitoring reaction progress with NMR techniques. The mixture of **7-H**/PIDA/I_2 was therefore irradiated off-site for 5 min (370 nm), followed by ^{1}H NMR measurements during a full reaction sequence (see Supporting Information). In addition to signals of the starting material, two sets of new signals appeared, which is consistent with the formation of two products. These two cannot be clearly assigned, but the observed signal motifs and chemical shift values support the formation of two halogenated structures, one of them being the expected C_5-halogenated product **8-I**.

https://doi.org/10.1021/acs.jpca.3c07892
J. Phys. Chem. A 2024, 128, 2574−2583

Figure 2. EPR spectra of spin-trapped radical intermediates generated with 370 nm irradiation of **7-Br**. The experimental spectrum is in purple, while blue, orange, green, and red correspond to simulated spectra for **10-PBN**, **8/9-PBN**, **7-PBN**, and total simulated spectra, respectively. Residuals from subtracted simulation from experimental spectra are at the bottom. More information on deconvolution and simulation is deposited in Supporting Information.

The assignment of the other product was not possible without ambiguity but clearly did not correspond to the C_6-halogenated product **9-I**, or $\mathbf{10}_{\mathbf{imine}}$, observed previously. To our knowledge, this is the first reaction monitoring HLF with NMR spectroscopy, with a large signal from excess PIDA covering the aromatic region of the spectra.

After NMR experiments, we monitored the complete reaction sequence with EPR spectrometry. Using continuous irradiation with the same UV lamp from the bottom of the cavity resonator, compound **7-I** was EPR-silent. This is in stark contrast to the published results,[12] but as mentioned before, radicals observed in that experiment might stem from different oxidation pathways and rearrangement reactions that are not part of the HLF sequence.

Next, we tried to capture nascent radicals from the reaction with PBN, but oxidizing and halogenating species present in the mixture reacted with PBN and produced an **oxo-PBN** (acylaminoxyl) radical, with $\alpha_{N,exp}$ = 8.0 G, as well as additional (**oxo-PBN**)-**PBN** adducts (see Figure 2).[49] To summarize, we have not been able to detect short-lived radical intermediates of the HLF reaction using this procedure.

As in situ halogenation inhibits PBN's ability to spin-trap radicals, the preparation of **7-Cl** and **7-Br** was performed in a separate step. While **7-Cl** was easily isolated and proved stable for a couple of days,[50] **7-Br** had to be synthesized, cleaned, isolated, and measured without any delay. Another major point is the sensitivity of the reaction to air. Line widths measured with EPR and reaction yields were greatly influenced by the effectiveness of air removal using freeze−pump−thaw cycles with backfill of argon or nitrogen gas. Experimental line widths of less than 0.4 G were deemed satisfactory for optimal resolution of radical adducts. Under these conditions with illumination with 370 nm light, we were able to observe a **Cl-PBN** adduct, proving homolytic cleavage of N−Cl bonds generating a chlorine radical that quickly combines with PBN (see Figure S20 in Supporting Information). From both **7-Cl** and **7-Br**, a PBN adduct **7-PBN** (g_{exp} = 2.0064, $\alpha_{N,exp}$ = 14.14 G, $\alpha_{N',exp}$ = 1.58 G, and $\alpha_{H,exp}$ = 3.95 G) formed from an N-centered radical **7** was detected for the first time using EPR spectroscopy, proving that this is the correct method for investigating the HLF reaction and corresponding intermediates (see Figure 2). Calculated EPR parameters for **7-PBN** ($g_{\mathbf{7\text{-}PBN},calc}$ = 2.00616, $\alpha_{\mathbf{7\text{-}PBN},N,calc}$ = 13.81 G, $\alpha_{\mathbf{7\text{-}PBN},N',calc}$ = 1.52 G, and $\alpha_{\mathbf{7\text{-}PBN},H,calc}$ = 2.89 G) are in satisfactory agreement with experimental values.

In the EPR spectrum (see Figure 2), one signal corresponding to the two PBN adducts of C-centered radicals was expected, namely, C_5 radical (**8**) and C_6 radical (**9**). PBN adducts of those radicals, **8-PBN** and **9-PBN**, have similar calculated hfcs and *g*-factors ($g_{\mathbf{8\text{-}PBN},calc}$ = 2.00595, $\alpha_{\mathbf{8\text{-}PBN},N,calc}$ = 15.09 G, and $\alpha_{\mathbf{8\text{-}PBN},H,calc}$ = 2.36 G and $g_{\mathbf{9\text{-}PBN},calc}$ = 2.00597, $\alpha_{\mathbf{9\text{-}PBN},N,calc}$ = 14.80 G, and $\alpha_{\mathbf{9\text{-}PBN},H,calc}$ = 2.27 G), and it is thus difficult to distinguish between them, due to both being secondary alkyl C-centered radicals with similar environments around the radical center. A signal with g_{exp} = 2.0061, α_N = 13.84 G, and α_H = 2.47 G was observed that can be assigned to both **8-PBN** and **9-PBN**. The unexpected result was the formation and detection of PBN adduct **10-PBN**. It is characterized with g_{exp} = 2.0064, α_N = 13.80 G, and α_H = 7.34 G, which is different from the previously described radicals (more information about deconvolution can be found in the Supporting Information). The **10-PBN** radical adduct can be tentatively assigned as a C_2 radical (**10**) due to having an hfc from N and H atoms in PBN and to different

https://doi.org/10.1021/acs.jpca.3c07892
J. Phys. Chem. A 2024, 128, 2574−2583

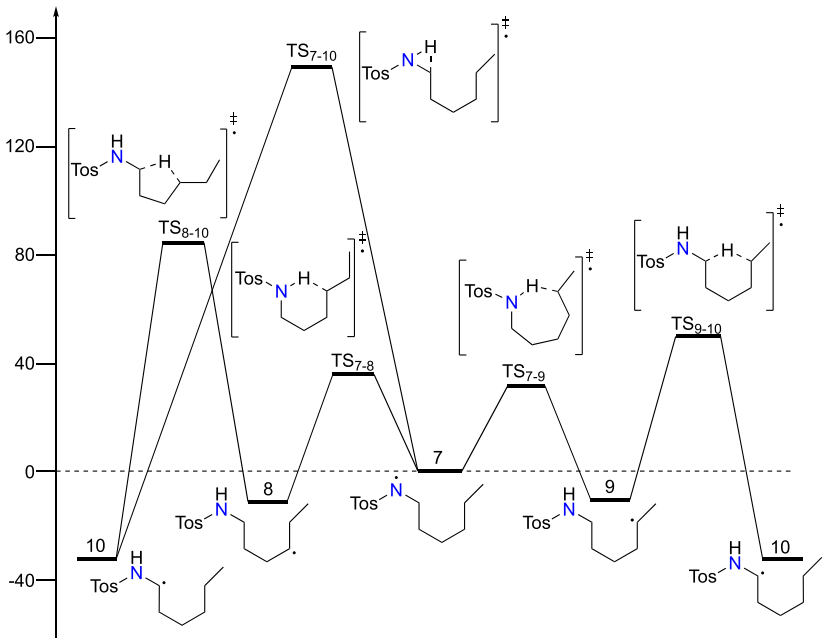

Figure 3. Energy diagram of intramolecular radical rearrangements from **7** calculated at RO-B2PLYP/G3MP2Large//B3LYP/6-31G(d).

connectivities closer to the radical center, although it has an unusually high hfc value for a C-centered radical. To confirm this assignment, extensive computational analyses were performed. The calculated Boltzmann averaged values for **10-PBN** ($g_{\mathbf{10\text{-}PBN},calc}$ = 2.00610, $\alpha_{\mathbf{10\text{-}PBN},N,calc}$ = 14.08 G, and $\alpha_{\mathbf{10\text{-}PBN},H,calc}$ = 5.46 G) demonstrated a trend similar to the experimental parameters, with significantly larger hfc values than computed for radicals **8**/**9-PBN**. A detailed analysis of the structural factors contributing to these values revealed interactions between the Tos-N(alkyl)-H and the O−N−PBN radical center, significantly impacting the α_H value in the lowest lying minima. Conformers of **10-PBN**, where this interaction is not present, are higher in energy by more than 10 kJ/mol from the global minima and have calculated $\alpha_{\mathbf{10\text{-}PBN},H,calc}$ 2.40 G, which is almost the same as that for radicals **8**/**9-PBN**. For more details on deconvolution and structure analysis, please consult Supporting Information.

From theoretical predictions calculated at the RO-B2PLYP-D3/G3MP2-large//B3LYP/6-31G(d) level of theory,[47,51] the N-centered radical **7** rearranges in HAT steps with $\Delta H_{298}^{\ddagger}$ = +35.4 and +31.2 kJ/mol for 1,5-HAT and 1,6-HAT steps to C_5-centered radical **8** and C_6-centered radical **9** with reaction enthalpies $\Delta H_{rx,298}$ of −11.4 and −10.8 kJ/mol, respectively (see Supporting Information). Radical **10** can be produced through different HAT reactions: (a) intermolecular HAT from any N-centered or C-centered radical, (b) intramolecular from an N-centered radical (**7** → **10**) via 1,2-HAT_{NC}, (c) intramolecular from C_5 radical (**8** → **10**) via 1,4-HAT_{CC}, and (d) intramolecular from C_6 radical (**9** → **10**) via 1,5-HAT_{CC}. Intermolecular HAT (**7-H** + **7** → **10** + **7-H**), involving neutral molecule (**7-H**) and N-centered radical (**7**), proceeds with a thermodynamic driving force of $\Delta H_{rx,298}$ = −50.6 kJ/mol and a predicted barrier of $\Delta H_{298}^{\ddagger}$ = 22.1 kJ/mol ($\Delta G_{298}^{\ddagger}$ = 37.2 kJ/mol from reaction complex). Intramolecular 1,2-HAT, a direct transformation from N-centered radical to C_2 radical (**7** → **10**), has a predicted barrier of $\Delta H_{298}^{\ddagger}$ = 148.8 kJ/mol with a strong thermodynamic driving force of $\Delta H_{rx,298}$ = −32.3 kJ/mol, making it a kinetically prohibitive process.

Rearrangement to a C_2 radical can occur from less stable distant C-centered radicals (**8** → **10** and **9** → **10**). Both inter- and intramolecular reactions are feasible with the latter (**7-H** + **8** → **10** + **7-H** and **7-H** + **9** → **10** + **7-H**) being characterized with $\Delta H_{298}^{\ddagger}$ = 33.5 kJ/mol and a thermodynamic driving force of $\Delta H_{rx,298}$ = −23.4 kJ/mol. This was calculated with the propane/propyl radical reference system as a reasonable model for the distant C-centered radicals in the hydrocarbon chain, due to negligible differences in reactivity and stability between the C_5 radical, C_6 radical, and propyl radical (RSEs and TS) toward the C_2 radical. As seen in Figure 3, the barrier for intramolecular 1,4-HAT_{CC} rearrangement of the C_5 radical to the C_2 radical (**8** → **10**) is prohibitively high ($\Delta H_{298}^{\ddagger}$ = 84.1 kJ/mol), while 1,5-HAT_{CC} from the C_6 radical to the C_2 radical (**9** → **10**) proceeds through a 6-membered transition state with $\Delta H_{298}^{\ddagger}$ = 56.1 kJ/mol and a reaction enthalpy of $\Delta H_{rx,298}$ = −21.5 kJ/mol. These results indicate that this second intramolecular rearrangement, with the lowest energy of activation, is the probable origin of the experimentally observed regioselectivity in HLF reactions. It significantly decreases the lifetime of the C_6 radical required for halogen atom abstraction and thus the yield of C_6-functionalized products.

As mentioned before, different radical fragments present in systems **7**−**14** can be used to gauge the thermodynamic driving force for rearrangement reactions (see Figure 4).[44−47,51] In our system, going from a tosylated methylamine radical (**7**) to a secondary C-centered radical (**8** and **9**) corresponds to an exothermic reaction ($\Delta H_{predict,298}$ = −19.8 kJ/mol, see Supporting Information). Additionally, rearrangement from a secondary C-centered radical to a tosylamide-substituted C-centered radical fragment such as **10** is also predicted to be exothermic (see Supporting Information), which is in line with our experimental observation.

The same rationale can be used to explain the regioselectivity reported in a recent study[52] with different sulfonamide derivatives. While radical generation was achieved using visible light photoredox catalysis with $Ru(bpy)_3Cl_2$ in

https://doi.org/10.1021/acs.jpca.3c07892
J. Phys. Chem. A 2024, 128, 2574−2583

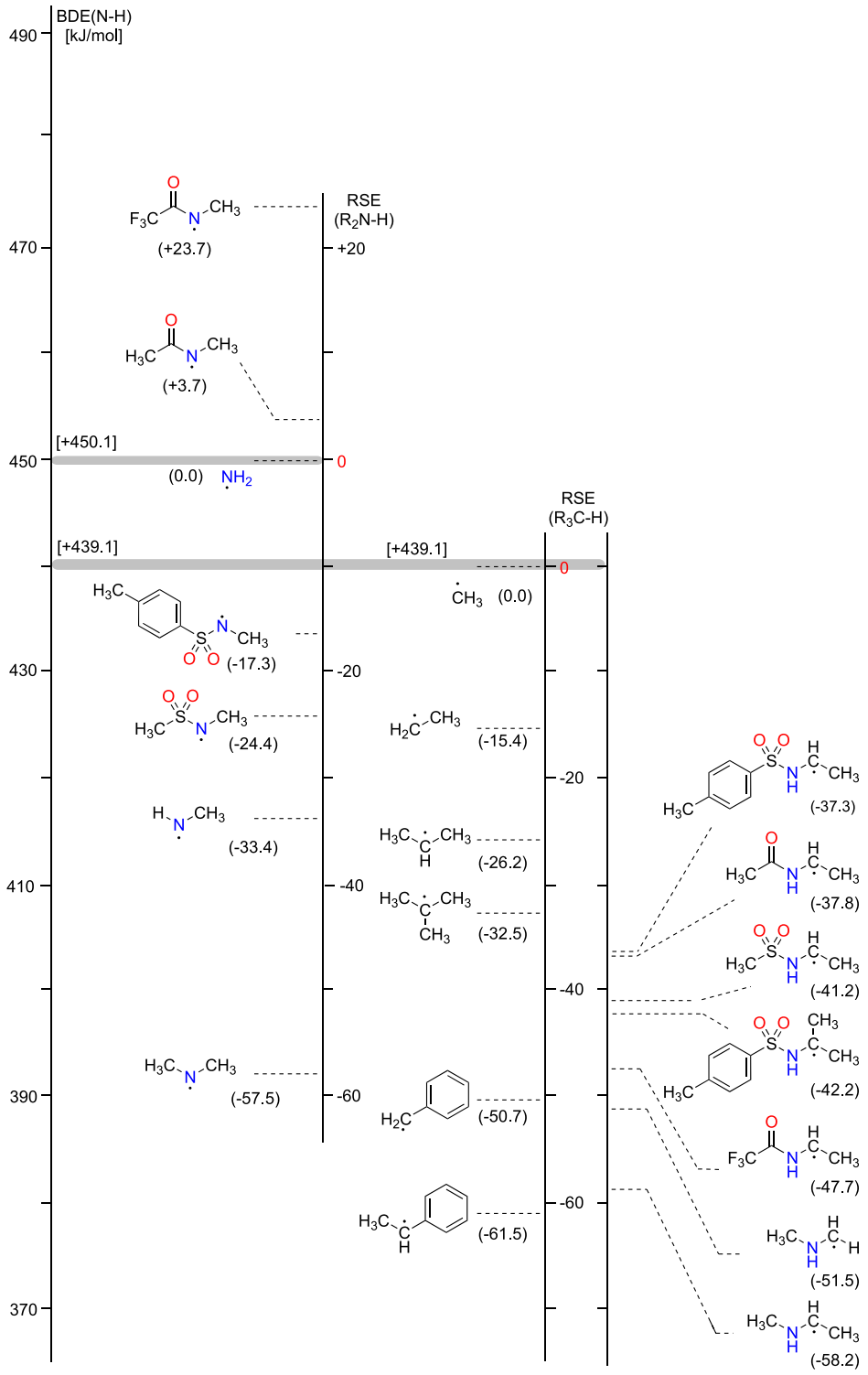

Figure 4. RSEs for selected N- and C-centered radicals present in systems **7**−**14**. The gray bands denote the anchor points for N-centered and C-centered radical RSE scales to a global BDE scale.

conjunction with blue LEDs, high yields and regioselectivity toward 1,5-HAT$_{NC}$ rearrangement were observed when C_5 and C_6 positions were secondary and primary radicals. This stems from a notable difference in the radical stability ($\Delta RSE_{prim/sec}$ = 10.8 kJ/mol). When additional substituents at the C_6 position are introduced to generate a (stabilized) tertiary C_6 radical, a mixture of a 56% C_5 product and a 40% C_6 product is obtained ($\Delta RSE_{sec/tert}$ = 6.3 kJ/mol), making both 1,5-HAT$_{NC}$ and 1,6-HAT$_{NC}$ equivalent reactions. Proof of the existence of a C_2 radical in HLF-type reactions is available in the literature. It was observed indirectly as an imine side product in electrochemically driven N-centered radical generation.[53] The proposed generation of imine was either via elimination of HBr from an N-brominated precursor or via 1,2-HAT from a transient N-centered radical. The possible sequence of 1,6-HAT$_{NC}$ followed by 1,5-HAT$_{CC}$ was not explored.

https://doi.org/10.1021/acs.jpca.3c07892
J. Phys. Chem. A 2024, 128, 2574−2583

In the ^{1}H NMR spectra of the reaction mixture obtained after off-site irradiation of the **7-Cl** precursor, only two (main) products were observed and measured in the same proportion. The two pairs of triplets in the upfield and downfield regions are consistent with product structures **10-Cl** and **12-Cl** (see Supporting Information), which supports the formation of C_5- and C_6-radical intermediates, the latter undergoing a 1,5-H shift to the respective C_2-centered radical. The same NMR results were obtained after irradiation of precursor **7-Br**.

To further investigate the second rearrangement process, we opted for a methyl-substituted derivative, *N*-(hept-2-yl)-4-methylbenzenesulfonamide (**11-H**, Scheme 2), which is a precursor for a more stable C_2-centered radical [RSE(propyl/propane) = −26.2 kJ/mol vs RSE(*tert*-butyl/*tert*-butane) = −32.5 kJ/mol]. After chlorination to **11-Cl**, and sequential off-site irradiation, two products were observed in the NMR spectra. One product corresponds to the C_5-chlorinated product **12-Cl**,[54] without formation of a pyrrolidine ring (see Supporting Information).[55] The C_6-chlorinated product, **13-Cl**, was not observed, although the calculated barriers and driving forces are again similar ($\Delta H_{298}^{\ddagger}$ = +31.5 kJ/mol and +36.1 kJ/mol; $\Delta H_{rx,298}$ = −13.0 kJ/mol and −9.4 kJ/mol, for 1,5-HAT and 1,6-HAT, respectively). The second product is the C_2-chlorinated product, **14-Cl**, with a characteristic triplet at 0.81 ppm (see Supporting Information). The lack of formation of **13-Cl** (or a piperidine ring product)[56] indicates that **13** is a reactive intermediate, that quickly rearranges to **14**, which is converted to **14-Cl**. This is supported by calculations with the expected barrier for the second step 1,5-HAT rearrangement between C_6 and C_2 carbon centers of $\Delta H_{298}^{\ddagger}$ = 57.6 kJ/mol and $\Delta H_{rx,298}$ = −18.1 kJ/mol.

In the EPR spectra, when **11-Cl** was illuminated, a chlorine PBN adduct was formed (**Cl-PBN**), alongside N-centered radical adduct **11-PBN**. Both **7-PBN** and **11-PBN** have similar hfcs, namely, $g_{\mathbf{11\text{-}PBN},exp}$ = 2.0062, $\alpha_{\mathbf{11\text{-}PBN},N,exp}$ = 14.1 G, $\alpha_{\mathbf{11\text{-}PBN},N',exp}$ = 1.3 G, and $\alpha_{\mathbf{11\text{-}PBN},H,exp}$ = 4.21 G. Those results fit nicely with the calculated results (see Supporting Information). As expected, the C-centered radical signal corresponds well to the C_5- and C_6-radical adducts **12/13-PBN**, with the same hfc values as observed for **8/9-PBN** ($g_{\mathbf{12/13\text{-}PBN},exp}$ = 2.0061, $\alpha_{\mathbf{12/13\text{-}PBN},N,exp}$ = 13.6 G, and $\alpha_{\mathbf{12/13\text{-}PBN},H,exp}$ = 2.6 G). The tentatively proposed C_2-radical **14**, similar to radical **10**, made an adduct with PBN, **14-PBN** with a characteristic signal at $g_{\mathbf{14\text{-}PBN},exp}$ = 2.0061, with hfc $\alpha_{14\text{-}PBN,N,exp}$ = 13.7 G and $\alpha_{\mathbf{14\text{-}PBN},H,exp}$ = 6.4 G, confirming our hypothesis that this species stems from rapid rearrangement from **13**. Again, a rather high hfc value for $\alpha_{\mathbf{14\text{-}PBN},H}$ can be attributed to the interaction between the sulfonamide hydrogen moiety and the oxygen-centered radical of the PBN in the thermodynamically stable conformers. Extensive calculations on radical adducts confirm the assignments (see Supporting Information). Similar results were obtained with **11-Br**, although the most pronounced peaks were **12/13-PBN. 11-PBN** was weak and **14-PBN** is not directly visible, possibly overshadowed by **11-PBN**. The lack of full correspondence between **11-Cl** and **11-Br** is most likely due to the instability of **11-Br**, which was already decomposing in the dark (see Supporting Information). We plan to continue the investigation on the weak components of the EPR spectrum deconvolution, currently assigned as **10/14-PBN**. Additional compounds with different substitution patterns on the C_5 and C_6 positions, with added modifications on C_2 (blocking the route) and C_3 positions (steric hindrance), will further test the origin of regioselectivity in HLF reactions.

CONCLUSIONS

Using NMR and EPR spectroscopy in combination with DFT calculations, we successfully monitored the reaction profile and identified all significant intermediate radicals and products in the HLF reaction. The initial rearrangement step allows the N-centered radical to transform into both C_5 and C_6 radicals. The observed regioselectivity favoring 1,5-HAT products can be attributed to an additional rearrangement reaction exclusive to the C_6 radical. Through another 1,5-HAT step, the C_6 radical is transformed into the most stable C_2 radical. The existence of C_2 radical is experimentally proved not only through EPR spectroscopy but also via synthetic reactions and side products, notably imine and aldehyde. Future research should extend to more complex systems with additional substituents on the radical chain and varying functional groups, applying the methodology outlined in this study.

ASSOCIATED CONTENT

Supporting Information

The Supporting Information is available free of charge at https://pubs.acs.org/doi/10.1021/acs.jpca.3c07892.

Experimental details, synthesis procedure, reactant and product characterization, EPR simulation parameters, calculation procedures, geometries and energies of optimized structures, and recorded NMR and EPR spectra (PDF)

AUTHOR INFORMATION

Corresponding Author

Davor Šakić − *Faculty of Pharmacy and Biochemistry, University of Zagreb, 10000 Zagreb, Croatia;* orcid.org/0000-0002-8871-6622; Email: davor.sakic@pharma.unizg.hr

Authors

Gabrijel Zubčić − *Faculty of Pharmacy and Biochemistry, University of Zagreb, 10000 Zagreb, Croatia*

Jiangyang You − *Division of Physical Chemistry, Ruđer Bošković Institute, 10000 Zagreb, Croatia;* orcid.org/0000-0001-8881-9448

Fabian L. Zott − *Department of Chemistry, Ludwig-Maximilians-Universität München, D-81377 München, Germany;* orcid.org/0000-0002-4813-947X

Salavat S. Ashirbaev − *Department of Chemistry, Ludwig-Maximilians-Universität München, D-81377 München, Germany;* orcid.org/0000-0001-7744-4556

Maria Kolympadi Marković − *Faculty of Physics, and Centre for Micro- and Nanosciences and Technologies, University of Rijeka, 51000 Rijeka, Croatia*

Erim Bešić − *Faculty of Pharmacy and Biochemistry, University of Zagreb, 10000 Zagreb, Croatia*

Valerije Vrček − *Faculty of Pharmacy and Biochemistry, University of Zagreb, 10000 Zagreb, Croatia;* orcid.org/0000-0003-1624-8126

Hendrik Zipse − *Department of Chemistry, Ludwig-Maximilians-Universität München, D-81377 München, Germany;* orcid.org/0000-0002-0534-3585

Complete contact information is available at: https://pubs.acs.org/10.1021/acs.jpca.3c07892

Notes

The authors declare no competing financial interest.

■ ACKNOWLEDGMENTS

The authors would like to acknowledge financial support from the Croatian Science Foundation Installation grant UIP-2020-02-4857 LIGHT-N-RING, grant IP-2022-10-2634 PharmaEco, and computational resources provided by Advanced Computing Service on Cluster Supek, EU funded through KK.01.1.1.08.0001, at the University of Zagreb University Computing Centre—SRCE. This work was also supported by the project FarmInova at the Faculty of Pharmacy and Biochemistry University of Zagreb, (KK.01.1.1.02.0021) funded by the European Regional Development Fund, and Croatian Science Foundation Research grant IP-2019-04-8846.

■ REFERENCES

(1) Sinha, S. K.; Guin, S.; Maiti, S.; Biswas, J. P.; Porey, S.; Maiti, D. Toolbox for Distal C-H Bond Functionalizations in Organic Molecules. *Chem. Rev.* **2021**, *122* (6), 5682−5841.
(2) Roy, S.; Panja, S.; Sahoo, S. R.; Chatterjee, S.; Maiti, D. Enroute Sustainability: Metal Free C-H Bond Functionalisation. *Chem. Soc. Rev.* **2023**, *52* (7), 2391−2479.
(3) Flerlage, H.; Slootweg, J. C. Modern Chemistry Is Rubbish. *Nat. Rev. Chem* **2023**, *7* (9), 593−594.
(4) EUR-Lex—52019DC0640—EN—EUR-Lex; European Commission: Brussels, 2019; pp 1−24. https://eur-lex.europa.eu/legal-content/EN/TXT/?uri=COM%3A2019%3A640%3AFIN (accessed 2023-11-21).
(5) EUR-Lex—52020DC0667—EN—EUR-Lex; European Commission: Brussels, 2020; pp 1−24. https://eur-lex.europa.eu/legal-content/EN/TXT/?uri=COM%3A2020%3A667%3AFIN (accessed 2023-11-21).
(6) Pratley, C.; Fenner, S.; Murphy, J. A. Nitrogen-Centered Radicals in Functionalization of Sp2 Systems: Generation, Reactivity, and Applications in Synthesis. *Chem. Rev.* **2022**, *122* (9), 8181−8260.
(7) Kwon, K.; Simons, R. T.; Nandakumar, M.; Roizen, J. L. Strategies to Generate Nitrogen-Centered Radicals That May Rely on Photoredox Catalysis: Development in Reaction Methodology and Applications in Organic Synthesis. *Chem. Rev.* **2022**, *122* (2), 2353−2428.
(8) Hofmann, A. W. Ueber Die Einwirkung Des Broms in Alkalischer Lösung Auf Die Amine. *Ber. Dtsch. Chem. Ges.* **1883**, *16* (1), 558−560.
(9) Hofmann, A. W. Ueber Die Einwirkung Des Broms in Alkalischer Lösung Auf Amide. *Ber. Dtsch. Chem. Ges.* **1881**, *14* (2), 2725−2736.
(10) Hofmann, A. W. Zur Kenntniss Der Coniin-Gruppe. *Ber. Dtsch. Chem. Ges.* **1885**, *18* (1), 109−131.
(11) Löffler, K.; Freytag, C. Über Eine Neue Bildungsweise von N-alkylierten Pyrrolidinen. *Ber. Dtsch. Chem. Ges.* **1909**, *42* (3), 3427−3431.
(12) Bosnidou, A. E.; Duhamel, T.; Muñiz, K. Detection of the Elusive Nitrogen-Centered Radicals from Catalytic Hofmann-Löffler Reactions. *Eur. J. Org Chem.* **2020**, *2020* (40), 6361−6365.
(13) Korth, H. Comment on "Detection of the Elusive Nitrogen-Centered Radicals from Catalytic Hofmann-Löffler Reactions. *Eur. J. Org Chem.* **2020**, *2020* (40), 6366−6367.
(14) Balakirev, M. Yu.; Khramtsov, V. V. ESR Study of Free Radical Decomposition of N,N-Bis(Arylsulfonyl)Hydroxylamines in Organic Solution. *J. Org. Chem.* **1996**, *61* (21), 7263−7269.
(15) Liu, Y.; Shi, B.; Liu, Z.; Gao, R.; Huang, C.; Alhumade, H.; Wang, S.; Qi, X.; Lei, A. Time-Resolved EPR Revealed the Formation, Structure, and Reactivity of N-Centered Radicals in an Electrochemical C(Sp3)-H Arylation Reaction. *J. Am. Chem. Soc.* **2021**, *143* (49), 20863−20872.
(16) Fan, R.; Pu, D.; Wen, F.; Wu, J. δ and α SP3 C-H Bond Oxidation of Sulfonamides with PhI(OAc)2/I2 under Metal-Free Conditions. *J. Org. Chem.* **2007**, *72* (23), 8994−8997.
(17) Becker, P.; Duhamel, T.; Stein, C. J.; Reiher, M.; Muñiz, K. Cooperative Light-Activated Iodine and Photoredox Catalysis for the Amination of C-H Bonds. *Angew. Chem., Int. Ed.* **2017**, *56* (27), 8004−8008.
(18) Teng, X.; Yu, T.; Shi, J.; Huang, H.; Wang, R.; Peng, W.; Sun, K.; Yang, S.; Wang, X. Recent Advances in the Functionalization of Remote C-H Bonds by Hofmann-Löffler-Freytag-type Reactions. *Adv. Synth. Catal.* **2023**, *365* (19), 3211−3226.
(19) Guo, W.; Wang, Q.; Zhu, J. Visible Light Photoredox-Catalysed Remote C-H Functionalisation Enabled by 1,5-Hydrogen Atom Transfer (1,5-HAT). *Chem. Soc. Rev.* **2021**, *50* (13), 7359−7377.
(20) Zubčić, G.; Shkunnikova, S.; Šakić, D.; Marijan, M. Renesansa Hofmann-Löffler-Freytag Reakcije - Razvoj C-H Funkcionalizacijskih Strategija Po Principima Zelene Kemije. *Kem. Ind.* **2022**, *71* (5−6), 359−373.
(21) Short, M. A.; Blackburn, J. M.; Roizen, J. L. Modifying Positional Selectivity in C-H Functionalization Reactions with Nitrogen-Centered Radicals: Generalizable Approaches to 1,6-Hydrogen-Atom Transfer Processes. *Synlett* **2020**, *31* (02), 102−116.
(22) Bafaluy, D.; Muñoz-Molina, J. M.; Funes-Ardoiz, I.; Herold, S.; de Aguirre, A. J.; Zhang, H.; Maseras, F.; Belderrain, T. R.; Pérez, P. J.; Muñiz, K. Copper-Catalyzed N-F Bond Activation for Uniform Intramolecular C-H Amination Yielding Pyrrolidines and Piperidines. *Angew. Chem., Int. Ed.* **2019**, *58* (26), 8912−8916.
(23) Muñoz-Molina, J. M.; Bafaluy, D.; Funes-Ardoiz, I.; De Aguirre, A.; Maseras, F.; Belderrain, T. R.; Pérez, P. J.; Muñiz, K. Mechanistic Studies on the Synthesis of Pyrrolidines and Piperidines via Copper-Catalyzed Intramolecular C-H Amination. *Organometallics* **2022**, *41*, 1099.
(24) Zhang, H.; Muñiz, K. Selective Piperidine Synthesis Exploiting Iodine-Catalyzed Csp3-H Amination under Visible Light. *ACS Catal.* **2017**, *7* (6), 4122−4125.
(25) Kessil PR-160L 370-Gen2 specification. https://www.kessil.com/products/science_PR160L.php (accessed 2023-12-01).
(26) Willcott, M. R. MestRe Nova. *J. Am. Chem. Soc.* **2009**, *131* (36), 13180.
(27) Stoll, S.; Schweiger, A. EasySpin, a Comprehensive Software Package for Spectral Simulation and Analysis in EPR. *J. Magn. Reson.* **2006**, *178* (1), 42−55.
(28) Šakić, D.; Bešić, E.; Zubčić, G.; Chechik, V. VisualEPR. https://github.com/DSakicLab/visualEPR (accessed 2023-12-01).
(29) Pracht, P.; Bohle, F.; Grimme, S. Automated Exploration of the Low-Energy Chemical Space with Fast Quantum Chemical Methods. *Phys. Chem. Chem. Phys.* **2020**, *22* (14), 7169−7192.
(30) Bannwarth, C.; Caldeweyher, E.; Ehlert, S.; Hansen, A.; Pracht, P.; Seibert, J.; Spicher, S.; Grimme, S. Extended tight-binding Quantum Chemistry Methods. *Wiley Interdiscip. Rev. Comput. Mol. Sci.* **2021**, *11* (2), No. e1493.
(31) Bannwarth, C.; Ehlert, S.; Grimme, S. GFN2-XTB—An Accurate and Broadly Parametrized Self-Consistent Tight-Binding Quantum Chemical Method with Multipole Electrostatics and Density-Dependent Dispersion Contributions. *J. Chem. Theory Comput.* **2019**, *15* (3), 1652−1671.
(32) Becke, A. D. Density-Functional Thermochemistry. III. The Role of Exact Exchange. *J. Chem. Phys.* **1993**, *98* (7), 5648−5652.
(33) Stephens, P. J.; Devlin, F. J.; Chabalowski, C. F.; Frisch, M. J. Ab Initio Calculation of Vibrational Absorption and Circular Dichroism Spectra Using Density Functional Force Fields. *J. Phys. Chem.* **1994**, *98* (45), 11623−11627.
(34) Ditchfield, R.; Hehre, W. J.; Pople, J. A. Self-Consistent Molecular-Orbital Methods. IX. An Extended Gaussian-Type Basis for Molecular-Orbital Studies of Organic Molecules. *J. Chem. Phys.* **1971**, *54* (2), 724−728.
(35) Grimme, S. Semiempirical Hybrid Density Functional with Perturbative Second-Order Correlation. *J. Chem. Phys.* **2006**, *124* (3), 034108.

(36) Neese, F.; Schwabe, T.; Grimme, S. Analytic Derivatives for Perturbatively Corrected "Double Hybrid" Density Functionals: Theory, Implementation, and Applications. *J. Chem. Phys.* **2007**, *126* (12), 124115.
(37) Curtiss, L. A.; Redfern, P. C.; Raghavachari, K.; Rassolov, V.; Pople, J. A. Gaussian-3 Theory Using Reduced Mo/Ller-Plesset Order. *J. Chem. Phys.* **1999**, *110* (10), 4703−4709.
(38) Grimme, S.; Antony, J.; Ehrlich, S.; Krieg, H. A Consistent and Accurate *Ab Initio* Parametrization of Density Functional Dispersion Correction (DFT-D) for the 94 Elements H-Pu. *J. Chem. Phys.* **2010**, *132* (15), 154104.
(39) Vrček, I. V.; Šakić, D.; Vrček, V.; Zipse, H.; Biruš, M. Computational Study of Radicals Derived from Hydroxyurea and Its Methylated Analogues. *Org. Biomol. Chem.* **2012**, *10* (6), 1196−1206.
(40) Hermosilla, L.; Calle, P.; García de la Vega, J. M.; Sieiro, C. Density Functional Theory Study of ^{14}N Isotropic Hyperfine Coupling Constants of Organic Radicals. *J. Phys. Chem. A* **2006**, *110* (50), 13600−13608.
(41) Frisch, M. J.; Trucks, G. W.; Schlegel, H. B.; Scuseria, G. E.; Robb, M. A.; Cheeseman, J. R.; Scalmani, G.; Barone, V.; Petersson, G. A.; Nakatsuji, H.; et al.; *Gaussian 16*, Revision C. 01. Gaussian, Inc.: Wallingford CT, 2016.
(42) *HR-ZOO, Cluster Supek*; University of Zagreb University Computing Centre—SRCE. KK.01.1.1.08.0001, EU funded within OPCC for Republic of Croatia: Zagreb, 2023.
(43) *PharmInova Project, Cluster Sw.Pharma.Hr*; University of Zagreb Faculty of Pharmacy and Biochemistry. KK.01.1.1.02.0021, EU funded by the European Regional Development Fund: Zagreb, 2023.
(44) Šakić, D.; Zipse, H. Radical Stability as a Guideline in C-H Amination Reactions. *Adv. Synth. Catal.* **2016**, *358* (24), 3983−3991.
(45) Hioe, J.; Šakić, D.; Vrček, V.; Zipse, H. The Stability of Nitrogen-Centered Radicals. *Org. Biomol. Chem.* **2015**, *13* (1), 157−169.
(46) Hioe, J.; Zipse, H. Radical Stability—Thermochemical Aspects. In *Encyclopedia of Radicals in Chemistry, Biology and Materials*; Chatgilialoglu, C., Studer, A., Eds.; Wiley: UK, 2012, pp 449−476..
(47) Shkunnikova, S.; Zipse, H.; Šakić, D. Role of Substituents in the Hofmann-Löffler-Freytag Reaction. A Quantum-Chemical Case Study on Nicotine Synthesis. *Org. Biomol. Chem.* **2021**, *19* (4), 854−865.
(48) Corey, E. J.; Hertler, W. R. A Study of the Formation of Haloamines and Cyclic Amines by the Free Radical Chain Decomposition of N-Haloammonium Ions (Hofmann-Löffler Reaction). *J. Am. Chem. Soc.* **1960**, *82* (7), 1657−1668.
(49) Carloni, P.; Eberson, L.; Greci, L.; Sgarabotto, P.; Stipa, P. New Insights on N-Tert-Butyl-α-Phenylnitrone (PBN) as a Spin Trap. Part 1. Reaction between PBN and N-Chlorobenzotriazole. *J. Chem. Soc. Perkin Trans. 2* **1996**, *7* (7), 1297−1305.
(50) Constantinou, C. T.; Gkizis, P. L.; Lagopanagiotopoulou, O. T. G.; Skolia, E.; Nikitas, N. F.; Triandafillidi, I.; Kokotos, C. G. Photochemical Aminochlorination of Alkenes without the Use of an External Catalyst. *Chem.—Eur. J.* **2023**, *29* (45), No. e202301268.
(51) Korotenko, V.; Zipse, H. The Stability of Oxygen-Centered Radicals and Its Response to Hydrogen Bonding Interactions. *J. Comput. Chem.* **2024**, *45*, 101−114.
(52) Zhu, Y.; Wang, J. J.; Wu, D.; Yu, W. Visible-Light-Driven Remote C-H Chlorination of Aliphatic Sulfonamides with Sodium Hypochlorite. *Asian J. Org. Chem.* **2020**, *9* (10), 1650−1654.
(53) Nikolaienko, P.; Jentsch, M.; Kale, A. P.; Cai, Y.; Rueping, M. Electrochemical and Scalable Dehydrogenative C(Sp3)-H Amination via Remote Hydrogen Atom Transfer in Batch and Continuous Flow. *Chem.—Eur. J.* **2019**, *25* (29), 7177−7184.
(54) Herron, A. N.; Hsu, C. P.; Yu, J. Q. δ-C-H Halogenation Reactions Enabled by a Nitrogen-Centered Radical Precursor. *Org. Lett.* **2022**, *24* (20), 3652−3656.
(55) Leijondahl, K.; Borén, L.; Braun, R.; Bäckvall, J. E. Enantiopure 1,5-Diols from Dynamic Kinetic Asymmetric Transformation. Useful Synthetic Intermediates for the Preparation of Chiral Heterocycles. *Org. Lett.* **2008**, *10* (10), 2027−2030.
(56) Marichev, K. O.; Takacs, J. M. Ruthenium-Catalyzed Amination of Secondary Alcohols Using Borrowing Hydrogen Methodology. *ACS Catal.* **2016**, *6* (4), 2205−2210.

https://doi.org/10.1021/acs.jpca.3c07892
J. Phys. Chem. A 2024, 128, 2574−2583

4. MECHANISTIC INSIGHTS INTO THE PROPAGATION CYCLE OF THE HOFMANN–LÖFFLER–FREYTAG REACTION. HALOGEN *VS* HYDROGEN ATOM TRANSFER

JOC The Journal of Organic Chemistry

pubs.acs.org/joc

Article

Mechanistic Insights into the Propagation Cycle of the Hofmann–Löffler–Freytag Reaction: Halogen vs Hydrogen Atom Transfer

Published as part of The Journal of Organic Chemistry special issue "Physical Organic Chemistry: Never Out of Style".

Gabrijel Zubčić, Luka Andrijanić, Iva Džeba, Jiangyang You, Tomislav Friganović, Tomislav Portada, Kristina Pavić, Erim Bešić, Valerije Vrček, and Davor Šakić*

Cite This: https://doi.org/10.1021/acs.joc.4c02997

Read Online

ACCESS | Metrics & More | Article Recommendations | Supporting Information

ABSTRACT: The Hofmann–Löffler–Freytag (HLF) reaction is a method that employs N-chlorinated precursors in radical-mediated rearrangement cycles to synthesize pyrrolidine rings and C–H functionalized products. This study aims to elucidate the mechanism of the propagation cycle, identify the rate-limiting step, and uncover the factors influencing the regioselectivity of the HLF reaction. Combining experimental techniques—laser flash photolysis (LFP), electron paramagnetic resonance (EPR), and nuclear magnetic resonance (NMR)—with computational density functional theory (DFT) calculations and kinetic modeling, we challenge the previous assumption that the hydrogen atom transfer (HAT) step was rate-limiting and regioselectivity was under both thermodynamic and kinetic control. We have identified that the halogen atom transfer (XAT) step in the propagation cycle of the HLF reaction follows pseudo-first-order kinetics and has the largest transition-state barrier. Additionally, we observed that regioselectivity is exclusively controlled by the intramolecular hydrogen atom transfer kinetics, while no thermodynamic preference exists in the formation of C_6- and C_5-chlorinated products. Our work predicts how to accelerate the HLF reaction and how we can control the regioselectivity by the smarter selection of substrates based on calculations, which could provide better control of the reaction when implemented in organic synthesis.

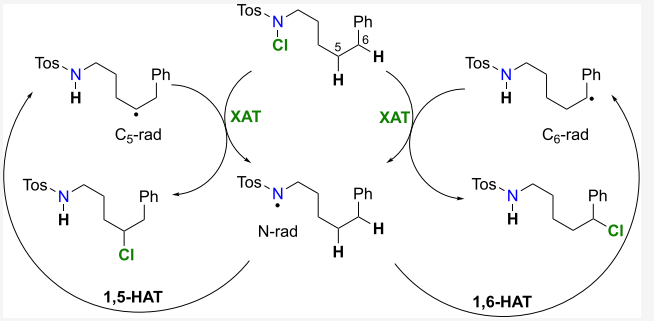

INTRODUCTION

The foundation for the use of N-centered aminyl radicals in organic synthesis, albeit not recognized as such, was laid more than a century ago. In 1881–1885, Hofmann[1] discovered that treating *N*-bromo-2-propylpiperidine, an *N*-halodialkylamine, with hot sulfuric acid produced a tertiary amine, eventually identified[2] as octahydroindolizine. Löffler and Freytag[3] extended the Hofmann reaction to simple secondary amines and discovered it to be a general approach for synthesizing pyrrolidines.[4] Around 70 years after its discovery, Wawzonek and Helen,[5] followed by Corey and Hertler,[6] identified a free radical chain mechanism for this reaction. Upon the activation of *N*-chloroamine **1** with sulfuric acid (Scheme 1), protonated *N*-chloroamine **2** undergoes homolytic cleavage in the presence of heat, light, or initiators. The resulted protonated aminyl radical **3** takes part in an intramolecular hydrogen atom transfer (HAT) abstracting a sterically favorably orientated hydrogen atom to afford, regioselectively, an alkyl radical **4**, which in turn abstracts a chlorine atom to form a

Scheme 1. Cyclization of N-Halogenated Amines (the Hofmann–Löffler–Freytag Reaction)[4]

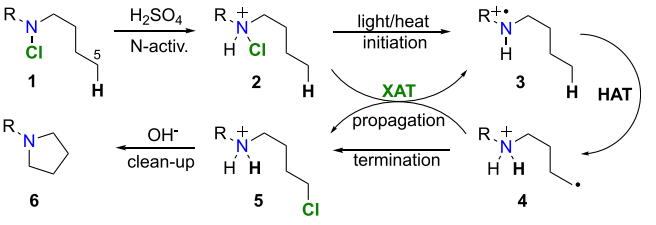

Received: December 5, 2024
Revised: March 11, 2025
Accepted: March 18, 2025

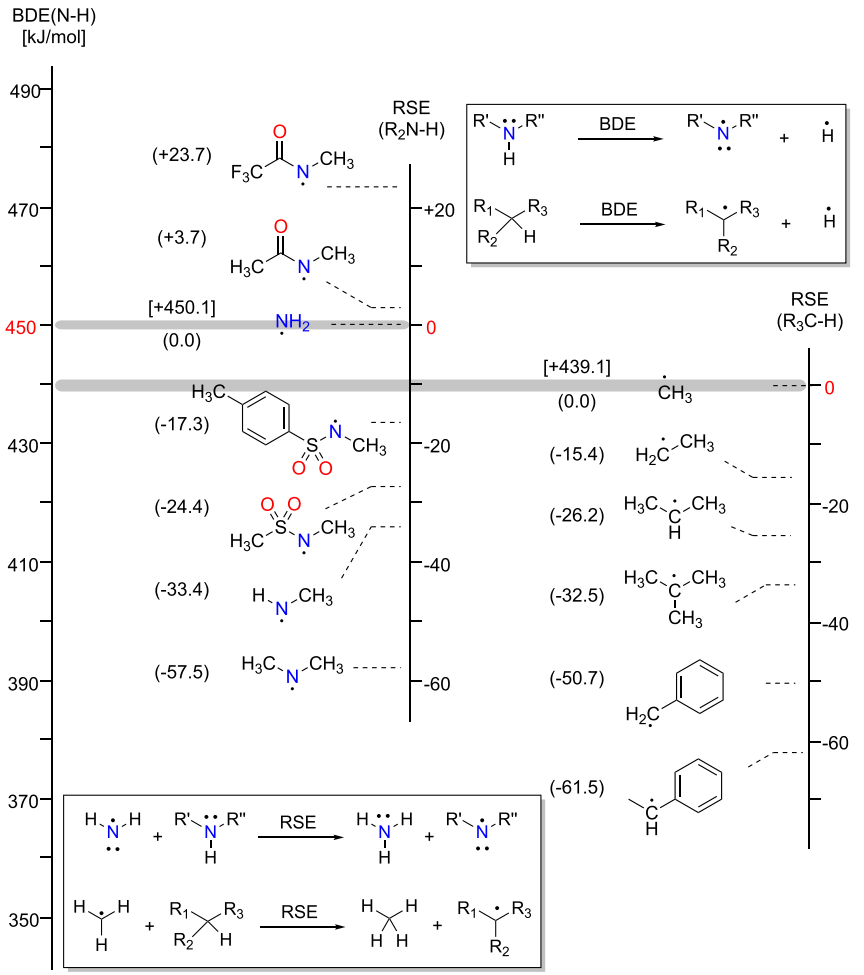

Figure 1. Bond dissociation energies (BDEs) and radical stabilization energies (RSEs) for selected small radical species commonly involved in HLF reactions. Gray bands denote anchor points between RSE and BDE scales. Data calculated at RO-B2PLYP/G3MP2large//B3LYP/6−31G(d) from refs 16, 22, and 25.

chloroalkylammonium ion **5**, which then cyclizes in the presence of a base, providing cyclic tertiary amine **6**.

There are two well-documented modern variants of the Hofmann−Löffler−Freytag Reaction (HLF), one developed by Suarez and co-workers,[7−10] who used *in situ* halogenation and photochemical activation of *N*-iodoamides to produce cyclization products, and another reported by Corey et al.,[11] where the required bromoamide precursor was synthesized and characterized in a separate first step. Subsequent irradiation of the bromoamide precursor in CCl_4 results in the formation of the C_5-bromo derivative, which can be cyclized to methyl 1-acetyl-3-methylpyrrolidine-2-carboxylate with a 90% yield using a hindered base.

Mechanistic investigations, from the discovery of the HLF reaction until today, point conclusively to a radical chain mechanism involving intramolecular HAT as the first step of the propagation cycle, with halogen atom transfer (XAT) as the second step.[4,6,12−15] Intermolecular reactions involving neutral or protonated aminyl radicals have been documented but only occur as additions to olefinic and acetylenic hydrocarbons and not as intermolecular HAT.[16−21] When olefins are present in the solvent, the intermolecular addition of protonated or neutral aminyl radicals to olefins competes with the intramolecular HAT step of the HLF propagation cycle, depending on the reaction conditions.

To the best of our knowledge, few published studies have investigated the rate-limiting step of the HLF reaction and the inherent causes that guide the regioselectivity. Wolff[4] has argued that the second step, XAT, has a smaller activation barrier, and from this point on, it was assumed that the HAT step is rate-limiting. In this context, extensive computational studies have been published investigating it,[22−25] where the thermodynamics of this step is evaluated via the radical stabilization energies (RSEs) for a family of isodesmic reactions and plotted against corresponding activation barriers (Bell−Evans−Polanyi principle). The main conclusion from these studies is that the selectivity of attack by the aminyl radical on a carbon atom depends on the reactivity of the aminyl radical and on the stability of the ensuing carbon radical (see Figure 1). Therefore, aminyl radicals that can abstract hydrogen atoms from carbon generally show a preference for hydrogen in the order of tertiary > secondary > primary. Furthermore, by changing the activating group on the N-centered aminyl radical, the outcome of the reaction can be dramatically influenced. This, however, does not provide an answer to whether the regioselectivity is determined by thermodynamics or kinetics and has not been placed in the context of the propagation cycle.

The vast majority of papers dealing with HLF reaction report on pyrrolidine formation, and there has been just one

https://doi.org/10.1021/acs.joc.4c02997
J. Org. Chem. XXXX, XXX, XXX−XXX

Scheme 2. Expected Products and Intermediates of the HLF Reaction Were Measured Using Three Different Techniques[a]

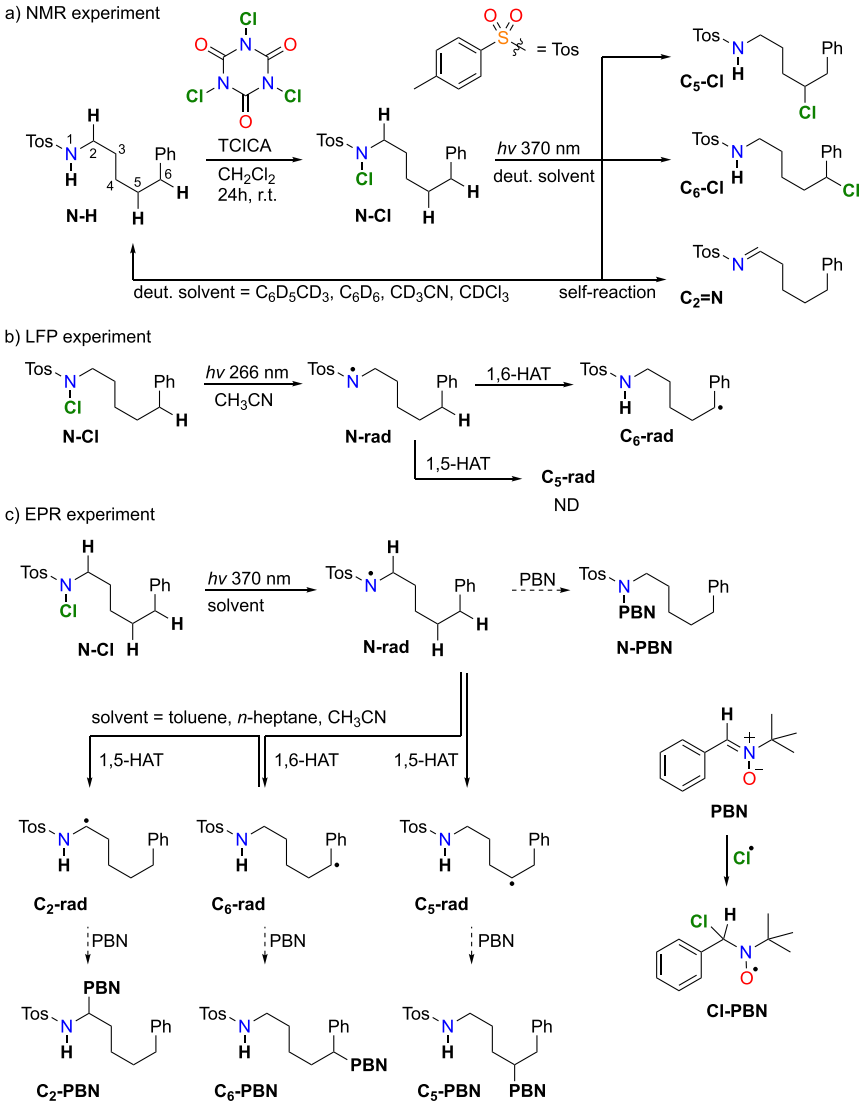

[a](a) Synthesis of **N-Cl** and NMR observed products of the reaction mixture after 370 nm irradiation of **N-Cl**, (b) radical intermediates observed after laser excitation at 266 nm of **N-Cl** in flow cuvettes (3 mL; 3×10^{-4} M) at 266 nm in N_2-purged acetonitrile, and (c) radical intermediates after 370 nm irradiation and PBN spin-trapped products in EPR experiment. Details of the experiments are found in the SI.

paper reporting on exclusive piperidine formation.[26] However, there have been a couple of papers reporting on the functionalization of the C_6 position with a chlorine atom.[27−29] To investigate the factors determining regioselectivity and identify the rate-limiting step, we chose a joint experimental and computational approach to study a system that was employed in piperidine synthesis. Our aim is to detect as many as possible radical intermediate species involved in the propagation cycle and analyze major products formed. Quantum chemical calculations have been used extensively to identify these radical intermediates and reaction products. The proposed calculated reaction mechanism should explain the experimental results, observed regioselectivity, and kinetic measurements. Finally, we propose that a combined approach involving both computational techniques and experiments must be employed when addressing fundamental questions, such as regioselectivity, and the rate-limiting step of the reaction sequence must be answered.

RESULTS AND DISCUSSION

To provide experimental evidence for the interplay between two reaction steps in the propagation cycle, we employed NMR, LFP, and EPR techniques (Scheme 2). The overall reaction progress and major product analysis was observed with different NMR techniques, with *off-site* irradiation using a 370 nm Kessil lamp. Direct detection of radical intermediates with measurement of their rearrangement kinetics was performed using LFP via the fourth harmonic of the Nd:YAG laser (266 nm). Additionally, we attempted an *in situ* generation and spin-trapping of N- and C-centered radicals using the phenylbutylnitrone (PBN) spin trap and investigated the resulting adducts with EPR (see Scheme 2c). Finally, we performed extensive DFT calculations and kinetic modeling of the reaction pathways, with the full model described in detail in Section S12 of the Supporting Information.

Using continuous irradiation with a UV lamp from the bottom of the cavity resonator, the complete reaction sequence was monitored with EPR spectrometry for **N-Cl** (Scheme 2c).

https://doi.org/10.1021/acs.joc.4c02997
J. Org. Chem. XXXX, XXX, XXX−XXX

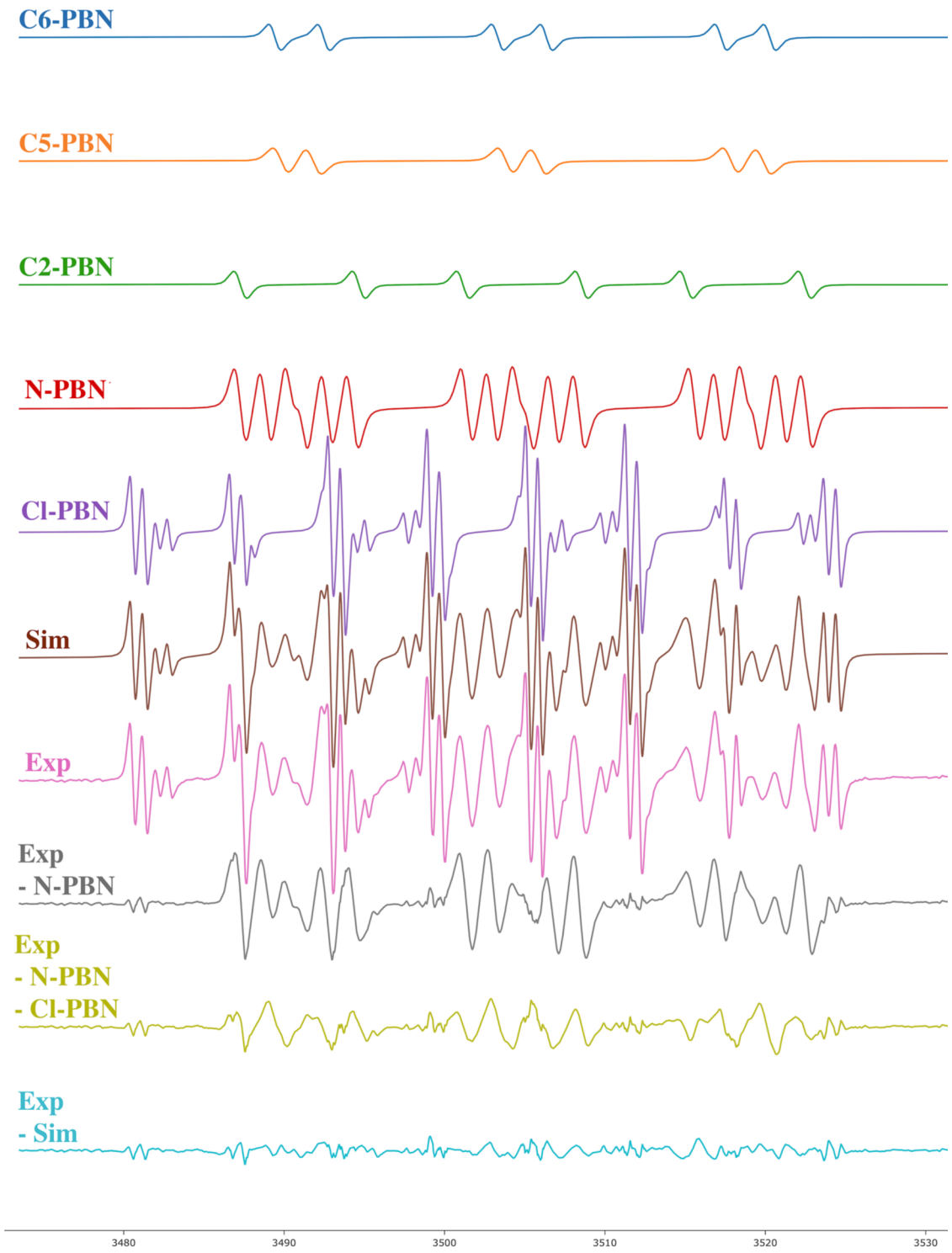

Figure 2. EPR spectra of spin-trapped radical intermediates generated with 370 nm irradiation of **N-Cl**. The simulated spectra of each radical adduct species are denoted in the spectra as **C_6-PBN**, **C_5-PBN**, **Cl-PBN**, **C_2-PBN**, and **N-PBN**. Total simulated spectrum is labeled as **Sim**, while the experimental spectrum is labeled as **Exp**, with residual signals provided as **Exp−N-PBN**, **Exp−N-PBN−Cl-PBN**, and **Exp−Sim**. Line widths measured with EPR and reaction yields were influenced by the effectiveness of air removal using freeze−pump−thaw cycles with backfill of argon or nitrogen gas. Experimental line widths of less than 0.4 G were deemed satisfactory for the optimal resolution of radical adducts. More information on deconvolution and simulation is deposited in the SI.

The resulting experimental spectrum is shown in Figure 2. The best decomposition of the experimental EPR spectrum for **N-Cl** was found to be the one with one N-centered radical adduct, **N-PBN**; a Cl radical adduct, **Cl-PBN**; and three C-centered radical adducts (assigned as **C_6-PBN**, **C_5-PBN**, and **C_2-PBN**) with different hydrogen hyperfine couplings (*hfc*) (Table 1). This total simulated spectrum, supported by our DFT calculations, aligns well with the experimental data (Figure 2). As a result, we were able to observe a **Cl-PBN** adduct, proving the homolytic cleavage of **N-Cl** bonds

https://doi.org/10.1021/acs.joc.4c02997
J. Org. Chem. XXXX, XXX, XXX−XXX

Table 1. Experimental and Calculated EPR Parameters for the Observed Radicals in the EPR Spectrum[a]

	N-PBN		Cl-PBN	C_6-PBN		C_5-PBN		C_2-PBN	
	EXP	CALC	EXP	EXP	CALC	EXP	CALC	EXP	CALC
g	2.00612	2.0063	2.0077	2.0064	2.00591	2.0064	2.00599	2.0062	2.00611
α_N	13.82	14.21	12.37	13.96	14.78	13.96	15.32	13.72	14.06
α_H	2.85	3.87	0.76	3.06	3.67	2.03	2.37	7.38	5.49
$\alpha_{N'}$	1.54	1.57	α_{Cl} 6.23						
ratio	1.00		0.72	0.12		0.17		0.11	

[a]Calculated at the B3LYP/(C,H,O)EPR-III/(S)def2-QZVP/(N)6-31G(d)//B3LYP/6-31G(d) level of theory. Hyperfine coupling (*hfc*) units are in Gauss.

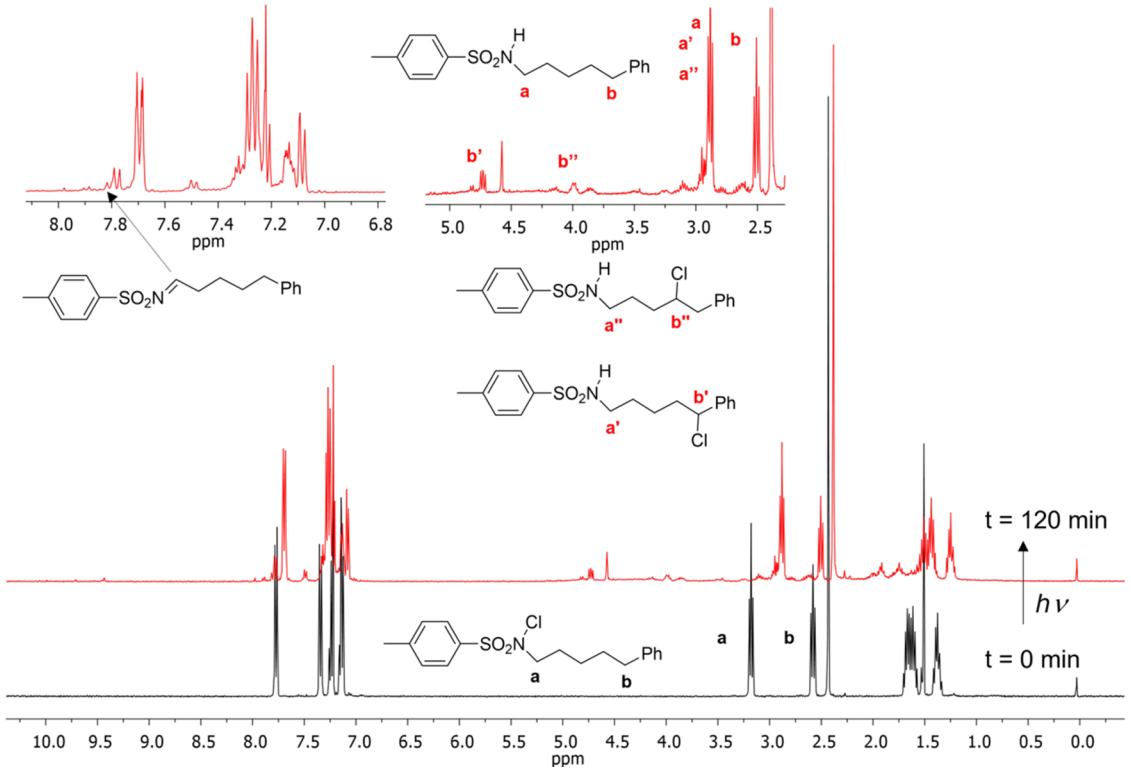

Figure 3. NMR spectra before and after *off-site* irradiation in $CDCl_3$. The black and red spectra correspond to the **N-Cl** and reaction mixture of **N-H**, **C_6-Cl**, **C_5-Cl**, and **C_2═N**, respectively. Insets depict selected signal ranges in more detail, with chosen signals assigned. The ^{1}H, HSQC, and $^{13}C\{^1H\}$ APT spectra for experiments in C_6D_6 are deposited in the SI.

generating a chlorine radical that quickly combines with **PBN**. An **N-PBN** adduct was formed from the addition of an N-centered radical to a **PBN** molecule. Calculated EPR parameters for **N-PBN** are in good agreement with the experimental values. Finally, we were able to observe three distinct PBN adducts of C-centered radicals, namely, **C_6-PBN**, **C_5-PBN**, and **C_2-PBN**. Experimental *hfc* values of these three PBN adducts differ enough to distinguish them, although in DFT calculations, **C_6-PBN** and **C_5-PBN** have similar calculated *g*-factor values, while **C_2-PBN** differs from them. Calculated EPR parameters for **C_6-PBN** and **C_5-PBN** are in satisfactory agreement with the experimental values. The difference in *g*-factors and *hfc* values of the **C_2-PBN** radical adduct compared to the rest of C-centered radicals is due to the different connectivity and closer secondary N atom to the radical center.[16] Again, calculated values for **C_2-PBN** have the same trend as the experimental parameters. Additional support to the correct assignment of radicals comes from similar experimental *g*-factors and *hfc* values for **C_2-PBN**, **N-PBN**, and **C_5-PBN** radicals generated from *N*-chloro-*N*-hexyl-4-methylbenzenesulfonamide.[16] At this point, it is worth noting that the relative weights of the radical adducts are as follows: **N-PBN**, 1; **Cl-PBN**, 0.72; **C_6-PBN**, 0.12; **C_5-PBN**, 0.17; and **C_2-PBN**, 0.11.

Before *off-site* irradiation, ^{1}H NMR and ^{13}C APT spectra of **N-Cl** (Scheme 2a) were recorded. All signals observed for the starting material are consistent with the expected signals for **N-Cl**. After *off-site* irradiation of the **N-Cl** precursor in toluene, a mixture of products was obtained with total conversion of the starting material, as indicated by the ^{1}H NMR spectrum of the reaction mixture. Out of the total **N-Cl** compound in the NMR tube, ~42% corresponds to the **N-H** product (Figure 3). The mechanism by which this reversal to the amine parent compound occurs has baffled us, although it is a common phenomenon reported in the literature.[18,28−30] Our first mechanism proposal involves the reaction of chlorine radical or N-centered radical **N-rad** with solvents,[20] producing solvent radicals and polymerization side reactions resulting in a cloudy reaction mixture.

https://doi.org/10.1021/acs.joc.4c02997
J. Org. Chem. XXXX, XXX, XXX−XXX

The analysis of the other products using the ^{1}H NMR spectrum combined with the 2D technique, HSQC and ^{13}C APT spectra, provides unambiguous evidence that the signals observed at 4.47 and 3.75 ppm correspond to **C_6-Cl** and **C_5-Cl** products, respectively, with an overall NMR yield of ∼47% (**C_6-Cl**/**C_5-Cl** = 71:29%) (Figure 3). This was determined from the integral ratios (SI). From additional NMR experiments in other solvents, we found that approximately 50% of **N-H** and 50% of the **C_6-Cl** and **C_5-Cl** mixture (72:28%) were obtained in deuterated benzene. In deuterated acetonitrile, we obtained 66% of **N-H** and 34% of the **C_6-Cl** and **C_5-Cl** mixture (57:43%). We can safely conclude that the H atom from the trace water is not involved in the mechanism of converting **N-Cl** back to the parent **N-H** species due to the same pattern of product ratios in a wide selection of solvents. Alas, by examination, we have observed a peak (δ 7.76, t, J = 11 Hz, in $CDCl_3$) in the aromatic NMR that corresponds to the imine signal and an NMR yield of ∼11%. This indicates the occurrence of a self-reaction facilitated by hydrogen atom transfer (HAT) between two **N-rad** molecules, leading to their termination and the formation of the starting amine (**N-H**) and imine (**C_2═N**) products. These disproportionation products are described in the literature,[31,32] and it is not a coincidence that many chemists deliberately design precursors with the C_2 position blocked or unavailable.[28−30] Additionally, the necessity of blocking the C_2 position in HLF reactions has been studied in detail in our previous work.[15] Our calculations predict a barrier of $\Delta G^{\ddagger}_{298}$ = +59.4 kJ mol^{-1}, with a thermodynamic driving force of ΔG_{298} = −134.6 kJ mol^{-1} for this reaction.

LFP measurements were performed on **N-Cl** in acetonitrile to directly detect the transient species generated after laser excitation at 266 nm (4.66 eV) (Scheme 2b). This resulted in the homolytic cleavage of the weakest N−Cl bond (4.03 eV)[33] and the formation of an aminyl radical and, through subsequent rearrangement reactions, corresponding C-centered radicals. This is confirmed by EPR experiments in toluene, acetonitrile, and *n*-heptane, in which we detected **N-PBN** and **Cl-PBN** after the irradiation of **N-Cl** (Figure 2).

The intramolecular HAT from one of the five carbon atoms of **N-Cl** to the nitrogen atom enables the formation of one or more C-centered radicals. Among these, a benzyl radical, **C_6-rad**, is the most likely to be detected by LFP due to the benzene ring acting as a chromophore. The transient absorption spectrum (Figure 4) displays three distinct maxima: one at 280 nm, the second at 310 nm, and the third at 460 nm. The shape of these spectra does not change significantly within the 1500 ns time frame after the laser excitation. However, it is understandable from the spectra that multiple transient species are present, which are deduced from the fact that some maxima disappear faster than others. Furthermore, there are no major changes in the shape of the spectra, which imply that the transient moieties are related and have major structural features in common. Conclusive evidence to support this comes from kinetic data collected at the respective wavelengths. We have a first-order decay with two contributions at 290 and 330 nm. The shorter time scale at 290 nm better reflects the kinetics of the shorter-lived transient species, which lives less than 20 ns and is close to the detection limit, while the longer-lived transient determined from the extended time scale has a lifetime (τ) of 25 μs at 290 nm and 47 μs at 330 nm. Kinetics at 450 nm follows the single exponential decay with only one component. The lifetime of this component is

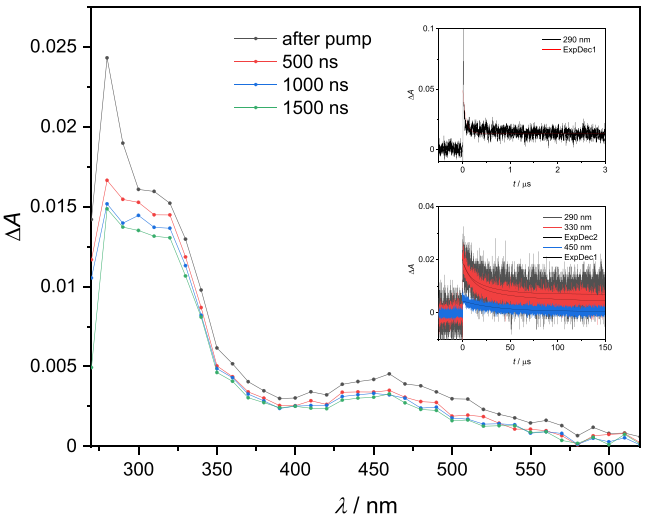

Figure 4. Transient absorption spectra of a N_2 purged solution of 0.3 mM **N-Cl** in acetonitrile. Flow rate: 2.4 mL/min. E_{266} = 22 mJ. A_{266} = 0.27. Insets: corresponding time profiles at 290, 330, and 450 nm.

35 μs. The small differences between the lifetime values may be due to variations in the signal-to-noise ratio (SNR) or due to different quantitative shares of the radicals presented (see the SI). The shorter-lived transient at 290 nm is assigned to an aminyl radical formed by the N−Cl bond cleavage. Amidyl and aminyl radicals have previously been generated by LFP, and their τ values have been reported whether they were directly detected with LFP or indirectly from the detected C-centered radical formed by cyclization/intramolecular HAT. Reported τ values of amidyl and aminyl N-centered radicals range from 5 to 454 ns.[34−37] This is in agreement with our experimental results.

To check if the aminyl N-centered radical, **N-rad**, absorbs at 290 nm, we have done extensive TD-DFT calculations that indicate a strong absorption peak at 280 nm with an oscillator strength (f) of 0.0238 (SI). We conclude that the longer-lived transient is one of the generated C-centered radicals, most likely a benzyl-type **C_6-rad**. This is in good agreement with the literature, which reports a lifetime of 40 μs for benzyl radicals, generated from benzyl chloride in hexane, with a maximum at about 315 nm.[38] Additionally, our measurements of the benzyl radical generated from BnCl in acetonitrile show a maximum at 310 nm and a lifetime of 30 μs (see Section S8 in the SI).S8 in the SI).

As seen in Figure 5, DFT calculations of the 1,6-HAT step involves rearrangement from the global minimum on the reactant side (**N-rad$_{gm}$**) to a prereactive conformer (**N-rad$_{ric1,6}$**) that is ΔG_{298} = +25.3 kJ mol^{-1} less stable. From there, transition state **TS-1,6-HAT$_{uni}$** is reached with an overall barrier of $\Delta G^{\ddagger}_{298,gm}$(**1,6-HAT$_{uni}$**) = +38.0 kJ mol^{-1}. When the barrier is defined as in eq 2, $\Delta G^{\ddagger}_{298,ric}$(**1,6-HAT$_{uni}$**) equals 12.8 kJ mol^{-1}. In the first case ($\Delta G^{\ddagger}_{298,gm}$), the calculated $t_{1/2}$ of the aminyl radical is 514 ns, while for the second case ($\Delta G^{\ddagger}_{298,ric}$), the calculated $t_{1/2}$ of 0.02 ns is in far better agreement with LFP experimental results. This led us to the conclusion that upon homolytic cleavage (hc) of the N−Cl bond, the N-centered aminyl radical **N-rad$_{hc,pic}$** exists as a high energy conformer on the potential energy surface and is almost equal in energy to the prereactive conformer **N-rad$_{ric1,6}$** of the IRC path. This is a case where Boltzmann distribution does not apply, and the low energy state is unavailable due to kinetic

https://doi.org/10.1021/acs.joc.4c02997
J. Org. Chem. XXXX, XXX, XXX−XXX

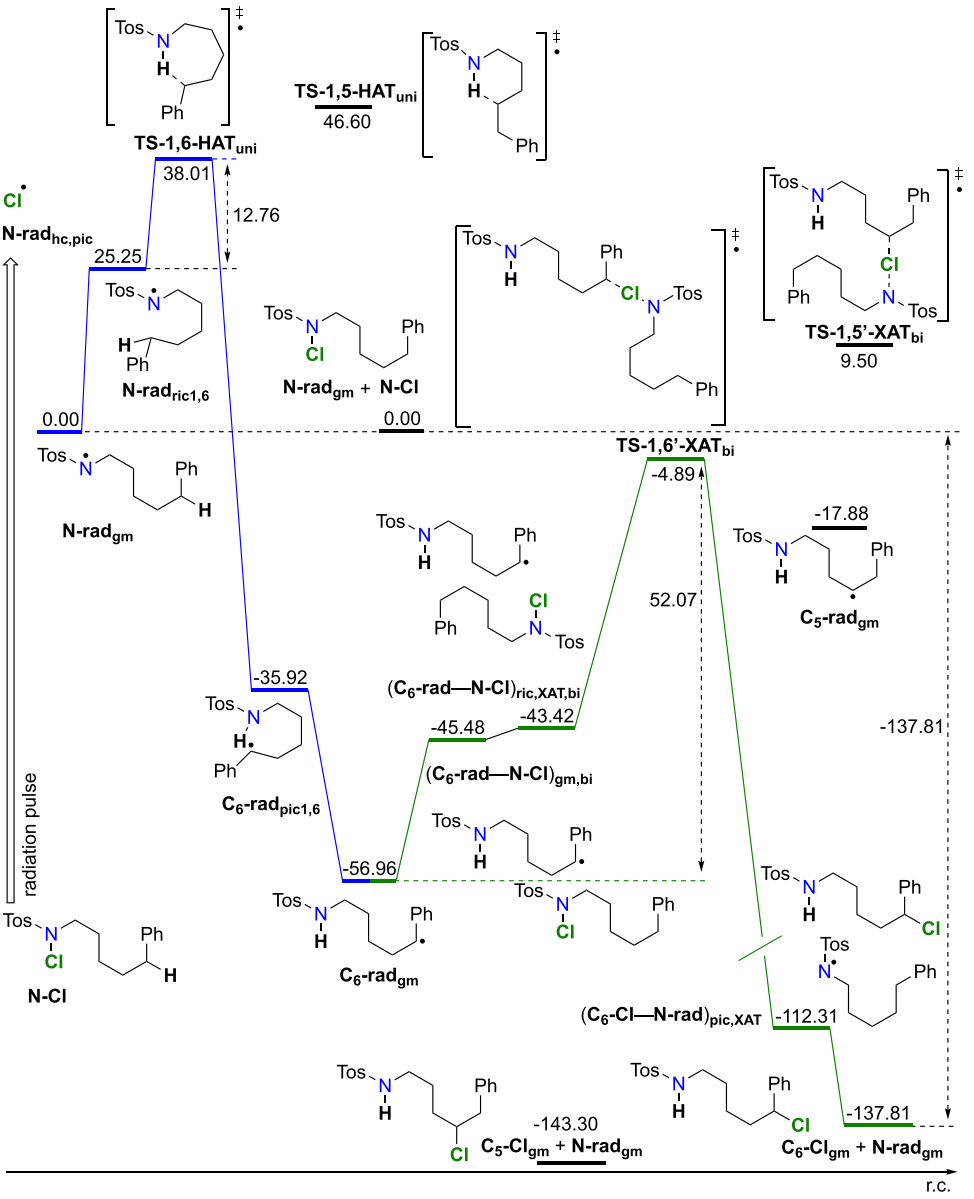

Figure 5. Energy diagram of intra- and intermolecular radical rearrangements for the propagation cycle of HLF for the 1,6-pathway. From the starting N-centered radical **N-rad**, it rearranges via **TS-1,6-HAT** to the **C$_6$-rad**. The next step is the bimolecular reaction from **C$_6$-rad** and **N-Cl**, via **TS-1,6'-XAT**, to **C$_6$-Cl** and **N-rad** formation. Calculated at the RO-B2PLYP/G3MP2Large(SMD,CH_3CN)//B3LYP/6-31G(d) level of theory. Included in the diagram are chosen points of the 1,5-pathway. The global minimum structure **N-rad$_{gm}$** was taken as the starting point in the unimolecular process, while the global minima of separated reactants, namely, **N-rad$_{gm}$** and **N—Cl$_{gm}$**, were taken as the starting point in the bimolecular reaction. Units are given in kJ mol^{-1}.

reasons, with **N-rad$_{hc,pic}$** quickly rearranging to **N-rad$_{ric1,6}$**. On the product side, the first local minimum encountered is **C$_6$-rad$_{pic1,6}$** at ΔG_{298} = −35.9 kJ mol^{-1}, which then rearranges to the most stable conformer, a global minima (gm) **C$_6$-rad$_{gm,uni}$** with an overall Gibbs free energy of reaction of ΔG_{298} = −57.0 kJ mol^{-1}. At this point, **C$_6$-rad** and **N—Cl** species are separated in the solvent. When they meet in the solvent cage due to diffusion, a complex **(C6-rad—N-Cl)$_{gm,bi}$** is formed at ΔG_{298} = −45.5 kJ mol^{-1}, after which a prereactive conformer for the **XAT** is formed, **(C6-rad—N-Cl)$_{ric,XAT,bi}$**, at ΔG_{298} = −43.4 kJ mol^{-1}. From there, the transition state **TS-1,6'-XAT$_{bi}$** is reached with an overall barrier of $\Delta G^{\ddagger}_{298,gm}$**(1,6'-XAT$_{bi}$)** = +52.1 kJ mol^{-1}. If the barrier is calculated according to eq 2, the $\Delta G^{\ddagger}_{298,ric}$**(1,6'-XAT$_{bi}$)** value is at +38.5 kJ mol^{-1}. For the first case, the $t_{1/2}$ of the **C$_6$-rad** species is 149 μs, and for the second case, the $t_{1/2}$ is 633 ns. The first case describes the $t_{1/2}$ of radical **C$_6$-rad** closer to the experimental results.

Hence, due to the better fit with the experiment, we use $\Delta G^{\ddagger}_{298,ric}$**(1,6-HAT$_{uni}$)** calculated from the prereactive minimum for the HAT reaction as a first step in the propagation cycle, while for the second step, which involves a bimolecular XAT reaction, we use $\Delta G^{\ddagger}_{298,gm}$**(1,6'-XAT$_{bi}$)** again due to the better fit to the experimental results.

We also performed TD-DFT calculations that show that **C$_6$-rad** has an absorption peak at 295.36 nm with an oscillator strength of f = 0.0362 and that the N-centered aminyl radical, **N-rad**, has a strong absorption peak at 290 nm with an oscillator strength (f) of 0.0238 (SI). Our experimental lifetimes of the radicals in the LFP agree with the lifetimes reported in the literature sources and with the calculated data.

https://doi.org/10.1021/acs.joc.4c02997
J. Org. Chem. XXXX, XXX, XXX−XXX

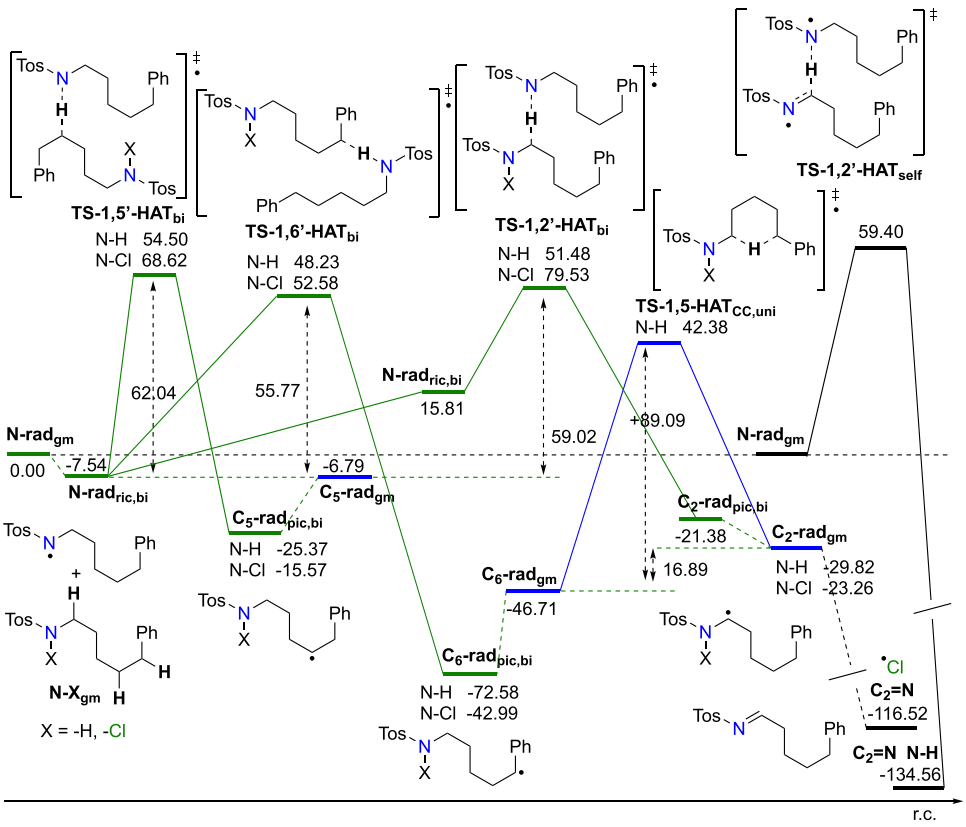

Figure 6. Energy diagram of intra- and intermolecular radical rearrangements to relevant C-centered radicals derived from **N-H** and **N-Cl**, and recombination through self-reaction to C_2=**N** and **N-H** species. Calculated at the RO-B2PLYP/G3MP2Large(SMD,CH_3CN)//B3LYP/6-31G(d) level of theory. Global minima of separated reactants, namely, **N-rad$_{gm}$**, **N−Cl$_{gm}$**, and **N−H$_{gm}$**, were taken as the starting point in the bimolecular reaction, while the global minimum structure on the reactant side, **N-rad$_{gm}$**, was taken as the starting point in the unimolecular process, and the dimer of **N-rad$_{gm}$** was taken as the starting point for the self-reaction. Units are in kJ mol^{-1}.

This leads us to the conclusion that we have observed an N-centered aminyl radical and benzylic-type **C$_6$-rad** in the LFP experiments.

As seen in Figure 2, there is a **C$_2$-rad** in the EPR spectra that can be formed via HAT from either **C$_6$-rad** (**1,5-HAT$_{CC,uni}$**) or **N-rad** (**1,2'-HAT$_{bi}$**). A similar radical has been observed in the EPR spectra in the *N*-hexyl-4-methylbenzenesulfonamide system.[16] When compared to the other bimolecular HAT reactions (Figure 6), the barrier for the formation via **1,2'-HAT$_{bi}$** is between the barriers for the C-centered alkylic-type radical and benzyl-type radical. Thermodynamically, **C$_2$-rad** is the second most stable C-centered radical, with stability closer to the **C$_6$-rad** than the **C$_5$-rad**. Calculated reaction energies for all these processes are slightly higher than the barriers calculated in the 1,6-pathway. This is especially true for the unimolecular HAT converting **C$_6$-rad** to **C$_2$-rad**, with the highest calculated barrier of $\Delta G^{\ddagger}_{298}$ = +89.1 kJ mol^{-1}. However, the **C$_2$**=**N** imine species, the product observed in the NMR experiment, is generated primarily by the self-reaction of two **N-rad** (see above) and then from **C$_2$-rad**. Another pathway for imine production involves 1,2'-HAT transfer between **N-Cl** and **N-rad**, but this reaction is kinetically less favored with a higher calculated barrier ($\Delta G^{\ddagger}_{298}$ = +79.53 kJ/mol).

At this point, it is worth noting that the first-order decay kinetics shown in the insets of Figure 4 does not reach zero but forms an onset close to zero. This implies that there is a steady state for a C-centered radical intermediate, which is presumably an intermediate species in the propagation cycle. Furthermore, the decay kinetics for **C$_6$-rad** can only be accurately described if the rate constant for the preceding elementary reaction is significantly larger or larger than the rate constant of the subsequent elementary reaction, assuming that these rate constants are the primary contributors to the observed experimental rate constants. This is corroborated by our DFT calculations as the calculated rate constant (eq 4) for 1,6-HAT is 2.4 × 10^{10} s^{-1}, while for the bimolecular **XAT**, the rate constant is 7 orders of magnitude lower, namely, 4.63 × 10^3 s^{-1}. Additionally, the lifetime of the N-centered aminyl radical **N-rad** is much shorter when compared to the lifetime of the C-centered radical **C$_6$-rad**. This is viable only when the second step is slower than the first. Thus, we conclude that the slow step of the propagation cycle is intermolecular **XAT**. On the product side, the first local minimum encountered is (**C$_6$-Cl−N-rad**)$_{pic,XAT}$ at ΔG_{298} = −112.3 kJ mol^{-1}, which then rearranges to the most stable conformer **C$_6$-Cl$_{gm}$** with an overall Gibbs free energy of reaction of $\Delta G_{298,rx,gm}$ = −137.8 kJ mol^{-1}.

For the 1,5-pathway (Figure 7), the HAT step involves rearrangement from the global minimum on the reactant side (**N-rad$_{gm}$**) to a prereactive conformer (**N-rad$_{ric1,5}$**) that is ΔG_{298} = +23.8 kJ mol^{-1} less stable. From there, transition state **TS-1,5-HAT$_{uni}$** is reached with an overall barrier of $\Delta G^{\ddagger}_{298}$ = +46.6 kJ mol^{-1}. When the barrier is defined from **N-rad$_{ric1,5}$**, it amounts to only 22.8 kJ mol^{-1}, which includes a fast rearrangement step between high-energy conformer **N-rad$_{hc,pic}$** and **N-rad$_{ric1,5}$**. On the product side, the first local minimum encountered is **C$_5$-rad$_{pic}$** at ΔG_{298} = −1.9 kJ mol^{-1}, which then

https://doi.org/10.1021/acs.joc.4c02997
J. Org. Chem. XXXX, XXX, XXX−XXX

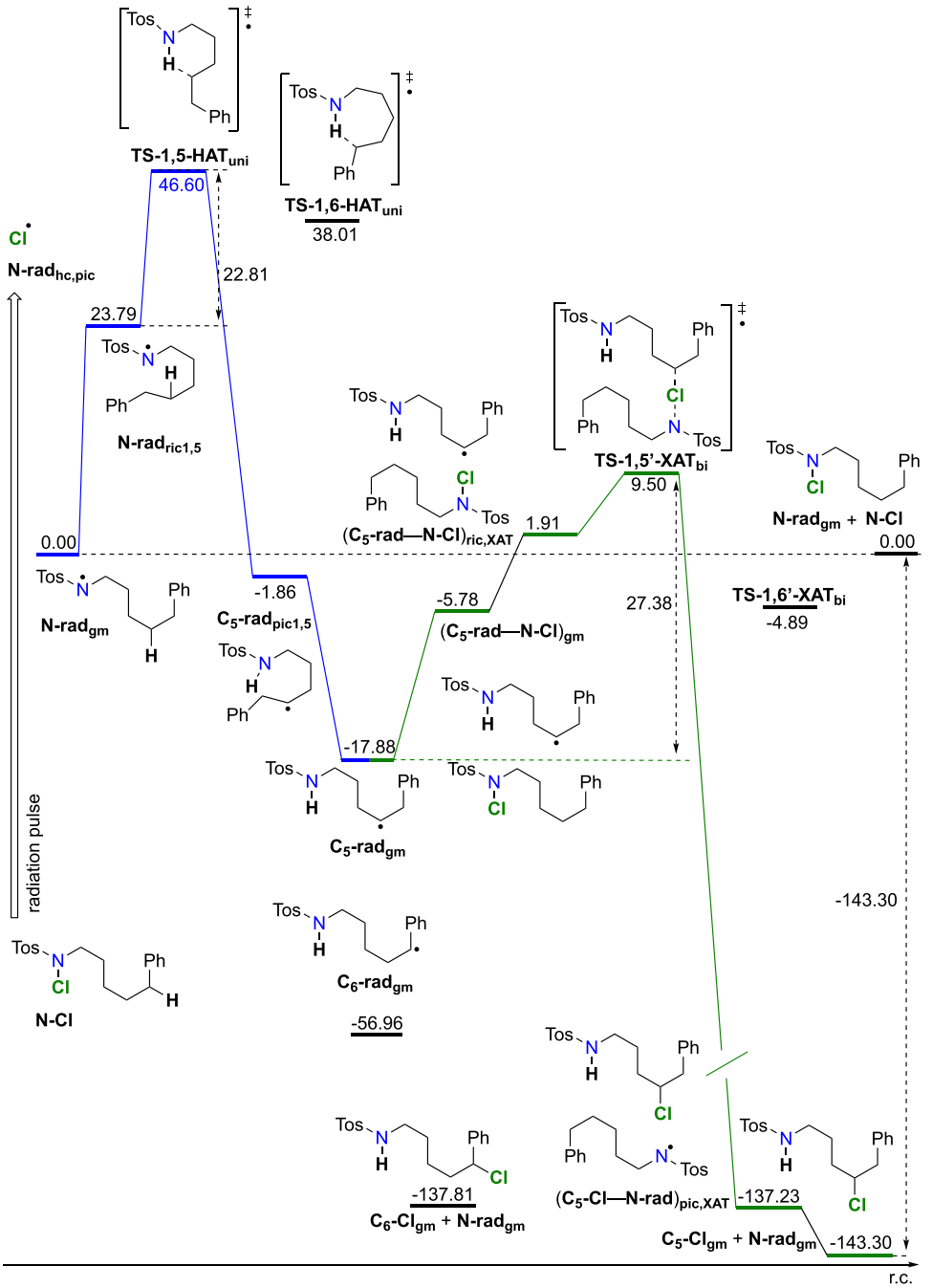

Figure 7. Energy diagram of intra- and intermolecular radical rearrangements for the propagation cycle of HLF for the 1,5-pathway. From the starting N-centered radical **N-rad**, it rearranges via **TS-1,5-HAT** to the **C$_5$-rad**. The next step is the bimolecular reaction from **C$_5$-rad** and **N-Cl**, via **TS-1,5′-XAT**, to **C$_5$-Cl** and **N-rad** formation. Calculated at RO-B2PLYP/G3MP2Large(SMD,CH_3CN)//B3LYP/6-31G(d) level of theory. Included in the diagram are chosen points of the 1,6-pathway. The global minimum structure on the reactant side, **N-rad$_{gm}$**, was taken as the starting point in unimolecular process, while the global minima of separated reactants, namely, **N-rad$_{gm}$** and **N-Cl$_{gm}$**, were taken as the starting point in bimolecular reaction. Units are in kJ mol^{-1}.

rearranges to the most stable conformer **C$_5$-rad$_{gm,uni}$** with an overall Gibbs free energy of reaction of ΔG_{298} = −17.9 kJ mol^{-1}. Species needed for the bimolecular reaction, namely, the **C$_5$-rad** radical and **N-Cl**, are still separated in the solvent. When they meet in the solvent cage due to diffusion, the complex **(C$_5$-rad−N-Cl)$_{gm,bi}$** is formed at ΔG_{298} = 1.9 kJ mol^{-1}, which leads to the prereactive conformer of the **XAT** reaction **(C$_5$-rad−N-Cl)$_{ric,XAT}$** at ΔG_{298} = 5.8 kJ mol^{-1}. From there, the transition state is reached with an overall barrier of $\Delta G^{\ddagger}_{298,gm}$**(1,5′-XAT$_{bi}$)**= +27.4 kJ mol^{-1}, while it amounts to $\Delta G^{\ddagger}_{298,ric}$**(1,5′-XAT$_{bi}$)** = 7.6 kJ mol^{-1} when the barrier is defined as in eq 2. On the product side, the first local minimum encountered is **(C$_5$-Cl−N-rad)$_{pic,XAT}$** at ΔG_{298} = −137.2 kJ mol^{-1}, which then rearranges to the most stable conformer **C$_6$-Cl$_{gm}$** with an overall Gibbs free energy of reaction of $\Delta G_{298,rx,gm}$ = −143.3 kJ mol^{-1}. To check if the **C$_5$-rad** radical moiety was detected in our LFP measurements at 290 nm, we have done TD-DFT calculations that show that it has a strong absorption peak at 238.04 nm with an oscillator strength of f = 0.0290

https://doi.org/10.1021/acs.joc.4c02997
J. Org. Chem. XXXX, XXX, XXX−XXX

(SI). This excludes the possibility of it being detected in this experimental setup.

The complete energy schemes (Figures 5 and 7) for the 1,6- and 1,5-pathways allow us to compare similarities between the two processes. As observed, we notice that there is an early transition state for the second step and that the second step is irreversible, which in turn makes the whole cycle irreversible, even though the N-centered aminyl radical is regenerated. Furthermore, there is no thermodynamic preference for the formation of **C6-Cl** over **C5-Cl**, with both products in the same energy range (∼−140 kJ mol^{-1}), as compared to the starting **N-Cl** compound. The definition of the barrier from the global minimum, as in eq 3, describes experimental results much better for the second step, namely, the XAT reaction, while the definition of the barrier from the prereactive minimum, as in eq 2, fits much better with the experimental results for the first step, namely, the HAT step. Moreover, NMR analysis of the product mixture in toluene shows that we have 71.5% **C_6-Cl** and 28.5% **C_5-Cl**. This is an indication that the kinetics of the HAT step determines regioselectivity, as the barrier for 1,6-HAT is 13.8 kJ mol^{-1} and that for 1,5-HAT is 23.8 kJ mol^{-1}. When Bodenstein approximation of quasi-stationary behavior[39,40] and the long chain approximation are applied to radical chain reactions, the reaction rates of the individual steps in the cycle are equal. However, different rate constants strongly imply the quite large steady-state concentration of the C-centered radicals, **C_5-rad** and **C_6-rad**, each in its own cycle, compared to **N-rad** created in the propagation step. When these approximations are applied in our kinetic model, we obtained that the HLF reaction follows pseudo-first-order kinetics with respect to the second step. Thus, we propose that the rate of the propagation cycle of the HLF reaction is controlled by the XAT step, which is additionally supported by both the LFP experiments and DFT calculations.

There is another interpretation of the reaction sequence in the literature, which was proposed by Muñiz for the selective synthesis of piperidines.[26] Instead of uni(intra)molecular HAT, they considered a bi(inter)molecular HAT, where the N-centered succinimide radical extracts selectively only the C_6-H, providing the C-centered benzylic radical. Since there is no outside chlorinating agent in our reaction (halogenation was performed in the previous reaction step and quantitatively removed), the only possible **1,6'-HAT_{bi}** is the reaction of **N-rad** with **N-Cl**, where the hydrogen extraction comes from the N-Cl species. The calculated barrier is $\Delta G^{\ddagger}_{298,ric}$(**1,6'-$HAT_{bi}$**) = +52.6 kJ mol^{-1}, which corresponds to a $t_{1/2}$ of 8.73 ms for the **N-Cl−C_6-rad** species. Similar results, $\Delta G^{\ddagger}_{298,ric}$(**1,5'-$HAT_{bi}$**) = +68.62 kJ mol^{-1} and $t_{1/2}$ of 98.28 ms, are obtained for the 1,5-pathway (see Figure 6). This is in stark contrast to the experimental values obtained from the LFP experiments, where degradation is much quicker. Products of these reactions, **N-Cl−C_6-rad** and **N-Cl−C_5-rad**, are lower in energy, with a thermodynamic driving force of − 43.0 and − 15.6 kJ mol^{-1}, respectively. As discussed above, **C_2-rad** is also a good candidate for the HAT reaction.[16] Yet this radical or downstream products (imine and **C_2-Cl**) were not observed in the Muñiz synthesis,[26] which is another reason why this reaction should be re-examined. After the C-centered radical formation, a uni(intra)molecular XAT process can be envisioned as the final step in the reaction sequence. It should be noted that Muñiz and co-workers make this a bimolecular XAT process with their halogen source (*N*-bromo-succinimide complex with I_2). For the unimolecular TS-1,6-XAT, from the **N-Cl−C_6-rad_{ric}** structure, the kinetic barrier is $\Delta G^{\ddagger}_{298,ric}$(**1,6-$XAT_{uni}$**) = +101.9 kJ mol^{-1} due to a very extended structure. The thermodynamics of this reaction is exergonic, with postreactive intermediate complex **N-rad−C_6-Cl_{pic}** being −70.5 kJ mol^{-1}. For the similar unimolecular TS-1,5-XAT, the reaction barrier is lower ($\Delta G^{\ddagger}_{298,ric}$(**1,5-$XAT_{uni}$**) = +75.1 kJ mol^{-1}), with thermodynamics of this step comparable to the 1,6-XAT. It should be noted that the starting points for both **XAT_{uni}** processes, namely, **N-Cl−C_6-rad_{ric}** and **N-Cl−C_5-rad_{ric}**, have a 50.4 kJ mol^{-1} difference in energy, with the benzyl type of C-radical more stable than the alkyl type of C-radical. In conclusion, pathways with bimolecular HAT and unimolecular XAT are unfavorable and thus should be excluded as possible mechanisms of the propagation cycle.

To support our experimental and computational results, we have done kinetic modeling of the HLF reactions in the case when only one major product is formed in a yield greater than 99%. In our kinetic modeling, we applied a steady-state approximation for the concentration of the N-centered radical **N-rad**, which we consider reasonable since the **N-rad** is continuously consumed and regenerated throughout the reaction cycle (see Section S12 in the SI)Section S12 in the SI). This approximation also indirectly implies steady states for the **C_5-rad** and **C_6-rad** intermediates, as their concentrations are tied to the steady state behavior of **N-rad** through the dominant **C_6-Cl** pathway. Additionally, the reverse reactions in the second step of each pathway (reactions from chlorinated products **C_5-Cl**, **C_6-Cl**, and **C_2−Cl** back to their respective radicals and **N-Cl**) were neglected. This is supported by Gibbs energy profiles (Figures 5−7), which indicate significantly higher energy barriers for these reverse reactions. As a result, they are unlikely to contribute significantly to the overall kinetics. Using the approximations, we derived a simplified equation that describes the formation of all (final) chlorinated products, as presented in eq 1.

$$\mathbf{C_6} - \mathrm{rad} + \mathrm{N} - \mathrm{Cl} \underset{k_{5r}}{\overset{k_{5f}}{\rightleftharpoons}} \mathbf{C_6} - \mathrm{Cl} + \mathrm{N} - \mathrm{rad}$$

$$[\mathrm{product}](t) = c_{max}(\mathrm{product})(1 - e^{-k_{5f}[C_6]_0 t}) \quad (1)$$

Here, c_{max} represents the maximum concentration of the product, while k_{5f} and k_{5r} denote forward and reverse rate constants, respectively. The full derivation is presented in the SI. The exponent $-k_{5f}[C_6]_0$ applies to all products as **N-Cl** depletion is predominantly controlled by the **C_6-Cl** pathway. As this pathway dictates the overall reaction kinetics, the time-dependent behavior of all products follows the same exponential decay. This pseudo-first-order approximation is in good accordance with the experimental data from the LFP measurements. In addition, we also estimated the reaction half-lives and product ratios, which support the model's consistency and generally align with the experimental data (see Section S12 in the SI).Section S12 in SI).

Understanding that XAT is the bottleneck step in the HLF reaction is crucial for controlling the reaction kinetics, predicting the duration of each step and the overall process, and designing specific termination steps.[69] Formed carbon-centered radicals can react with common halogenating agents in a one-pot reaction setup, such as trichloroisocyanuric acid (TCICA), *N*-chlorosuccinimide (NCS), *N*-bromosuccinimide (NBS), *N*-iodosuccinimide (NIS), or even iodine/sodium

https://doi.org/10.1021/acs.joc.4c02997
J. Org. Chem. XXXX, XXX, XXX−XXX

Scheme 3. Propagation vs Termination Step in the HLF Reactions[a]

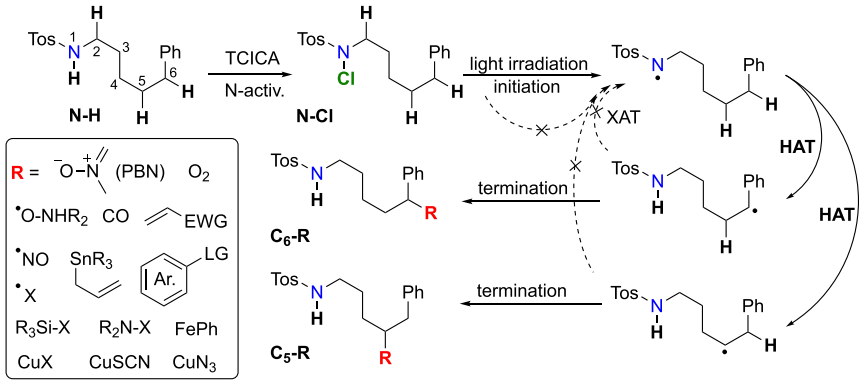

[a]Different selection of termination traps may compete with XAT and the closing of the propagation site.

iodide (I_2/NaI), with lower or negligible activation barriers, leading to functionalized sp^3-hybridized carbon centers (see Scheme 3). This pathway bypasses the propagation step, where nitrogen-centered radicals are converted to carbon-centered radicals that promptly terminate with the halogen source. New nitrogen-centered radicals must then be generated via irradiation, which can occur under one-pot reaction conditions, where N-halogenation happens simultaneously with the HLF reaction.Scheme 3

Moreover, this mechanism opens possibilities for remote δ- and ε-site functionalization if suitable targets for radical addition are present. For such transformations to occur, the termination reaction must be both faster than the XAT step and thermodynamically more favorable than the halogenated products. An example is the reaction of carbon-centered radicals with a PBN spin trap, yielding an extremely stable NO-type radical in our EPR experiments. Other potential reactions can involve weakly bonded main group molecules (N−X, Si−X, Sn−H, and Sn−allyl), metal salts (CuX, CuSCN, and CuN_3), and π-systems (alkenes and arenes). We are currently exploring these possibilities in our laboratory and encourage other researchers to investigate these avenues, as they may lead to novel strategies in radical chemistry and synthetic methodologies.

CONCLUSIONS

Using NMR spectroscopy, laser flash photolysis LFP, and EPR spectroscopy in combination with DFT calculations and kinetic modeling, we monitored the reaction profile and identified significant intermediate radicals and products in the Hofmann−Löffler−Freytag reaction (HLF). Our results indicate that there is no thermodynamic preference for the formation of **C_6-Cl** over **C_5-Cl**, and the difference in ratios (72 vs 28%, respectively) is due to the **C_6-Cl** being a kinetic product. Thus, the kinetics of the HAT step in the propagation cycle guides the regioselectivity of the HLF reaction, and by calculating the barrier for the HAT step, we can predict the major product formed. Moreover, we deduce that the slow step of the HLF reaction is the bimolecular XAT step. Additionally, we propose that adding halogen sources, typically used as chlorinating agents, or other traps may interfere with the XAT step of the propagation cycle, promoting the earlier termination of a reaction cycle. We recommend that future research on radical mechanisms be conducted using a combination of experimental techniques paired with rigorous quantum-chemical calculations and kinetic modeling for a comprehensive overview of the reaction.

MATERIALS AND METHODS

The purchased compounds were sourced from Sigma-Aldrich (St. Louis, MO, USA) (trichloroisocyanuric acid (TCICA), Celite S, hydrochloric acid (37%), acetone, silicone oil, petroleum ether, and cyclohexane), Fisher Scientific (Waltham, MA, USA) (toluene (anhydrous), acetonitrile (anhydrous), 1,4-dioxane (anhydrous), tetrahydrofuran (anhydrous), *N*,*N*-dimethylformamide (anhydrous), *N*,*N*-dimethylacetamide, 1,2-dichloroethane (anhydrous), dichloromethane (anhydrous), dichloromethane (CH_2Cl_2)), and Kemika (Zagreb, Croatia) (sodium hydroxide). All reagents and chemicals were obtained commercially and used without further purification unless otherwise noted. The starting material, 4-methyl-*N*-(5-phenylpentyl)benzenesulfonamide, **N-H**, was provided by the research group of Prof. Hendrik Zipse from Ludwig-Maximilian University, Munich, Germany, and ^{1}H and ^{13}C{^{1}H} NMR spectra values of the compound (see the SI) correspond to the previously reported values.[26]

Chromatographic purification of the products was carried out using column chromatography filled with silica gel (Macherey-Nagel) 0.063−0.2 mm, and appropriate solvent mixtures of petroleum ether/ethyl acetate were used as eluents. Thin-layer chromatography (TLC) was performed on precoated ALUGRAM SIL G/UV254 0.20 mm silica gel 60 plates with a fluorescent indicator UV254 (Macherey-Nagel) in the appropriate solvent system. TLC spots were observed via the illumination with UV light at a wavelength of 254 nm after the immersion of the plate in an aqueous solution of $KMnO_4$ (3 g $KMnO_4$, 20 g K_2CO_3, 5 mL aq. NaOH 5%, and 300 mL water) followed by heating. If TLC spots were not visible after illumination with UV light, they were detected using an iodine chamber.

NMR spectra of the reaction mixture were obtained on a Varian Inova 400 NMR spectrometer operating at 399.90 MHz for ^{1}H NMR and 100.6 MHz for ^{13}C{^{1}H} NMR and are reported as chemical shifts (δ) in ppm. The spectra were imported and processed in the MestreNova 11.0.4 program.[41]

EPR spectroscopy was performed by using a Bruker ELEXSYS E500 EPR spectrometer with an ER4122SHQE cavity resonator. As this cavity resonator does not have an optical window for illumination, the light source was mounted underneath the cavity with light coming through the bottom of the EPR 4 mm inner-diameter tube. EPR deconvolution and simulation were done using an EasySpin module with the MATLAB program package.[42] EPR visualization and spectroscopy were done using the VisualEPR Web page.[43] For experiments, 35 mg of **N-Cl** was dissolved in the 0.3 mL of solvent (~0.04 M), degassed, and then mixed with degassed 10 mg of **PBN** dissolved in 0.3 mL of the same solvent (~0.015 M).

Transient absorption spectroscopy (TAS) measurements were performed by using a nanosecond laser flash photolysis setup. The

https://doi.org/10.1021/acs.joc.4c02997
J. Org. Chem. XXXX, XXX, XXX−XXX

setup consisted of a Nd:YAG laser (Quantel, Q-smart 450) and an LP980 transient absorption spectrometer (Edinburgh Instruments). The ground state absorption of the samples was adjusted to 0.3 at the 266 nm laser excitation wavelength (5 ns pulse duration and 10 Hz). The laser pulse energy at 266 nm was in the range of 10−23 mJ (30−70 mJ cm^{-2}). Kinetic measurements were performed in 1 cm quartz cells sealed with rubber septa. The transient absorption spectra were measured in a flow cell with a flow rate set to 2.4 mL/min to ensure that no light was absorbed by the photoproducts. All solutions were prepared immediately before the experiments. Solutions were purged with high-purity N_2 for 20 min prior to the kinetics measurements and for 1 h before spectra measurements. All measurements were performed at 25 °C. UV−vis spectra of the sample solutions were recorded by using a Varian Cary 4000 spectrophotometer (Figures S15 and S16).

The conformational space for all the local minima and saddle points of the first order on the energy diagram was investigated using the Conformer−Rotamer Ensemble Sampling Tool (CREST)[44] coupled with the xtb-GFN2 program package and meta-dynamics simulation using xtb-GFN1[45] and xtb-GFN2.[46] The obtained structures were reoptimized using the B3LYP/6-31G(d) level of theory.[47−49] For each structure with a stable wave function, a frequency calculation was performed to identify the minima and transition-state structures. The lowest lying conformers, e.g., with the lowest energy value, for each species were labeled global minima (gm) on the potential energy surface (PES). Transition state structures were differentiated from the minima by having exactly one imaginary frequency. From all transition state conformers, an intrinsic reaction coordinate (IRC) search was performed to characterize the corresponding reaction/product channel, and the last point in the forward and reverse direction was then optimized to the nearest local minimum, i.e., reactive complex. On the reactant side, the obtained structure was termed prereactive intermediate complex (ric), while on the product side, the optimized structure was named postreactive intermediate complex (pic). Single point energies were obtained with the universal continuum solvation model SMD,[50] with acetonitrile as a solvent and RO-B2PLYP[52,53] with a G3MP2 large basis set[54] on geometries obtained at the B3LYP/6-31G(d) level of theory, with additional D3 dispersion correction.[55] The thermal corrections to the free energy were derived from the frequency calculations under conditions of 298.15 K and 1 atm. The activation free energies ($\Delta G^{\ddagger}_{298}$) of each elementary reaction are defined in two distinct ways through the following equations:

$$\Delta G^{\ddagger}_{298,\mathrm{ric}} = G(\text{transition state}) - G(\text{reactant complex}) \quad (2)$$

$$\Delta G^{\ddagger}_{298,\mathrm{gm}} = G(\text{transition state}) - G(\text{global minimum}) \quad (3)$$

According to transition state theory (TST),[56,57] approximate reaction rate constants for elementary reactions, in which the reactants directly generate products, were estimated based on the Eyring−Polanyi equation as eq. 4:

$$k_{\mathrm{calc}} = \frac{k_B T}{h} e^{-\Delta G^{\neq}/RT} \quad (4)$$

where k_B is the Boltzmann constant, T is the temperature, h is Planck's constant, R is the molar gas constant, and $\Delta G^{\ddagger}$ is the activation free energy.

Calculations of EPR parameters were done using the B3LYP functional and a mixed basis set: EPR-III was used for C, H, and O atoms; def2-QZVP was used for the S atom; and 6−31G(d) was used for the N atom. A small basis set on the N atom is necessary for the correct calculations of the *g*-factor and hyperfine constants (*hfc*).[58,59] When using a larger basis set for the N atom, e.g., EPR-III or def2-QZVP, the obtained results systematically underestimate the *hfc*. Calculations were performed on Gaussian version 16.C01[60] using the advanced computing service (clusters Isabella and Supek) provided by the University of Zagreb University Computing Centre (SRCE)[61] and the computational resources of the PharmInova project (sw.pharma.hr) at the University of Zagreb Faculty of Pharmacy and Biochemistry.[62]

Electronic transition spectra were calculated at the gas phase and in acetonitrile with the time-dependent[63] CAM-B3LYP[64]/TZVP/PCM[51] method at the molecular geometries optimized at the B3LYP/TZVP level.

To account for the entropic effect of the presence of solvent molecules around a solute, the cell model presented by Ardura et al. was used.[65] This model is proposed to explicitly evaluate the effect of the loss of translation degrees of freedom in solution on the Gibbs activation energy in a bimolecular (or higher order of molecularity) reaction.[66]

We performed kinetic modeling of the reaction pathways, with the full model described in detail in Section S12 of the Supporting Information. The complete mathematical model, which incorporates all possible reaction steps, leads to a system of nonlinear differential equations that is exceedingly complex and likely impossible to solve analytically due to the nonlinearity and the interdependence of the species' concentrations.[67−70] Numerical methods like Runge−Kutta could be applied; however, the potential solution may be highly sensitive to the initial conditions, particularly to the concentration of radicals formed after the laser pulse.[71,72] In such calculations, the uncertainty in starting conditions may induce numerical instability.[69,73,74] Therefore, some necessary approximations were applied to reduce the complexity of the model.

■ ASSOCIATED CONTENT

Data Availability Statement

The data underlying this study are available in the published article and its Supporting Information.

Supporting Information

The Supporting Information is available free of charge at https://pubs.acs.org/doi/10.1021/acs.joc.4c02997.

Supporting information with experimental details, synthesis procedure, reactant and product characterization, EPR simulation parameters, calculation procedures, geometries and energies of optimized structures, and recorded NMR and EPR spectra (PDF)

■ AUTHOR INFORMATION

Corresponding Author

Davor Šakić − *University of Zagreb Faculty of Pharmacy and Biochemistry, Zagreb 10000, Croatia;* orcid.org/0000-0002-8871-6622; Email: davor.sakic@pharma.unizg.hr

Authors

Gabrijel Zubčić − *University of Zagreb Faculty of Pharmacy and Biochemistry, Zagreb 10000, Croatia;* orcid.org/0000-0003-3264-5826

Luka Andrijanić − *University of Zagreb Faculty of Science, Zagreb 10000, Croatia*

Iva Džeba − *Ruđer Bošković Institute, Zagreb 10000, Croatia*

Jiangyang You − *Ruđer Bošković Institute, Zagreb 10000, Croatia;* orcid.org/0000-0001-8881-9448

Tomislav Friganović − *University of Zagreb Faculty of Science, Zagreb 10000, Croatia*

Tomislav Portada − *Ruđer Bošković Institute, Zagreb 10000, Croatia;* orcid.org/0000-0002-7139-0881

Kristina Pavić − *University of Zagreb Faculty of Pharmacy and Biochemistry, Zagreb 10000, Croatia;* orcid.org/0000-0002-8523-6340

Erim Bešić − *University of Zagreb Faculty of Pharmacy and Biochemistry, Zagreb 10000, Croatia*

https://doi.org/10.1021/acs.joc.4c02997
J. Org. Chem. XXXX, XXX, XXX−XXX

Valerije Vrček − *University of Zagreb Faculty of Pharmacy and Biochemistry, Zagreb 10000, Croatia;* orcid.org/0000-0003-1624-8126

Complete contact information is available at: https://pubs.acs.org/10.1021/acs.joc.4c02997

Author Contributions

G.Z. conceived the idea for this work; G.Z. and D.Š. did computational work; K.P. and T.P. purified and prepared chemicals and respective solvents; L.A. and I.Dž. carried out the LFP experiments and data processing; E.B. and J.Y. did EPR studies; V.V. was responsible for NMR measurement and analysis; kinetic modeling was done by T.F.; supervision was provided by I.Dž., E.B., V.V., and D.Š.; and G.Z. and D.Š. wrote the manuscript with input from all authors. All authors participated in the discussion and revision of the manuscript.

Notes

The authors declare no competing financial interest.

■ ACKNOWLEDGMENTS

The authors would like to acknowledge the financial support from the Croatian Science Foundation Installation Grant UIP-2020-02-4857 LIGHT-N-RING and Research Grant IP-2022-10-2634 Pharma-Eco and the computational resources provided by the Advanced Computing Service on Cluster Supek, EU funded through KK.01.1.1.08.0001, at the University of Zagreb University Computing Centre (SRCE). Support from The Cryogenic Centre at the Institute of Physics (project KaCIF, KK.01.1.1.02.0012) is acknowledged. This work was also supported by the project FarmInova (KK.01.1.1.02.0021), funded by the European Regional Development Fund, and Croatian Science Foundation Research Grant IP-2019-04-8846. The authors would like to thank Prof. Hendrik Zipse and Dr. Salavat Ashirbaev from Ludwig-Maximilian University for collaboration and Assoc. prof. Boris Maryasin for fruitful discussions.

■ REFERENCES

(1) Hofmann, A. W. Ueber die Einwirkung des Broms in alkalischer Lösung auf Amide. *Ber. Dtsch. Chem. Ges.* **1881**, *14* (2), 2725−2736.
(2) Lellmann, E. Ueber die Conicëine. *Justus Liebigs Ann. Chem* **1890**, *259* (2-3), 193−208.
(3) Freytag, C. Über eine neue Bildungsweise von *N*-alkylierten Pyrrolidine. *Ber. Dtsch. Chem. Ges.* **1909**, *42* (3), 3427−3431.
(4) Wolff, M. E. Cyclization of N-Halogenated Amines (The Hofmann-Löffler Reaction). *Chem. Rev.* **1963**, *63* (1), 55−64.
(5) Wawzonek, S.; Thelen, P. J. Preparation of N-Methylgranatanine. *J. Am. Chem. Soc.* **1950**, *72* (5), 2118−2120.
(6) Corey, E. J.; Hertler, W. R. A Study of the Formation of Haloamines and Cyclic Amines by the Free Radical Chain Decomposition of N-Haloammonium Ions (Hofmann-Löffler Reaction) [1]. *J. Am. Chem. Soc.* **1960**, *82* (7), 1657−1668.
(7) Hernández, R.; Medina, M. C.; Salazar, J. A.; Suárez, E.; Prangé, T. Intramolecular Functionalization of Amides Leading to Lactams. *Tetrahedron Lett.* **1987**, *28* (22), 2533−2536.
(8) de Armas, P.; Francisco, C. G.; Hernandez, R.; Salazar, J. A. Steroidal N-Nitroarnines. Part 4.'Intramolecular Functionalization of N - Nitroamine Radicals: Synthesis of I, 4-Nitroimine Compounds. *J. Chem. Soc., Perkin Trans. 1* **1988**, *11*, 3255.
(9) Dorta, R. L.; Francisco, C. G. Hypervalent Organoiodine Reagents in the Transannular Functionalisation of Medium-Sized Lactams: Synthesis of I-Azabicyclo Compounds. *J. Chem. Soc., Chem. Commun.* **1989**, *16*, 1168−1169.
(10) Carrau, R.; Hernández, R.; Suárez, E.; Betancor, C. Intramolecular Functionalization of N-Cyanamide Radicals: Synthesis of 1,4-and 1,5-N-Cyanoepimino Compounds. *J. Chem. Soc., Perkin Trans. 1* **1987**, *0*, 937−943.
(11) Reddy, L. R.; Reddy, B. V. S.; Corey, E. J. Efficient Method for Selective Introduction of Substituents as C(5) of Isoleucine and Other α-Amino Acids. *Org. Lett.* **2006**, *8* (13), 2819−2821.
(12) Coleman, G. H.; Goheen, G. E. Preparation of Pyrrolidines. *J. Am. Chem. Soc.* **1938**, *60* (3), 730.
(13) Corey, E. J.; Hertler, W. R. A Study of the Formation of Haloamines and Cyclic Amines by the Free Radical Chain Decomposition of N-Haloammonium Ions (Hofmann-Löffler Reaction)[1]. *J. Am. Chem. Soc.* **1960**, *82* (7), 1657−1668.
(14) Minisci, F. Free-Radical Additions to Olefins in the Presence of Redox Systems. *Acc. Chem. Res.* **1975**, *8* (5), 165−171.
(15) Wawzonek, S.; Nelson, M. F.; Thelen, P. J. Preparation of Quinuclidines [1]. *J. Am. Chem. Soc.* **1951**, *73* (6), 2806−2808.
(16) Zubčić, G.; You, J.; Zott, F. L.; Ashirbaev, S. S.; Kolympadi Marković, M.; Bešić, E.; Vrček, V.; Zipse, H.; Šakić, D. Regioselective Rearrangement of Nitrogen- and Carbon-Centered Radical Intermediates in the Hofmann−Löffler−Freytag Reaction. *J. Phys. Chem. A* **2024**, *128* (13), 2574−2583.
(17) Neale, R. The Chemistry of Nitrogen Radicals. V. The Free-Radical Addition of Dialkyl-N-Chloramines to Olefinic and Acetylenic Hydrocarbons. *J. Org. Chem.* **1967**, *32* (11), 3263−3273.
(18) Neale, R. S.; Hinman, R. L. The Chemistry of Ion Radicals. The Free Radical Addition of N-Chlorodialkylamines to Butadiene. *J. Am. Chem. Soc.* **1963**, *85* (17), 2666−2667.
(19) Neale, R. S.; Marcus, N. L. Chemistry of Nitrogen Radicals. VI. The Free-Radical Addition of Dialkyl-N-Chloramines to Substituted Olefins. *J. Org. Chem.* **1967**, *32* (11), 3273−3284.
(20) Stein, C.; Tyler, J. L.; Wiener, J.; Boser, F.; Daniliuc, C. G.; Glorius, F. Anomeric Amide-Enabled Alkene-Arene and Alkene-Alkene Aminative Coupling. *Angew. Chem. Int. Ed* **2025**, *64* (5), No. e202418141.
(21) Constantinou, C. T.; Gkizis, P. L.; Lagopanagiotopoulou, O. T. G.; Skolia, E.; Nikitas, N. F.; Triandafillidi, I.; Kokotos, C. G. Photochemical Aminochlorination of Alkenes without the Use of an External Catalyst. *Chem. - Eur. J.* **2023**, *29* (45), No. e202301268.
(22) Šakić, D.; Zipse, H. Radical Stability as a Guideline in C-H Amination Reactions. *Adv. Synth. Catal.* **2016**, *358* (24), 3983−3991.
(23) Hioe, J.; Šakić, D.; Vrček, V.; Zipse, H. The Stability of Nitrogen-Centered Radicals. *Org. Biomol. Chem.* **2015**, *13* (1), 157−169.
(24) Hioe, J.; Zipse, H. Radical Stability—Thermochemical Aspects. In *Encyclopedia of Radicals in Chemistry, Biology and Materials*; Chatgilialoglu, C., Studer, A., Eds.; Wiley, 2012. .
(25) Shkunnikova, S.; Zipse, H.; Šakić, D. Role of Substituents in the Hofmann−Löffler−Freytag Reaction. A Quantum-Chemical Case Study on Nicotine Synthesis. *Org. Biomol. Chem.* **2021**, *19* (4), 854−865.
(26) Zhang, H.; Muñiz, K. Selective Piperidine Synthesis Exploiting Iodine-Catalyzed C $_{sp}$ ^{3} − H Amination under Visible Light. *ACS Catal.* **2017**, *7* (6), 4122−4125.
(27) Short, M. A.; Shehata, M. F.; Sanders, M. A.; Roizen, J. L. Sulfamides Direct Radical-Mediated Chlorination of Aliphatic C−H Bonds. *Chem. Sci.* **2020**, *11* (1), 217−223.
(28) Short, M. A.; Blackburn, J. M.; Roizen, J. L. Sulfamate Esters Guide Selective Radical-Mediated Chlorination of Aliphatic C−H Bonds. *Angew. Chem., Int. Ed.* **2018**, *57* (1), 296−299.
(29) Short, M. A.; Blackburn, J. M.; Roizen, J. L. Modifying Positional Selectivity in C−H Functionalization Reactions with Nitrogen-Centered Radicals: Generalizable Approaches to 1,6-Hydrogen-Atom Transfer Processes. *Synlett* **2020**, *31* (02), 102−116.
(30) Short, M. A.; Shehata, M. F.; Sanders, M. A.; Roizen, J. L. Sulfamides Direct Radical-Mediated Chlorination of Aliphatic C−H Bonds. *Chem. Sci.* **2020**, *11* (1), 217−223.
(31) Sutcliffe, R.; Ingold, K. U. Kinetic Applications of Electron Paramagnetic Resonance Spectroscopy. 40. Intramolecular Reactions

of Some N-Alkylcarboxamidyl Radicals. *J. Am. Chem. Soc.* **1982**, *104* (22), 6071−6075.
(32) Rice, F. O.; Grelecki, C. J. The Dimethylamino Radical. *J. Am. Chem. Soc.* **1957**, *79* (11), 2679−2680.
(33) Luo, Y.-R. *Comprehensive Handbook of Chemical Bond Energies*; CRC Press, London, 2007.
(34) Musa, O. M.; Horner, J. H.; Shahin, H.; Newcomb, M. A Kinetic Scale for Dialkylaminyl Radical Reactions. *J. Am. Chem. Soc.* **1996**, *118* (16), 3862−3868.
(35) Esker, J. L.; Newcomb, M. Chemistry of Amidyl Radicals Produced from N-Hydroxypyridine-2-Thione Imidate Esters. *J. Org. Chem.* **1993**, *58* (18), 4933−4940.
(36) Horner, J. H.; Musa, O. M.; Bouvier, A.; Newcomb, M. Absolute Kinetics of Amidyl Radical Reactions. *J. Am. Chem. Soc.* **1998**, *120* (31), 7738−7748.
(37) Le Tadic-Biadatti, M.-H.; Callier-Dublanchet, A.-C.; Horner, J. H.; Quiclet-Sire, B.; Zard, S. Z.; Newcomb, M. Absolute Rate Constants for Iminyl Radical Reactions. *J. Org. Chem.* **1997**, *62* (3), 559−563.
(38) Nagano, M.; Suzuki, T.; Ichimura, T.; Okutsu, T.; Hiratsuka, H.; Kawauchi, S. Production and Excited State Dynamics of the Photorearranged Isomer of Benzyl Chloride and Its Methyl Derivatives Studied by Stepwise Two-Color Laser Excitation Transient Absorption and Time-Resolved Thermal Lensing Techniques. *J. Phys. Chem. A* **2005**, *109* (26), 5825−5831.
(39) Kozuch, S. Steady State Kinetics of Any Catalytic Network: Graph Theory, the Energy Span Model, the Analogy between Catalysis and Electrical Circuits, and the Meaning of "Mechanism.". *ACS Catal.* **2015**, *5* (9), 5242−5255.
(40) Perez-Benito, J. F. Some Considerations on the Fundamentals of Chemical Kinetics: Steady State, Quasi-Equilibrium, and Transition State Theory. *J. Chem. Educ.* **2017**, *94* (9), 1238−1246.
(41) Willcott, M. R. MestRe Nova. *J. Am. Chem. Soc.* **2009**, *131* (36), 13180−13180.
(42) Stoll, S.; Schweiger, A. EasySpin, a Comprehensive Software Package for Spectral Simulation and Analysis in EPR. *J. Magn. Reson.* **2006**, *178* (1), 42−55.
(43) Šakić, D. *DSakicLab/visualEPR*, 2023. https://github.com/DSakicLab/visualEPR (accessed 2024−10−30).
(44) Pracht, P.; Bohle, F.; Grimme, S. Automated Exploration of the Low-Energy Chemical Space with Fast Quantum Chemical Methods. *Phys. Chem. Chem. Phys.* **2020**, *22* (14), 7169−7192.
(45) Bannwarth, C.; Caldeweyher, E.; Ehlert, S.; Hansen, A.; Pracht, P.; Seibert, J.; Spicher, S.; Grimme, S. Extended TIGHT-BINDING Quantum Chemistry Methods. *WIREs Comput. Mol. Sci.* **2021**, *11* (2), No. e1493.
(46) Bannwarth, C.; Ehlert, S.; Grimme, S. GFN2-xTB—An Accurate and Broadly Parametrized Self-Consistent Tight-Binding Quantum Chemical Method with Multipole Electrostatics and Density-Dependent Dispersion Contributions. *J. Chem. Theory Comput.* **2019**, *15* (3), 1652−1671.
(47) Becke, A. D. Density-Functional Thermochemistry. III. The Role of Exact Exchange. *J. Chem. Phys.* **1993**, *98* (7), 5648−5652.
(48) Stephens, P. J.; Devlin, F. J.; Chabalowski, C. F.; Frisch, M. J. Ab Initio Calculation of Vibrational Absorption and Circular Dichroism Spectra Using Density Functional Force Fields. *J. Phys. Chem.* **1994**, *98* (45), 11623−11627.
(49) Ditchfield, R.; Hehre, W. J.; Pople, J. A.; et al. *J. Chem. Phys.* **1971**, *54* (2), 724−728.
(50) Marenich, A. V.; Cramer, C. J.; Truhlar, D. G. Universal Solvation Model Based on Solute Electron Density and on a Continuum Model of the Solvent Defined by the Bulk Dielectric Constant and Atomic Surface Tensions. *J. Phys. Chem. B* **2009**, *113* (18), 6378−6396.
(51) Mennucci, B.; Tomasi, J.; Cammi, R.; Cheeseman, J. R.; Frisch, M. J.; Devlin, F. J.; Gabriel, S.; Stephens, P. J. Polarizable Continuum Model (PCM) Calculations of Solvent Effects on Optical Rotations of Chiral Molecules. *J. Phys. Chem. A* **2002**, *106* (25), 6102−6113.
(52) Grimme, S. Semiempirical Hybrid Density Functional with Perturbative Second-Order Correlation. *J. Chem. Phys.* **2006**, *124* (3), No. 034108.
(53) Neese, F.; Schwabe, T.; Grimme, S. Analytic Derivatives for Perturbatively Corrected "Double Hybrid" Density Functionals: Theory, Implementation, and Applications. *J. Chem. Phys.* **2007**, *126* (12), No. 124115.
(54) Curtiss, L. A.; Redfern, P. C.; Raghavachari, K.; Rassolov, V.; Pople, J. A. Gaussian-3 Theory Using Reduced Mo/Ller-Plesset Order. *J. Chem. Phys.* **1999**, *110* (10), 4703−4709.
(55) Grimme, S.; Antony, J.; Ehrlich, S.; Krieg, H. A Consistent and Accurate *Ab Initio* Parametrization of Density Functional Dispersion Correction (DFT-D) for the 94 Elements H-Pu. *J. Chem. Phys.* **2010**, *132* (15), No. 154104.
(56) Hill, T. L. *An Introduction to Statistical Thermodynamics*. 1st ed.; Dover Publications Inc., New York, 1986.
(57) Steinfeld, J. I., Francisco, J. S., Hase, W. L. *Chemical Kinetics and Dynamics*. 2nd Illustrated ed.; Prentice Hall, 1999.
(58) Vrček, I. V.; Šakić, D.; Vrček, V.; Zipse, H.; Biruš, M. Computational Study of Radicals Derived from Hydroxyurea and Its Methylated Analogues. *Org. Biomol. Chem.* **2012**, *10* (6), 1196−1206.
(59) Hermosilla, L.; Calle, P.; García De La Vega, J. M.; Sieiro, C. Density Functional Theory Study of ^{14} N Isotropic Hyperfine Coupling Constants of Organic Radicals. *J. Phys. Chem. A* **2006**, *110* (50), 13600−13608.
(60) Frisch, M. J.; Trucks, G. W.; Schlegel, H. B.; Scuseria, G. E.; Robb, M. A.; Cheeseman, J. R.; Scalmani, G.; Barone, V.; Petersson, G. A.; Nakatsuji, H.et al.*Gaussian 16, Revision C. 01*. Gaussian, Inc.: Wallingford CT, 2016.
(61) HR-ZOO *Cluster Supek*; University of Zagreb University Computing Centre SRCE. KK.01.1.1.08.0001, EU Funded within OPCC for Republic of Croatia: Zagreb, 2023.
(62) PharmInova Project *Cluster Sw.Pharma.Hr*. University of Zagreb Faculty of Pharmacy and Biochemistry. KK.01.1.1.02.0021, EU Funded by the European Regional Development Fund: Zagreb, 2023.).
(63) Bauernschmitt, R.; Häser, M.; Treutler, O.; Ahlrichs, R. Calculation of Excitation Energies within Time-Dependent Density Functional Theory Using Auxiliary Basis Set Expansions. *Chem. Phys. Lett.* **1997**, *264* (6), 573−578.
(64) Yanai, T.; Tew, D. P.; Handy, N. C. A New Hybrid Exchange−Correlation Functional Using the Coulomb-Attenuating Method (CAM-B3LYP). *Chem. Phys. Lett.* **2004**, *393* (1−3), 51−57.
(65) Ardura, D.; López, R.; Sordo, T. L. Relative Gibbs Energies in Solution through Continuum Models: Effect of the Loss of Translational Degrees of Freedom in Bimolecular Reactions on Gibbs Energy Barriers. *J. Phys. Chem. B* **2005**, *109* (49), 23618−23623.
(66) Šakić, D.; Šonjić, P.; Tandarić, T.; Vrček, V. Chlorination of *N*-Methylacetamide and Amide-Containing Pharmaceuticals. Quantum-Chemical Study of the Reaction Mechanism. *J. Phys. Chem. A* **2014**, *118* (12), 2367−2376.
(67) El-Ajou, A.; Al-ghananeem, H.; Saadeh, R.; Qazza, A.; Oqielat, M. N. A modern analytic method to solve singular and non-singular linear and non-linear differential equations. *Front. Phys.* **2023**, *11*, 1−13.
(68) Cheng, C. M.; Peng, Z. K.; Zhang, W. M.; Meng, G. Volterra-Series-Based Nonlinear System Modeling and Its Engineering Applications: A State-of-the-Art Review. *Mechanical Systems and Signal Processing* **2017**, *87*, 340−364.
(69) Gavalas, G. R. *Nonlinear Differential Equations of Chemically Reacting Systems*; Coleman, B. D., Aris, R., Collatz, L., Ericksen, J. L., Germain, P., Gurtin, M. E., Schiffer, M. M., Sternberg, E., Truesdell, C., Series Eds.; Springer Tracts in Natural Philosophy; Springer Berlin Heidelberg: Berlin, Heidelberg, 1968; Vol. *17*.
(70) Pachpatte, B. G. *Mathematics in Science and Engineering: Nonlinear Integral Inequalities I. 197*; Elsevier, 1998.

https://doi.org/10.1021/acs.joc.4c02997
J. Org. Chem. XXXX, XXX, XXX−XXX

(71) Wang, W.-S.; Li, S.-F.; Su, K. Nonlinear Stability of Runge−Kutta Methods for Neutral Delay Differential Equations. *Journal of Computational and Applied Mathematics* **2008**, *214* (1), 175−185.
(72) Zennaro, M. Asymptotic Stability Analysis of Runge-Kutta Methods for Nonlinear Systems of Delay Differential Equations. *Numerische Mathematik* **1997**, *77* (4), 549−563.
(73) Iserles, A. Stability and Dynamics of Numerical Methods for Nonlinear Ordinary Differential Equations. *IMA J. Numer Anal* **1990**, *10* (1), 1−30.
(74) Ricardo, H. J. Systems of Nonlinear Differential Equations. In *A Modern Introduction to Differential Equations*; Elsevier, 2021; pp 361−420.

https://doi.org/10.1021/acs.joc.4c02997
J. Org. Chem. XXXX, XXX, XXX−XXX

5. LIGHT-INDUCED REARRANGEMENT FROM MACROCYCLIC TO BICYCLIC LACTAM: A CASE STUDY OF *N*-CHLORINATED LAUROLACTAM

Acta Pharm. **74** (2024) 725–737
https://doi.org/10.2478/acph-2024-0035

Original research paper

Light-induced rearrangement from macrocyclic to bicyclic lactam: A case study of *N*-chlorinated laurolactam

GABRIJEL ZUBČIĆ[1]
KRISTINA PAVIĆ[1]
JIANGYANG YOU[2]
VALERIJE VRČEK[1]
TOMISLAV PORTADA[2]
ERIM BEŠIĆ[1]
DAVOR ŠAKIĆ[1]*

[1] *University of Zagreb Faculty of Pharmacy and Biochemistry 10 000 Zagreb, Croatia*

[2] *Ruđer Bošković Institute 10 000 Zagreb, Croatia*

Accepted September 14, 2024
Published online September 15, 2024

ABSTRACT

Converting macrocycle lactams into bicyclic lactams is proposed as an additional way to further increase the metabolic stability of peptide-based drugs. Unfortunately, the synthesis of bicyclic lactams has to start almost from scratch. This study explores the Hofmann-Löffler-Freytag (HLF) reaction mechanism and products as a potential late-stage functionalisation strategy for facile conversion of macrocyclic to bicyclic ring. Laurolactam, a macrocyclic amide, exhibits significant potential for transformation into bioactive bicyclic structures with smaller, β-, γ-, δ-, and ε-lactam rings, further increasing rigidity and hydrolytic stability. With irradiation provided by a 370 nm lamp, light-induced rearrangement reaction was monitored using nuclear magnetic resonance (NMR), while involved radical intermediates were trapped using *N-tert*-butyl-α-phenylnitrone (PBN) spin-trap and characterised *via* EPR. While only two radical adduct types were identified in the electron paramagnetic resonance (EPR) (*C*-centered radical and chlorine radical), all eight possible products are observed in the NMR. Quantum chemical calculations provide deeper insights into reaction thermodynamics and kinetics, explaining why the *N*-centered radical was not observed. This research highlights the feasibility of using the HLF reaction to transform macrocyclic lactams into stable bicyclic drug candidates, paving the way for new therapeutic developments.

Keywords: radical rearrangement, radical thermodynamics, ring-contraction, late-stage functionalisation, synthetic strategy

INTRODUCTION

Late-stage functionalisation (LSF) has emerged as a transformative strategy in medicinal chemistry, providing powerful means to generate new potential drugs from existing lead compounds. This approach involves the modification of complex molecules at a late synthetic stage, allowing for the introduction of diverse functional groups without the need for extensive synthetic reroutes. By enabling the fine-tuning of pharmacological

* Correspondence; e-mail: davor.sakic@pharma.unizg.hr

properties such as potency, selectivity, and metabolic stability, LSF plays a crucial role in optimising lead compounds and accelerating the drug development process (1, 2).

Among the "reaction toolbox" for LSF are ring-expansion reactions, which are particularly valuable for synthesising medium-sized and macrocyclic rings (3). These large-ring frameworks are critical in medicinal chemistry, with many drugs based on these structures on the market. The ability to create and modify these ring systems through LSF enables the development of drug candidates with unique structural and functional properties (4).

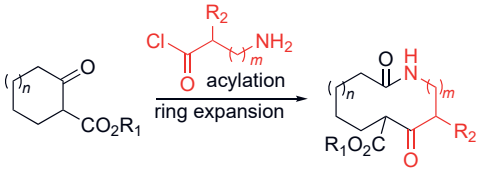

Scheme 1. Example of ring expansion in the late-stage functionalisation protocols. Adapted from reference (3).

Among macrocyclic drugs, a special place is reserved for lactams, as some of the most significant heterocycles in a variety of natural products and drugs, including antimicrobial drugs. Lactams as cyclic amides are classified by ring size, including four-membered (β-lactams, 2-azetidinones), five-membered (γ-lactams, 2-pyrrolidinones), six-membered (δ-lactams, 2-piperidinones), seven-membered (ε-lactams, 2-azepanones), medium-sized (8–11-membered), and macrocyclic (≥ 12-membered) rings. Moreover, lactams serve as conformationally restricted scaffolds that enhance the potency, selectivity, and metabolic stability of peptide-based drugs. They exhibit a broad spectrum of biological activities, making them valuable in the treatment of cancer, diabetes, infectious diseases, and more (5).

Changing macrocyclic lactams to bicyclic lactams with smaller ring motifs, such as β-, γ-, δ, and ε-lactams, may provide new opportunities for drug development. To make a ring contraction, a previously unfunctionalized C–H bond has to be activated to form a novel C–N bond (6). The photocatalytic Hofmann-Löffler-Freytag (HLF) reaction (7–11) is a

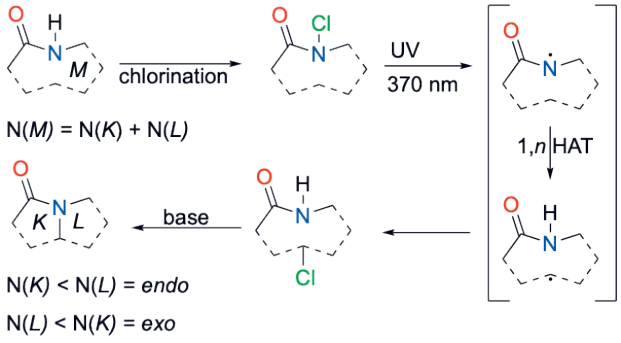

Scheme 2. Example of ring-contraction using Hofmann-Löffler-Freytag reaction.

promising method for achieving this transformation and has been used in alkaloid synthesis (12, 13). It employs *N*-centered radicals to functionalise remote C–H bonds. Our recent investigations into the mechanistic details of the HLF reaction have provided insights into its utility in synthesising nicotine derivatives in a cost-effective way while conserving stereoconfiguration (14). The cause of regioselectivity in the HLF reaction, where more pyrrolidine than piperidine products are formed, has recently been explained, and that could steer in producing only select bicyclic structures in the macrocycle (15).

In this study, we aim to modify laurolactam (azacyclotridecan-2-one, dodecalactam), which is industrially utilised as a monomer in the polymerisation of nylon-12, to serve as a model compound and potential scaffold for further bicyclic lactam synthesis. By leveraging the HLF reaction, we intend to demonstrate the feasibility of this approach, paving the way for the development of new, stable bicyclic drug candidates from macrocyclic leads.

EXPERIMENTAL

General

The purchased compounds were sourced from Sigma-Aldrich (USA) (azacyclotridecan-2-one, trichloroisocyanuric acid (TCICA), Celite® S), Fisher Scientific (USA) (dichloromethane, DCM) and Kemika (Croatia) (sodium hydroxide). All chemicals and solvents were obtained commercially and used without further purification unless otherwise noted.

Reactions were routinely checked by thin-layer chromatography (TLC) with Merck silica gel 60F-254 glass plates (Merck, Germany) using cyclohexane/ethyl acetate/methanol 3:1:0.5 as a solvent system. Spots were visualized by spraying the TLC plates with an ethanolic solution of phosphomolybdic acid followed by heating.

Photocatalysed reactions were performed *in situ* (reaction of **1-Cl** and EPR studies) and *off-site* (NMR) with Kessil PR-160L 370 ± 10 nm gen-2 LED UV (DiCon, USA), with an average intensity of 137 mW cm^{-2} when the sample is at a 6-cm distance from the lamp, according to the manufacturer (16).

Syntheses

*1-Chloroazacyclotridecan-2-one (**1-Cl**)*

TCICA (0.561 g, 2.414 mmol) was added to a stirred solution of azacyclotridecan-2-one (**1**) (0.433 g, 2.194 mmol) in DCM (17 mL) at 0 °C. The reaction mixture was stirred overnight at room temperature. The mixture was filtered through Celite® and the filtrate evaporated under reduced pressure to give the *N*-chloro derivative (0.488 g, 96 %).

Cyclisation

After one-hour long irradiation of **1-Cl** using a 370 nm lamp in the round-bottom flask, while checking the reaction progress with TLC, the reaction was quenched with an excess of 0.1 mol L^{-1} solution of NaOH. Products were filtrate evaporated under reduced pressure and washed with deionised water.

NMR and EPR reaction monitoring

NMR spectra of the reaction mixture were obtained on a Varian Inova 400 NMR spectrometer (Varian, USA) operating at 399.90 MHz for ^{1}H NMR and 100.6 MHz for ^{13}C NMR. Chemical shifts (δ) are reported in parts per million (ppm). First, ^{1}H and APT-^{13}C spectra of the starting compound **1-Cl** were acquired. Then the sample was irradiated off-site for 5 minutes from the bottom of the NMR tube using the UV lamp at 25 % power. Reaction progress was monitored with ^{1}H spectra, and for every three irradiation intervals, APT-^{13}C was recorded. Deuterated chloroform was used as a solvent, with some precipitation forming during the reaction. Quenched and washed products were analysed in DMSO-d_6 solvent. The spectra were processed in the MNova 11.0.4 software (Mestrelab, Spain) (17) and using the NMRium online platform (Zakodium, Switzerland) (18).

EPR spectroscopy was done using a Bruker E500 ELEXSYS EPR spectrometer (Bruker, USA) with an ER4122SHQE cavity resonator. As this cavity resonator does not have an optical window for illumination, the light source was mounted underneath the cavity, with light coming through the bottom of the EPR 4 mm-inner-diameter tube, with toluene as a solvent. EPR deconvolution and simulation were done using an EasySpin module (19) with the MATLAB program package. (MATLAB, Natick, USA) EPR visualization and simulations were done using the VisualEPR Web page (20).

Computational methods

Initial structures were optimised using the semi-empirical tight-binding quantum chemical method xtb program package (21). Conformational space for reactants, products, and transition states was sampled and investigated using the Conformer-Rotamer Ensemble Sampling Tool – CREST (22) coupled with meta-dynamic simulations (23) on the GFN2-xtb level of theory (24). Selected 50 lowest energy conformations were re-optimised using density functional theory on B3LYP/6-31G(d) level of theory (25, 26) using Gaussian 16 program package (27). For each structure, frequency calculation was performed to identify if the structure is a minimum or a saddle point (minimum in all directions except in one path, identifying transition-state structure) on the potential energy surface. From the transition-state structure, an intrinsic reaction coordinate search was performed to characterise the corresponding reaction and product complexes/reactive conformers. All conformer ensembles were sorted via the CREGEN procedure, and improved energetics were obtained *via* single-point calculations using RO-B2PLYP-D3/G3MP2Large level of theory (28–31). Calculations were performed using the advanced computing service (cluster Supek) provided by the University of Zagreb University Computing Centre – SRCE (32) and the computational resources of the PharmInova project (sw.pharma.hr) at the University of Zagreb Faculty of Pharmacy and Biochemistry (33), and all visualisations were done using IQmol (34).

RESULTS AND DISCUSSION

HLF reaction is governed by the thermodynamic factors, namely the difference in the radical stability between reactants and products in the rate-determining step (35). A well-proven method used for the calculation and prediction of radical stabilities among the

N-centered and *C*-centered radicals is done *via* modelling of isodesmic reactions involving one experimentally well-defined standard. For *C*-centered radicals, the standard is methane/methyl radical, while for *N*-centered radicals ammonia/aminyl radical is used as an anchor point, with bond-dissociation energies (BDEs) of 439.3 ± 0.4 kJ mol^{-1} and 450.1 ± 0.24 kJ mol^{-1}, respectively (36). Reaction enthalpy of such isodesmic reactions is called radical stabilisation energy (RSE) and can be used to gauge the relative difference between the same class of radicals, but also a good approximation of BDE, when added to the referent BDE. In Scheme 3, different relevant *N*-centered and *C*-centered radicals present in lactams and similar compounds (amidyl, aminyl, and alkyl radicals) are shown. A clear effect of sterical influence on the stability of amidyl radicals can be observed. Namely, for *N*-methyl-acetamide

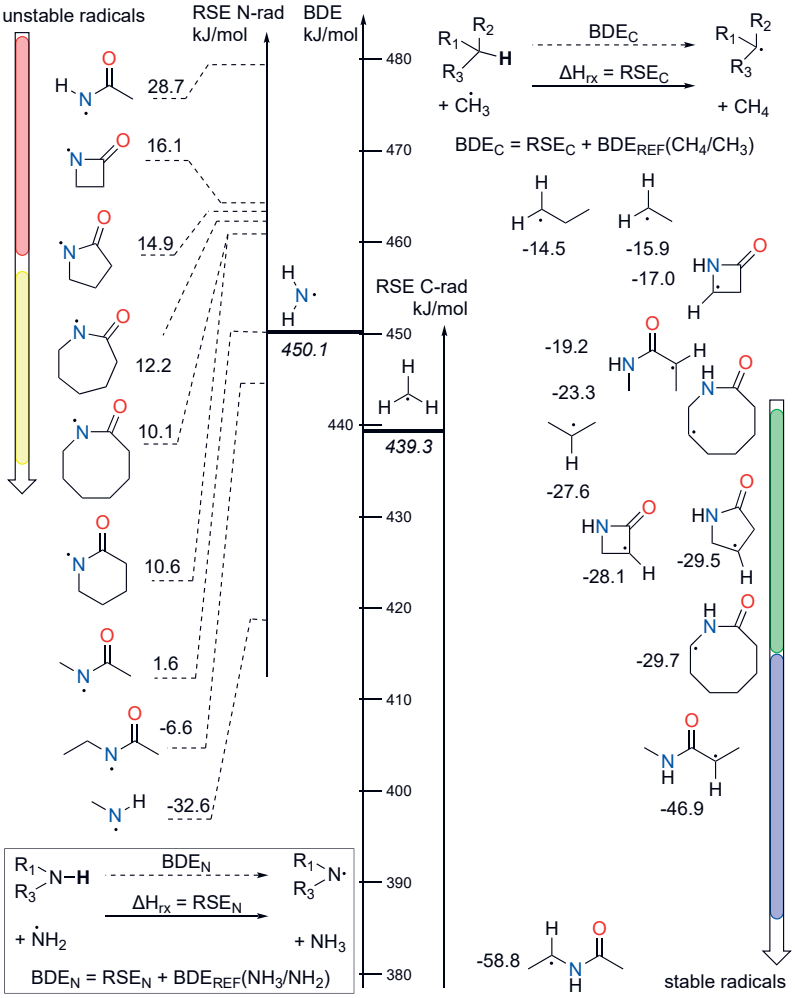

Scheme 3. BDE/RSE of selected *N*-centered radicals and *C*-centered radicals.

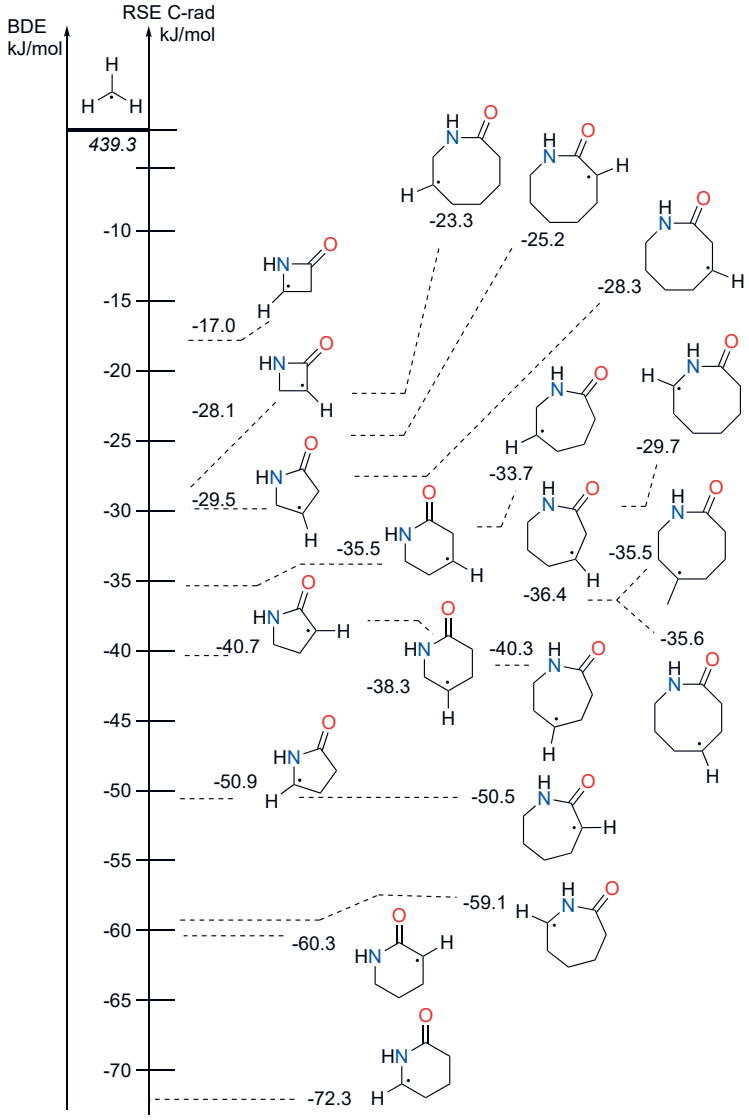

Scheme 4. BDE/RSE of *C*-centered radicals in lactam structures.

amidyl radical, RSE is 1.6 kJ mol^{-1}, but when constricted in 2-azetidinone, 2-pyrrolidinone, 2-pepridinone, 2-azepanone, and 2-azocanone less stable amidyl radicals are formed, with RSEs in the range of 10.1 to 16.1 kJ mol^{-1}. But as the ring grows, the structural effect on the radical is less pronounced, and for laurolactam amidyl radical (**1-Nrad**), RSE od –1.9 kJ mol^{-1} is between radical stability of *N*-methyl and *N*-ethyl (RSE = –6.6 kJ mol^{-1}) derivatives of acetamide.

C-centered radicals are generally more stable than *N*-centered amidyl radicals (see Schemes 3 and 4). Alkyl radicals have RSE around that of C_2-radical in propane (–27.6 kJ mol^{-1}), ranging from –23.3 kJ mol^{-1} in C_7-radical of 2-azocanone to –40.3 kJ mol^{-1} in C_5-radical of 2-azepanone. While alkyl radicals surrounded by methylene neighbourghs are in the aforementioned range, *C*-centered radicals with carbonyl or amine part of amide next to it are more stable. The exceptions to that rule are radicals in β-lactam (2-azetidinone), which are heavily constrained and are among the least stable *C*-centered radicals, comparable only to the primary radicals.

From Schemes 3 and 4 it is obvious that the HLF reaction is exothermic in the radical rearrangement reaction, and can occur in lactam rings of various sizes.

Next, we wanted to test our theory on a real macrocyclic lactam, specifically on laurolactam, in order to model all transition states and products stemming from the HLF reaction. The first step of the HLF reaction is light-induced homolytic cleavage of the *N*-halogen bond. To that end, an *N*-chloro derivative (**1-Cl**) of laurolactam (**1**) was prepared by *N*-chlorination with TCICA (Scheme 5).

Quantum-chemical methods were used to model all transition states and all products stemming from the HLF reaction. Possible 1,*n*-HAT reactions include 1,4-HAT, 1,5-HAT, 1,6-HAT, and 1,7-HAT forming 4-, 5-, 6-, and 7-membered rings, respectively (see Scheme 5). However, there are two different ways to form those rings. One pathway generates the product with the carbonyl group inside the smaller, newly formed ring, titled *endo*. Consequently, newly formed rings with the carbonyl group outside the smaller ring are termed *exo*. In Table I, calculated parameters are presented for all combinations. The lowest barriers ($\Delta H^{\ddagger}_{298}$) are present in the *exo*-1,5-HAT and *exo*-1,6-HAT for the cyclisation. The *endo*-1,5-HAT process is more stable than both *endo*-1,6-HAT and *endo*-1,7-HAT for *endo*-type of cyclisation, and very similarly stable to the 1,7-HAT path of *exo*-type. To our surprise, the barrier for the *endo*-1,4-HAT reaction is lower than the *exo*-1,4-HAT reaction. The formation of the β-lactam ring by 1,4-HAT *endo*-type of cyclisation is two orders of magnitude

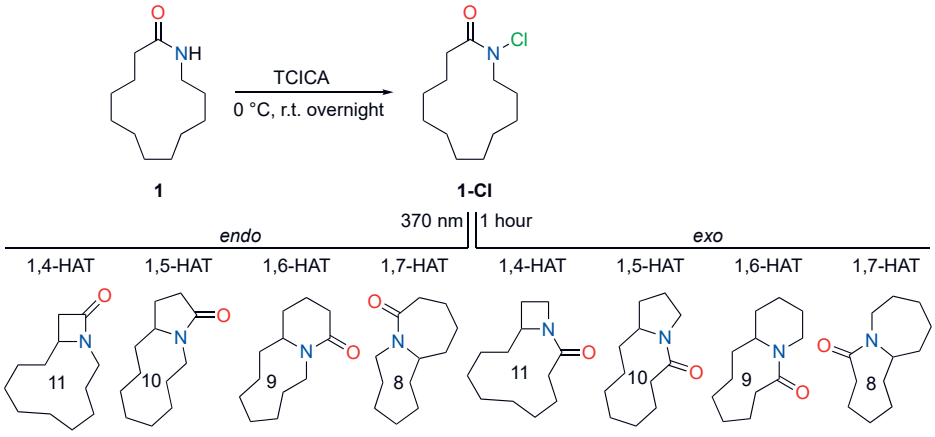

Scheme 5. *N*-chlorination of laurolactam and tentative products after 1-hour irradiation with 370 nm lamp.

Table I. Calculated reaction parameters in the 1,n-HAT rearrangement reactions between amidyl N-centered and C-centered radicals[a]

1,*n*-HAT	exo		endo	
	$\Delta H_{rx,298}$ (kJ mol^{-1})	$\Delta H^{\ddagger}_{298}$ (kJ mol^{-1})	$\Delta H_{rx,298}$ (kJ mol^{-1})	$\Delta H^{\ddagger}_{298}$ (kJ mol^{-1})
1,4-HAT	–38.38	61.41	–36.89	45.38
	azetidine		β-lactam	
1,5-HAT	–37.86	25.26	–33.37	32.13
	pyrrolidne/azolidine		γ-lactam	
1,6-HAT	–41.31	25.40	–40.28	35.04
	piperidine		δ-lactam	
1,7-HAT	–41.90	33.13	–41.27	34.56
	azepine		ε-lactam	

[a] The bottom row describes the formed ring in the subsequent reaction with the base.

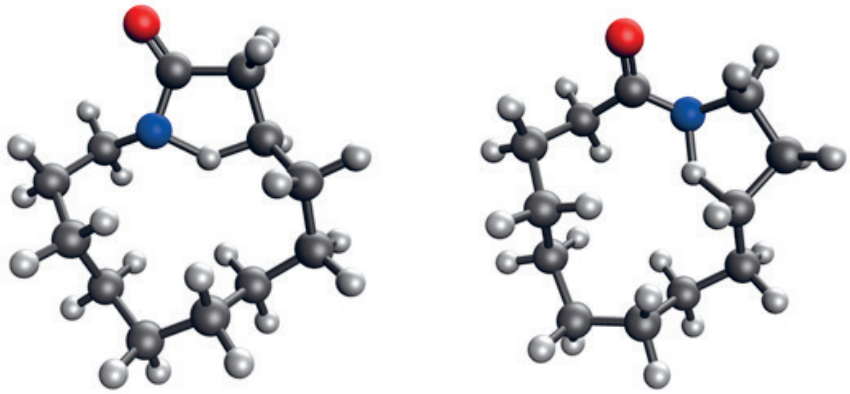

Fig. 1. Transition-state structures for *endo*-1,4-HAT and *exo*-1,4-HAT

faster than the formation of azetidine by the *exo*-1,4-HAT, as seen from the calculated rate constants for *endo*- ($k_{endo\text{-}1,4\text{-HAT}} = 6.899 \times 10^4$ s^{-1}) and *exo*- ($k_{exo\text{-}1,4\text{-HAT}} = 1.069 \times 10^2$ s^{-1}) pathways of 4-membered ring cyclisations (transition-state structures are shown in Fig. 1). The stabilities of all products are similar and provide a strong thermodynamic force (reaction enthalpy, $\Delta H_{rx,298}$) towards products.

Next, EPR experiments were performed as described in the method section. After spectra deconvolution, only two different radicals are observed. The major observed radical is the adduct of chlorine radical onto the *N-tert*-butyl-α-phenylnitrone (PBN), **Cl-PBN**, with hyperfine splitting constant (*hfc*) $A_N = 12.36$ G, $A_H = 0.75$ G and $A_H = 6.22$ G, with a line width of 0.22. Another radical is a *C*-centered radical adduct of PBN, **C-PBN**, with a difference in *g*-value of –0.0013 from **Cl-PBN**, and *hfc* $A_N = 13.44$ G, $A_H = 1.76$ G. After decomposition, some residual signals remain with some weak and broad components which are

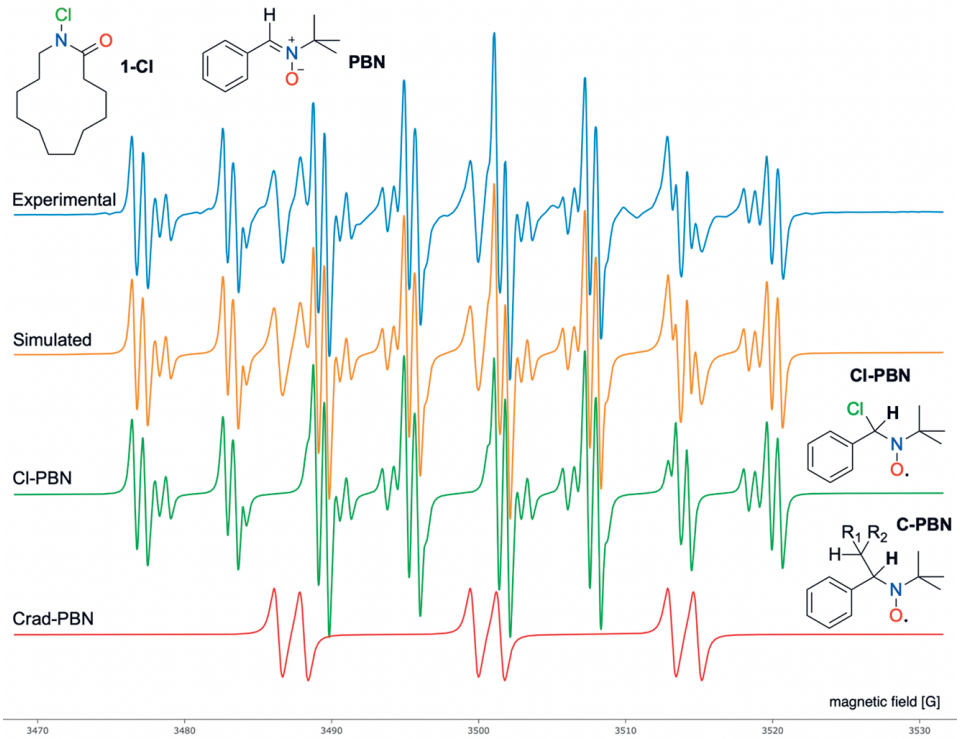

Fig. 2. EPR spectra of spin-trapped radical intermediates generated with a 370 nm irradiation of **1-Cl**. The experimental spectrum is in blue, while red, green, and orange correspond to simulated spectra for **Crad-PBN**, **Cl-PBN**, and total simulated spectra, respectively.

similar to the **N-PBN** adduct radical observed in our previous work (15). Yet the residue signal is extremely weak, making it difficult to achieve a satisfactory deconvolution. Since the reactions happen very quickly, the rearrangement of *N*-centered radical to the *C*-centered radicals occurs faster than the spin-trapping reaction of PBN.

Finally, NMR experiments were performed to identify the reaction products. The biggest obstacle encountered in the NMR experiments was the relative insolubility of the compound **1-Cl** and its products in $CDCl_3$ solvent. As the reaction progressed, precipitation was formed in the NMR tube, making prolonged spectra acquisition unfeasible. To address this issue, the photoreaction was quenched with 0.1 mol L^{-1} NaOH (added in excess), washed with water, and then 30 mg of the product mixture was resuspended in DMSO-d_6 for NMR spectroscopy. In Fig. 3, APT-^{13}C NMR spectra are shown, along with an enlarged portion of the spectra displaying signals of carbon atoms with an odd number of attached H-atoms. In the spectra, nine such signals can be observed, with a dubious signal at 62.05 ppm. If we disregard that signal, eight different signals actually correspond to the eight different products predicted *via* calculations (see Scheme 5).

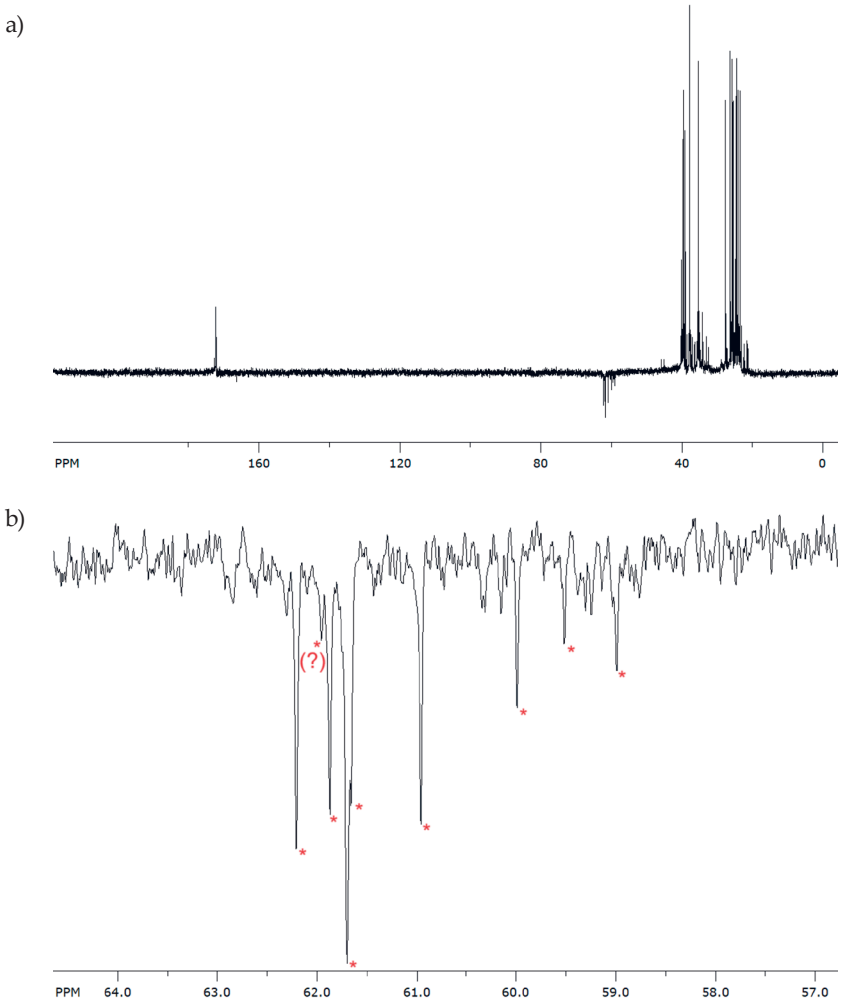

Fig. 3. a) APT-^{13}C NMR spectra of the quenched and washed reaction; b) eight different signals in the negative region from 57–64 ppm correspond to eight different products.

Thus, we have demonstrated that HLF reaction can be used in the LSF strategies to produce all types of bicyclic rings from lactam macrocycles, with ring sizes ranging from 4-membered rings, up to 7-membered rings.

CONCLUSIONS

This study successfully demonstrates the potential of the Hofmann-Löffler-Freytag (HLF) reaction as a viable method for late-stage functionalization (LSF) of macrocyclic lactams, as shown with laurolactam. The thermodynamically driven HLF reaction, char-

acterised by radical stability differences, effectively transforms laurolactam into various bicyclic lactams with ring sizes ranging from 4- to 7-membered rings. These transformations, investigated with theoretical and experimental approaches, underscore the versatility and efficiency of the HLF reaction in generating structurally diverse and stable products. Amidyl radicals in constrained lactam rings exhibit higher radical stabilization energy (RSE) values, indicating reduced stability. *C*-centered radicals, particularly those adjacent to carbonyl or amine groups, demonstrate enhanced radical stability, with notable exceptions in highly constrained structures like 2-azetidinone. Computational modelling reveals the lowest activation barriers for 1,5- and 1,6-HAT *exo*-type cyclizations with carbonyl moiety outside the smaller ring. The unexpected lower barrier for 1,4-HAT *endo*-type reactions compared to *exo*-type counterparts highlights the complexity and potential of the HLF mechanism in the formation of pharmacologically potent β-lactam motif. EPR spectroscopy identifies **Cl-PBN** and **C-PBN** as primary radical adducts to the spin-trap *N*-*tert*-butyl-α-phenylnitrone (PBN), underpinning rapid *N*- to *C*-centered radical rearrangement. NMR spectroscopy confirms the formation of eight distinct products, aligning with computational predictions. The findings affirm the HLF reaction's applicability in LSF strategies, enabling the production of various bicyclic rings from macrocyclic lactams. This approach not only broadens the scope of accessible ring structures but also facilitates the fine-tuning of pharmacological properties, crucial for drug development. Future research should focus on exploring different macrocyclic substrates, optimising reaction conditions, and conducting biological evaluations to fully harness the HLF reaction's potential in drug development.

Abbreviations, acronyms, symbols. – APT, attached proton test; BDE, bond dissociation energy; EPR, electron paramagnetic resonance; $\Delta H^{\ddagger}_{298}$, activation enthalpy at 298K; $\Delta H_{rx,298}$, reaction enthalpy at 298K; HAT, hydrogen atom transfer; hfc, hyperfine coupling constant; HLF, Hofmann-Löffler-Freytag; LED UV, light-emitting diode in ultraviolet radiation; LSF, late-stage functionalization; NMR, nuclear magnetic resonance; PBN, *N*-*tert*-butyl-α-phenylnitrone; RSE, radical stabilization energy; TCICA, trichloroisocyanuric acid.

Acknowledgments. – The authors would like to acknowledge financial support from the Croatian Science Foundation Installation grant UIP-2020-02-4857 LIGHT-N-RING, grant IP-2022-10-2634 PharmaEco, and computational resources available on Cluster Supek, EU funded through KK.01.1.1.08.0001, a part of the Advanced Computing Service provided by University of Zagreb University Computing Centre – SRCE. This work was also supported by the project FarmInova at the Faculty of Pharmacy and Biochemistry University of Zagreb (KK.01.1.1.02.0021) funded by the European Regional Development Fund. Support from The Cryogenic Centre at the Institute of Physics project (KaCIF, KK.01.1.1.02.0012) is acknowledged.

Funding. – This research received no external funding.

Conflicts of interest. – The authors declare no conflict of interest.

Authors contributions. – Conceptualization, D.Š. and G.Z.; calculations, data analysis, G.Z.; methodology, experimental, J.Y., K.P. and T.P; analysis, T.P. and V.V.; writing, original draft preparation, D.Š.; writing, review and editing, E.B. and D.Š.; funding, D.Š. All authors have read and agreed to the published version of the manuscript.

REFERENCES

1. T. Cernak, K. D. Dykstra, S. Tyagarajan, P. Vachal and S. W. Krska, The medicinal chemist's toolbox for late stage functionalization of drug-like molecules, *Chem. Soc. Rev.* **45**(3) (2016) 546–576; https://doi.org/10.1039/C5CS00628G

2. S. K. Sinha, S. Guin, S. Maiti, J. P. Biswas, S. Porey and D. Maiti, Toolbox for distal C–H bond functionalizations in organic molecules, *Chem. Rev.* **122**(6) (2022) 5682–5841; https://doi.org/10.1021/acs.chemrev.1c00220
3. Z. Yang, M. Arnoux, D. Hazelard, O. R. Hughes, J. Nabarro, A. C. Whitwood, M. A. Fascione, C. D. Spicer, P. Compain and W. P. Unsworth, Expanding the scope of the successive ring expansion strategy for macrocycle and medium-sized ring synthesis: unreactive and reactive lactams, *Org. Biomol. Chem.* **22** (2024) 2985–2991; https://doi.org/10.1039/D4OB00285G
4. L. G. Baud, M. A. Manning, H. L. Arkless, T. C. Stephens and W. P. Unsworth, Ring-expansion approach to medium-sized lactams and analysis of their medicinal lead-like properties, *Chem. Eur. J.* **23** (2017) 2225–2230; https://doi.org/10.1002/chem.201605615
5. F. I. Saldívar-González, E. Lenci, A. Trabocchi and J. L. Medina-Franco, Exploring the chemical space and the bioactivity profile of lactams: a chemoinformatic study, *RSC Adv.* **9** (2019) Article ID 27105 (12 pages); https://doi.org/10.1039/c9ra04841c
6. P. Bellotti, H.-M. Huang, T. Faber and F. Glorius, Photocatalytic late-stage C–H functionalization, *Chem. Rev.* **123**(8) (2023) 4237–4352; https://doi.org/10.1021/acs.chemrev.2c00478
7. A. W. Hofmann, Ueber die Einwirkung des Broms in alkalischer Lösung auf die Amine, *Ber. Dtsch. Chem. Ges.* **16**(1) (1883) 558–560; https://doi.org/10.1002/cber.188301601120
8. A. W. Hofmann, Ueber die Einwirkung des Broms in alkalischer Lösung auf Amide, *Ber. Dtsch. Chem. Ges.* **14**(2) (1881) 2725–2736; https://doi.org/10.1002/cber.188101402242
9. A. W. Hofmann, Zur Kenntniss der Coniin-Gruppe, *Ber. Dtsch. Chem. Ges.* **18**(1) (1885) 109–131; https://doi.org/10.1002/cber.18850180126
10. K. Löffler and C. Freytag, Über eine neue Bildungsweise von N-alkylierten Pyrrolidinen, *Ber. Dtsch. Chem. Ges.* **42**(3) (1909) 3427–3431; https://doi.org/10.1002/cber.19090420377
11. G. Zubčić, S. Shkunnikova, D. Šakić and M. Marijan, Renaissance of Hofmann-Löffler-Freytag reaction – Development of C–H functionalisation strategies based on green chemistry principles, *Kem. Ind.* **71**(5–6) (2022) 359–373; https://doi.org/10.15255/KUI.2021.070
12. S. W. Baldwin and R. J. Doll, Synthesis of the 2-aza-7-oxatricyclo[4.3.2.$0^{4,8}$]undecane nucleus of some gelsemium alkaloids, *Tetrahedron Lett.* **20**(35) (1979) 3275–3278; https://doi.org/10.1016/S0040-4039(01)95450-2
13. K. Löffler and S. Kober, Über die Bildung desi-Nicotins aus N-Methyl-p-pyridyl-butylamin (Dihydrometanicotin), *Ber. Dtsch. Chem. Ges.* **42** (1909) 3431–3438; https://doi.org/10.1002/cber.19090420378
14. S. Shkunnikova, H. Zipse and D. Šakić, Role of substituents in the Hofmann-Löffler-Freytag reaction. A quantum-chemical case study on nicotine synthesis, *Org. Biomol. Chem.* **19** (2021) 854–865; https://doi.org/10.1039/D0OB02187C
15. G. Zubčić, J. You, F. L. Zott, S. S. Ashirbaev, M. K. Marković, E. Bešić, V. Vrček, H. Zipse and D. Šakić, Regioselective rearrangement of nitrogen- and carbon-centered radical intermediates in the Hofmann-Löffler-Freytag reaction, *J. Phys. Chem. A* **128**(13) (2024) 2574–2583; https://doi.org/10.1021/acs.jpca.3c07892
16. Kessil PR-160L 370-Gen2 specification; https://www.kessil.com/products/science_PR160L.php; last access date June 28, 2024.
17. M. R. Willcott, MestRe Nova, *J. Am. Chem. Soc.* **131**(36) (2009) 13180; https://doi.org/10.1021/ja906709t
18. L. Patiny, H. Musallam, A. Bolaños, M. Zasso, J. Wist, M. Karayilan, E. Ziegler, J. C. Liermann and N. E. Schlörer, NMRium: Teaching nuclear magnetic resonance spectra interpretation in an online platform, *Beilstein J. Org. Chem.* **20** (2024) 25–31; https://doi.org/10.3762/bjoc.20.4
19. S. Stoll and A. Schweiger, EasySpin, a comprehensive software package for spectral simulation and analysis in EPR, *J. Magn. Reson.* **178**(1) (2006) 42–55; https://doi.org/10.1016/j.jmr.2005.08.013
20. D. Šakić, G. Zubčić, J. You, T. Weitner, V. Chechik and E. Bešić, VisualEPR; https://github.com/DSakicLab/visualEPR; last access date December 1, 2023.

21. C. Bannwarth, E. Caldeweyher, S. Ehlert, A. Hansen, P. Pracht, J. Seibert, S. Spicher and S. Grimme, *WIREs Comput. Mol. Sci.* **11** (2020) Article ID e01493 (49 pages); https://doi.org/10.1002/wcms.1493
22. P. Pracht, F. Bohle and S. Grimme, Automated exploration of the low-energy chemical space with fast quantum chemical methods, *Phys. Chem. Chem. Phys.* **22** (2020) 7169–7192; https://doi.org/10.1039/C9CP06869D
23. S. Grimme, Exploration of chemical compound, conformer, and reaction space with meta-dynamics simulations based on tight-binding quantum chemical calculations, *J. Chem. Theory Comput.* **15**(5) (2019) 2847–2862; https://doi.org/10.1021/acs.jctc.9b00143
24. C. Bannwarth, S. Ehlert and S. Grimme, GFN2-xTB – An accurate and broadly parametrized self-consistent tight-binding quantum chemical method with multipole electrostatics and density-dependent dispersion contributions, *J. Chem. Theory Comput.* **15**(3) (2019) 1652–1671; https://doi.org/10.1021/acs.jctc.8b01176
25. A. D. Becke, Density-functional thermochemistry. III. The role of exact exchange, *J. Chem. Phys.* **98**(7) (1993) 5648–5652; https://doi.org/10.1063/1.464913
26. R. Ditchfield, W. J. Hehre and J. A. Pople, Self-consistent molecular-orbital methods. IX. An extended gaussian-type basis for molecular-orbital studies of organic molecules, *J. Chem. Phys.* **54**(2) (1971) 724–728; https://doi.org/10.1063/1.1674902
27. M. J. Frisch, G. W. Trucks, H. B. Schlegel, G. E. Scuseria, M. A. Robb, J. R. Cheeseman, G. Scalmani, V. Barone, G. A. Petersson, H. Nakatsuji, X. Li, M. Caricato, A. V. Marenich, J. Bloino, B. G. Janesko, R. Gomperts, B. Mennucci, H. P. Hratchian, J. V. Ortiz, A. F. Izmaylov, J. L. Sonnenberg, D. Williams-Young, F. Ding, F. Lipparini, F. Egidi, J. Goings, B. Peng, A. Petrone, T. Henderson, D. Ranasinghe, V. G. Zakrzewski, J. Gao, N. Rega, G. Zheng, W. Liang, M. Hada, M. Ehara, K. Toyota, R. Fukuda, J. Hasegawa, M. Ishida, T. Nakajima, Y. Honda, O. Kitao, H. Nakai, T. Vreven, K. Throssell, J. A. Montgomery, Jr., J. E. Peralta, F. Ogliaro, M. J. Bearpark, J. J. Heyd, E. N. Brothers, K. N. Kudin, V. N. Staroverov, T. A. Keith, R. Kobayashi, J. Normand, K. Raghavachari, A. P. Rendell, J. C. Burant, S. S. Iyengar, J. Tomasi, M. Cossi, J. M. Millam, M. Klene, C. Adamo, R. Cammi, J. W. Ochterski, R. L. Martin, K. Morokuma, O. Farkas, J. B. Foresman and D. J. Fox. Gaussian 16. Wallingford CT, USA: Gaussian, Inc.; 2016.
28. S. Grimme, Semiempirical hybrid density functional with perturbative second-order correlation, *J. Chem. Phys.* **124**(3) (2006) Article ID 034108 (17 pages); https://doi.org/10.1063/1.2148954
29. S. Grimme, J. Antony, S. Ehrlich and H. Krieg, A consistent and accurate ab initio parametrization of density functional dispersion correction (DFT-D) for the 94 elements H-Pu, *J. Chem. Phys.* **132**(15) (2010) Article ID (20 pages) 154104; https://doi.org/10.1063/1.3382344
30. F. Neese, T. Schwabe and S. Grimme, Analytic derivatives for perturbatively corrected "double hybrid" density functionals: Theory, implementation, and applications, *J. Chem. Phys.* **126**(12) (2007) Article ID (16 pages) 124115; https://doi.org/10.1063/1.2712433
31. L. A. Curtiss, P. C. Redfern, K. Raghavachari, V. Rassolov and J. A. Pople, Gaussian-3 theory using reduced Möller-Plesset order, *J. Chem. Phys.* **110**(10) (1999) 4703–4709; https://doi.org/10.1063/1.478385
32. HR-ZOO, Cluster Supek; University of Zagreb University Computing Centre – SRCE, KK.01.1.1.08.0001, EU funded within OPCC for Republic of Croatia, Zagreb, 2023.
33. PharmInova Project, Cluster Sw.Pharma.Hr; University of Zagreb Faculty of Pharmacy and Biochemistry, KK.01.1.1.02.0021, EU funded by the European Regional Development Fund: Zagreb, 2023.
34. IQmol; https://github.com/nutjunkie/IQmol; last access date July 2, 2024.
35. D. Šakić and H. Zipse, Radical stability as a guideline in C–H amination reactions, *Adv. Synth. Catal.* **358** (2016) 3983–3991; https://doi.org/10.1002/adsc.201600629
36. Y.-R. Luo, *Comprehensive Handbook of Chemical Bond Energies*, CRC Press, London 2007.

6. DISCUSSION

Research in our scientific group was conducted with an aim to thoroughly investigate the mechanism of the HLF reaction. Within the framework of this research, three scientific articles were published (82,95,96).

As part of article **1** (82), a method for the *in situ* generation and trapping of radical intermediates using the PBN spin trap and investigation of the resulting adducts via EPR spectroscopy was developed. The method involves irradiation inside the cavity of the EPR and monitoring of the kinetics of the accumulations and decays of various spin adducts over time. These measurements were done on four different systems that were prepared in a two-step synthesis as part of article **1**. The analyzed systems were two bromine and two chlorine derivatives, namely, *N*-bromo-*N*-hexyl-4-methylbenzenesulfonamide, *N*-bromo-*N*-(heptan-2-yl)-4-methylbenzenesulfonamide, *N*-chloro-*N*-hexyl-4-methylbenzenesulfonamide, and *N*-chloro-*N*-(heptan-2-yl)-4-methylbenzenesulfonamide. The first step in the preparation of these systems involves introduction of a Tosyl activating group onto the nitrogen atom of an amine compound (97). The second step includes chlorination or bromination of the nitrogen atom. The two chlorine derivatives were prepared with relative ease in high yields as stable products following the procedure by De Luca (44). On the other hand, the two bromine derivatives were prepared using the newly developed methodology described in article **1** and have been shown to be unstable with respect to light or/and temperature. It has been reported in the literature (11,25,98) that *N*-bromo derivates are unstable when compared to *N*-chloro derivatives and, therefore, not as suitable substrates for the HLF reaction. However, there are reports (81) that both *N*-chloro and *N*-bromo derivatives are comparable in term of the yields of the cyclized products obtained or even in some cases, better yields of the cyclized products were obtained with *N*-bromo derivatives. Interestingly, iodine derivatives were not prepared, due to problems in the isolation of the *N*-iodine derivatives.

An improvised degassing procedure on a vacuum line instead of a Schlenk line of the solutions was developed and thoroughly described in article **1**. The instability of the *N*-bromo derivatives made the degassing procedure of the solutions of these compounds much more challenging. Effectiveness of the oxygen removal using freeze−pump−thaw cycles with backfill of argon or nitrogen gas was evidenced by the line widths measured with EPR. Experimental line widths of less than 0.4 Gauss proved that extremely little or no air was present in the solutions. Within the framework of article **1**, *in situ* progress of the HLF reaction on the synthesized compounds was monitored via NMR experiments. These experiments were done with off-site illumination and constitute first known monitoring of the progress of the HLF reaction via NMR.

As part of article **1**, preliminary experiments, in which PIDA, iodine and *N*-halo sulfonamide were used, proved to be unsuccessful. In these experiments, both PIDA, I_2 and *N*-halo sulfonamide were potential sources of free radical species. This proved to be the case as the obtained EPR spectra were complex in nature and no clear assignment could be made. Although two distinct radicals were formed in these experiments, both belonging to the oxidation products of spin-trap PBN. Namely, oxo-PBN was identified as the compound whose EPR signal has the typical *g*-factor of 2.0069 characteristic of nitroxide radical and hyperfine coupling of 8.0 G from nitrogen atom, making it a triplet. This compound was described earlier in the literature (99) and was observed in larger quantity in other EPR measurements after prolonged irradiation. Additional radical, with slightly different *g*-factor (2.0059) was still a nitroxide radical, but with distinct H-atom and *N*-atom couplings, making it a triplet of doublets. As part of article **1**, different options were investigated using DFT calculations, but only oxo-PBN adduct had good enough fit with experimental results. Deconvolution techniques were used to gain insights about this mixture of radicals. Within these deconvolution procedures, one major premise was followed – our goal was to deconvolute towards the least number of radicals that successfully describe experimental spectra. Additionally, deconvolution results were compared with results from quantum-chemical calculations. Conditional fitting of EPR spectra based on observations made from EPR experiments without simulations as well as NMR spectra, was done.

In article **1**, EPR spectra for compound *N*-bromo-*N*-hexylbenzenesulfonamide was disclosed. Spectrum for this compound provides evidence for a nitrogen radical adduct that is characterized by large triplet splitting coming from *N*-atom in PBN with doublet splitting coming from H-atom of PBN and the third triplet splitting coming from *N*-atom in from fragment belonging to the *N*-chloro-*N*-hexyl-4-methylbenzenesulfonamide. One signal corresponding to two indistinguishable PBN adducts of C_5- and C_6-centered radicals, was observed. This observation was corroborated by DFT calculations as both C_5- and C_6-radical adducts have similar calculated *hfc* and *g*-factors as they are both secondary alkyl *C*-centered radicals. In addition, a C_2-radical adduct was detected and assigned in accordance with DFT calculations (Table 2). No bromine radical adduct was observed as this adduct was too unstable and rapidly decomposed.

Table 2. Comparison of calculated and simulated EPR parameter for *N*-bromo-*N*-hexylbenzenesulfonamide. Radical adducts are denoted in the table as C_2-PBN, C_5-PBN, C_6-PBN, and N-PBN while *g* stands for *g* tensor, α_N, $\alpha_{N'}$ and α_H are hyperfine coupling values for each of the adducts, respectively.

	N-PBN[a]		**C_6-PBN**[a]		**C_5-PBN**[a]		**C_2-PBN**[a]	
	EXP	CALC	EXP	CALC	EXP	CALC	EXP	CALC
g^b	2.0064	2.0062	2.0061	2.00595	2.0061	2.00597	2.0064	2.00610
$\alpha_N{}^b$	14.14	13.81	13.84	15.09	13.84	14.80	13.80	14.08
$\alpha_H{}^b$	3.95	2.89	2.47	2.36	2.47	2.27	7.34	5.46
$\alpha_{N'}{}^b$	1.58	1.52						

[a] Radical adducts [b] *g* tensor and hyperfine coupling values for each of the adducts, respectively.

The same method was used to deconvolute the spectra of the *N*-bromo-*N*-(heptan-2-yl)-4-methylbenzenesulfonamide, showing a good agreement between the simulated and experimental spectrum along with a small residual signal. Although bromine radical adduct was not detected as it decomposed to quickly to form oxo-PBN, which was in this case observed. Evidence for both nitrogen radical as well as C_5- and C_6-radical adducts was provided. C_2-radical adduct was not discerned in the spectra.

From the comparison of the two EPR spectra of the compounds, in the case of *N*-bromo-*N*-hexylbenzenesulfonamide, no oxo-PBN adduct was observed, however a C_2 radical adduct was observed. As for the compound *N*-bromo-*N*-(heptan-2-yl)-4-methylbenzenesulfonamide, it is the opposite, oxo-PBN was observed and C_2-PBN was not observed. These EPR measurements constitute first detection of *N*- and *C*- centered radical intermediates generated from *N*-bromoamines in the literature.

In article **1**, EPR spectra (Figure 2) for compound *N*-chloro-*N*-hexyl-4-methylbenzenesulfonamide was disclosed. Chlorine radical adduct was identified in the spectra. EPR parameters of this radical adduct correspond to the literature references (100). Nitrogen radical adduct was detected as well as carbon radical adducts which are both indistinguishable *C*-centered alkyl radicals. Oxo-PBN and C_2-radical adducts have also been observed. For this compound, experimental and simulated spectra agree exceptionally well with some residual signal.

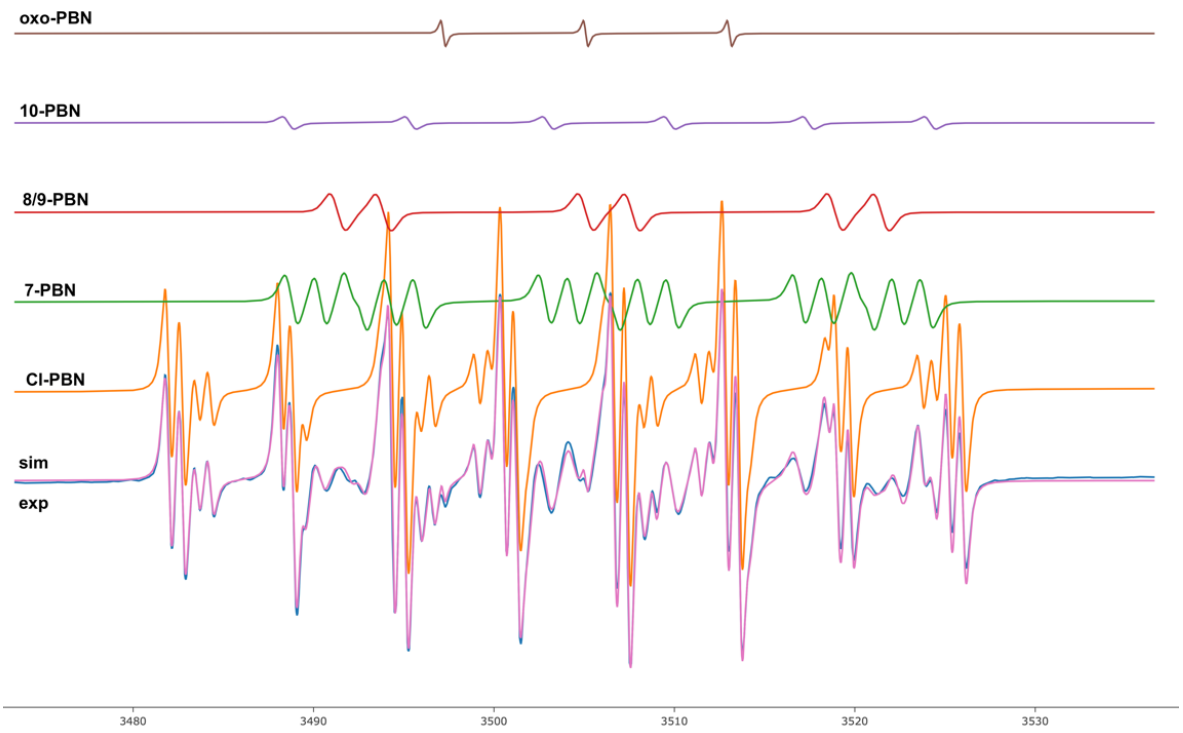

Figure 2. EPR spectra of spin-trapped radical intermediates generated with 370 nm irradiation of *N*-chloro-*N*-hexyl-4-methylbenzenesulfonamide. The experimental spectrum is in brown color, purple, red, green, orange, pink and blue correspond to simulated spectra for oxo-PBN, 10-PBN, 8/9-PBN, 7-PBN, Cl-PBN, total simulated spectrum and experimental spectrum, respectively.

Spectra for compound *N*-chloro-*N*-(heptan-2-yl)-4-methylbenzenesulfonamide were deconvoluted in the same manner, with an excellent agreement between the experimental and the simulated spectrum along with some residual signal. The spectra revealed the presence of a chlorine radical adduct, nitrogen radical adduct, C_5-, C_6- and C_2-radical adducts. In addition, the oxo-PBN species was also observed.

As seen from the comparison of the two compounds, the same number and type of PBN spin adducts were detected. Reproducibility of EPR measurements was achieved between these two systems. Based on these measurements a mechanism was proposed, *i.e.*, the homolytic cleavage of an N–Cl bond upon which *N* and Cl radicals are generated. *N*-radical rearranges to its carbon radical counterparts. *C*-centered radical then abstracts a halogen atom from a reactant molecule, thereby closing the cycle and yielding products. The expected products were observed in NMR measurements.

In these EPR measurements, different radical precursors in terms of the *N*-halogen bonds were used, however, remarkable reproducibility of *g* tensor and *hfc* values for both *N*-centered and

C-centered radical adducts was obtained across the board. Furthermore, the *N*- and *C*-centered radical adducts in these experiment were detected simultaneously, *i.e.*, while propagating. This was not observed by Sutcliffe and Ingold (88), although they had a tougher job of detecting *N*- and *C*-centered radicals directly. Therefore, this constitutes the first known detection of traces in the HLF reaction captured while propagating as there is little or no doubt (88) that at room temperature *N*-centered radical rearranges rapidly to its *C*-centered counterpart. This argument is also supported by the calculated rate constant of $4 \cdot 10^6$ s^{-1} for 1,5-HAT and $2 \cdot 10^7$ s^{-1} for 1,6-HAT for system *N*-chloro-*N*-(heptan-2-yl)-4-methylbenzenesulfonamide, while Sutcliffe and Ingold (88) reported on the estimated rate constants for 1,5-HAT processes of $1 \cdot 10^5$ s^{-1} and $4 \cdot 10^4$ s^{-1} for abstraction from a methyl group in alkly and acyl moieties, respectively.

As part of article **1**, a methodology for the calculation of EPR parameters was developed. Molecular dynamics (MD) simulations and conformer generation as well as DFT calculations for several hundred conformers for each PBN adducts were done. Boltzmann averages of *g* tensor and *hfc* values for all of the obtained conformers for a particular adduct were calculated using a program that was developed. These calculations were very precise in terms of explaining what was observed (Table 2).

Methodology was developed for DFT calculations on the thermodynamics and kinetics of the rearrangement of nitrogen and carbon radicals in the same article. Within this methodology a program for the calculation of Boltzmann averages was written. Stabilities of different nitrogen and carbon centered radicals were calculated as well and presented on a scale.

As part of article **2** (96), EPR measurements on model compound *N*-chloro-4-methyl-*N*-(5-phenylpentyl)benzensulfonamide were done.

The spectra for compound *N*-chloro-4-methyl-*N*-(5-phenylpentyl)benzensulfonamide were recorded in three different solvents, toluene, *n*-heptane and acetonitrile. Recorded spectrum in toluene exhibited an exceptional agreement with the simulated spectrum with some residual signal (Figure 3). Chlorine radical adduct and nitrogen radical adducts were first identified in the spectra. Two distinct *C*-centered radicals were detected, one alkyl radical that was assigned to be a C_5-centered radical, and the other C_6-centered benzyl radical along with a C_2-radical adduct**.**

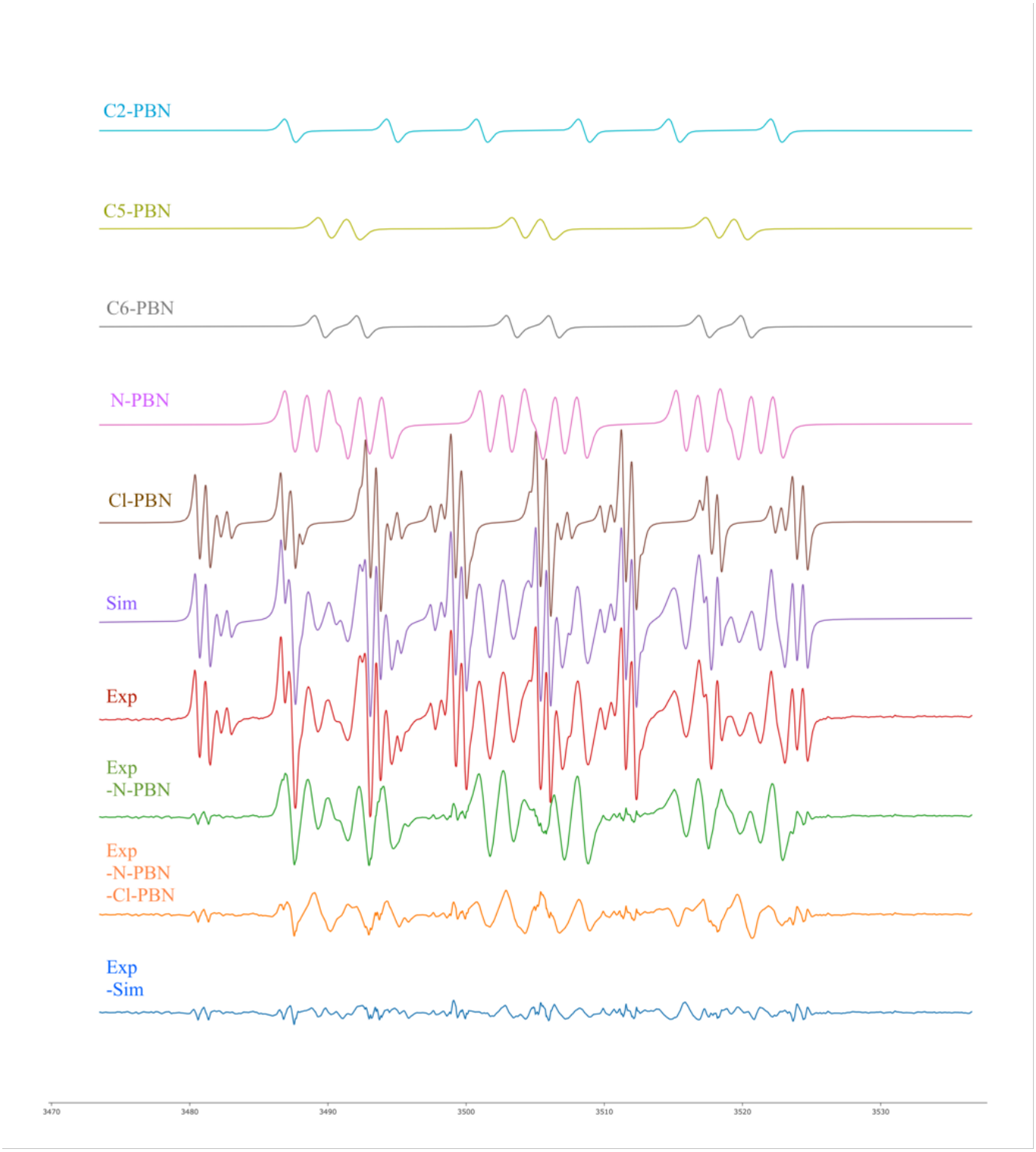

Figure 3. EPR spectra of spin-trapped radical intermediates generated with 370 nm irradiation of *N*-chloro-4-methyl-*N*-(5-phenylpentyl)benzensulfonamide. The simulated spectra of each radical adduct species are denoted on the spectra as C_2-PBN, C_5-PBN, Cl-PBN, C_6-PBN, and N-PBN. Total simulated spectrum is labelled as Sim, while experimental spectrum is labelled Exp, with residual signals provided as Exp – N-PBN, Exp – N-PBN – Cl-PBN, and Exp – Sim.

Spectrum in acetonitrile was deconvoluted in the same manner, in agreement with the simulated spectrum, along with some residual signal. All of the same types and the same number of radical adducts were detected. This was the case in *n*-heptane as well.

Reproducibility of EPR measurements was achieved. Based on our EPR results, we proposed homolytic cleavage of an N–Cl bond upon which *N*- and Cl radicals were generated. *N*-radical rearranged to its carbon radical counterparts. *C*-radical then abstracted a bromine atom from a reactant molecule thereby closing the cycle and yielding products.

In article **2**, NMR analysis of the product mixture after *off-site* irradiation of *N*-chloro-4-methyl-*N*-(5-phenylpentyl)benzensulfonamide in toluene revealed formation of four distinct products. It was established that these four products were parent amine, imine, and C_6- and C_5-chlorinated products (Figure 4). From additional NMR experiments in deuterated benzene and deuterated acetonitrile, the same mixture of products, albeit in different ratios, was obtained. It was established that parent amine and imine are disproportionation product of a self-reaction (32,33) and it was hypothesized that this is the reason why many chemists in their synthetic work block the C_2-position (74,77,101).

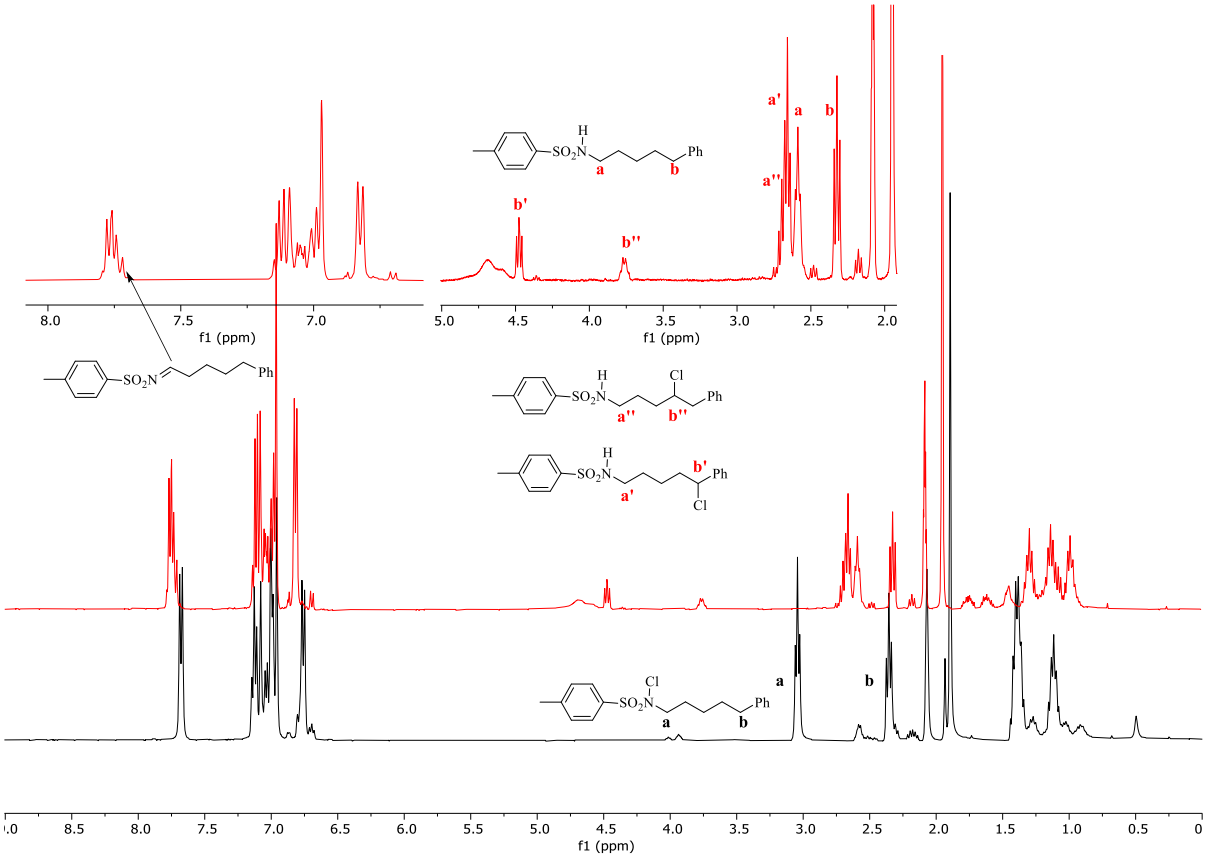

Figure 4. NMR spectra before and after *off-site* irradiation in toluene. The black and red spectra correspond to the *N*-chloro-4-methyl-*N*-(5-phenylpentyl)benzensulfonamide and reaction mixture of N-H, C_6-Cl, C_5-Cl, and C_2=N, respectively.

As part of article **2**, LFP measurements were conducted on *N*-chloro-4-methyl-*N*-(5-phenylpentyl)benzensulfonamide in acetonitrile through which the transient species generated after laser excitation were directly detected (Figure 5). It was established that a nitrogen centered radical as well as a benzyl radical were detected and their lifetimes estimated. This constituted the first detection of nitrogen centered radical and its rearranged carbon radical counterpart from *N*-halo amines in the context of the HLF reaction.

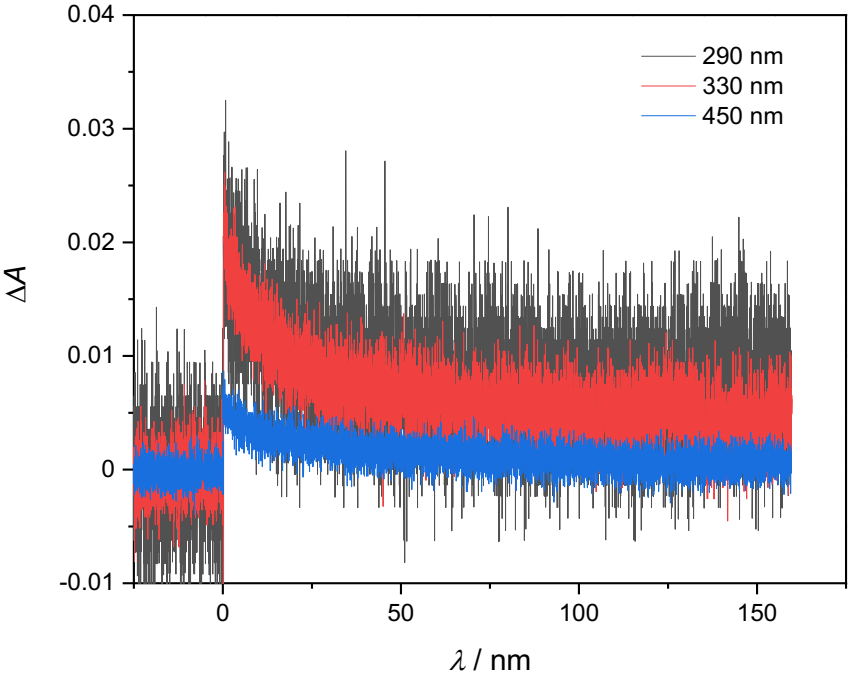

Figure 5. Superimposed time profiles at 290, 330 and 450 nm after laser excitation of 0.3 mM Tos-*N*-Cl-$(CH_2)_5$-Ph in acetonitrile saturated with N_2. E_{266} = 22 mJ, A_{266} = 0.27.

In the framework of article **2**, a computational methodology was developed in order to calculate the UV spectra of all possible radical species and to confirm what was detected via LFP measurements. It was established that the calculated UV spectrum explain the observed ones. These computational results were visualized and presented using a web-based implementation of a software (102).

Extensive DFT calculations were done in article **2** on the propagation cycle in which trace compounds detected *via* EPR and LFP measurements were observed. It was established that the calculated lifetimes are in good agreement with the experimentally determined ones and that the definition of the barrier from the global minimum describes experimental results much better for the second step, namely XAT. On the other hand, definition of the barrier from the pre-reactive minimum fits much better with the experimental results for the first, HAT step. Furthermore, it was determined that there is no thermodynamic preference for the formation of the C_6-Cl product over C_5-Cl product.

Based on these calculations and the observed regioselectivity of the chlorinated product mixture in the NMR measurements, a hypothesis was proposed that explains the observed

regioselectivity and the rate limiting step of the HLF reaction. The argument was that the formation of the two products occurs via two distinct and well-established radical chain reactions to which Bodenstein approximation, long-chain approximation, and approximation regarding chain-carrier concentrations apply. The Bodenstein approximation (103,104) states that "The net rate of formation of an intermediate that is and remains at trace level is negligible compared with its contributing formation and decay rates." Approximation that both radical chain reactions, 1,5-HAT and 1,6-HAT, have the same steady state concentration of the aminyl radicals. When this approximation was applied in the kinetic modelling done in article **2** on the HLF reaction, equations 7–17 were derived. From eqn. 5 follows that the rates of the propagation steps comprising a propagation cycle are the same and are equal to the overall rate of the cycle. It was argued that this is the case for the two propagation cycles leading to two distinct products, *i.e.*, C_5–Cl and C_6–Cl (Figure 6 and 7) and the following argument was made. The obtained mathematical expression state that the HLF reaction follows pseudo-first order kinetics with regard to the second step and that the rate of the cycle can, therefore, be controlled by the second step. This implies that the regioselectivity of the HLF reaction is determined by the first step and that the second step is rate limiting. Finally, this was supported by the experimental and computational results from which it was deduced that the different rate constants strongly imply the quite large steady-state concentration of the *C*-centered radicals.

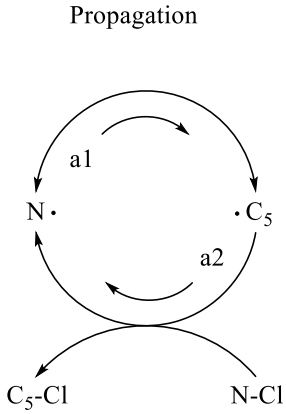

Figure 6. Propagation cycle leading to the formation of the C_5–Cl product.

$$r_{a1} = \lambda_{a1}N - \lambda_{-a1}C_5 \qquad \text{eqn 7.}$$

$$r_{a2} = \lambda_{a2}C_5 \qquad \text{eqn 8.}$$

$$r_X = (r_X)_{init} + \lambda_{a1}N - C_5(\lambda_{-a1} + \lambda_{a2}) + (r_X)_{trm} \cong 0 \qquad \text{eqn 9.}$$

$$N \cong C_5\left[\frac{\lambda_{a2} + \lambda_{-a1}}{\lambda_{a1}}\right] \qquad \text{eqn 10.}$$

$$r_{a1} \cong r_{a2} \cong \lambda_{a2} C_5 \qquad \text{eqn 11.}$$

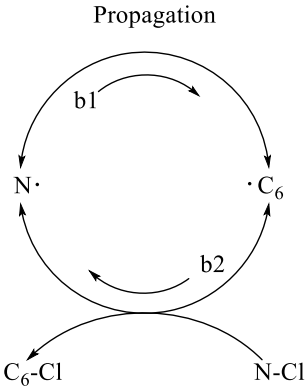

Figure 7. Propagation cycle leading to the formation of the C_6–Cl product.

$$r_{b1} = \lambda_{b1} N - \lambda_{-b1} C_6 \qquad \text{eqn 12.}$$

$$r_{b2} = \lambda_{b2} C_6 \qquad \text{eqn 13.}$$

$$r_X = (r_X)_{init} + \lambda_{b1} N - C_6(\lambda_{-b1} + \lambda_{b2}) + (r_X)_{trm} \cong 0 \qquad \text{eqn 14.}$$

$$N \cong C_6 \left[\frac{\lambda_{b2} + \lambda_{-b1}}{\lambda_{b1}}\right] \qquad \text{eqn 15.}$$

$$r_{b1} \cong r_{b2} \cong \lambda_{b2} C_6 \qquad \text{eqn 16.}$$

$$C_5 \left[\frac{\lambda_{a2} + \lambda_{-a1}}{\lambda_{a1}}\right] \cong C_6 \left[\frac{\lambda_{b2} + \lambda_{-b1}}{\lambda_{b1}}\right] \qquad \text{eqn 17.}$$

Following this work, the synthesis of macrocycles was pursued in article **3**(95). Within this article, a methodology was developed that modelled all transition states and all products of the rearrangement reactions of azacyclotridecan-2-one.

Within the context of article **3**, EPR experiments were performed. Spectra were deconvoluted and only two different radicals were observed. The major observed radical was the adduct of chlorine radical adduct. Another radical was a *C*-centered radical adduct. After decomposition, some residual signals remained with some weak and broad components which are similar to the *N*-PBN adduct radical observed in article **1**.

Finally, NMR experiments were performed to identify the reaction products. In the spectra, eight distinct products were identified.

All experiments done in article **3** combined, established that the thermodynamically driven HLF reaction, characterized by radical stability differences, transformed laurolactam into various bicyclic lactams with ring sizes ranging from 4- to 7-membered rings. Amidyl radicals in such constrained lactam rings exhibited a higher RSE values (Figure 8) as compared to unconstrained system (*N*-methylacetamide), indicating reduced stability, according to the DFT computations. C-centered radicals, particularly those adjacent to carbonyl or amine groups, demonstrated enhanced radical stability. Computational modelling revealed the lowest activation barriers for 1,5- and 1,6-HAT *exo*-type cyclizations with carbonyl moiety outside the smaller ring. It was calculated that 1,4-HAT *endo*-type reactions proceed with a lower barrier when compared to *exo*-type counterparts.

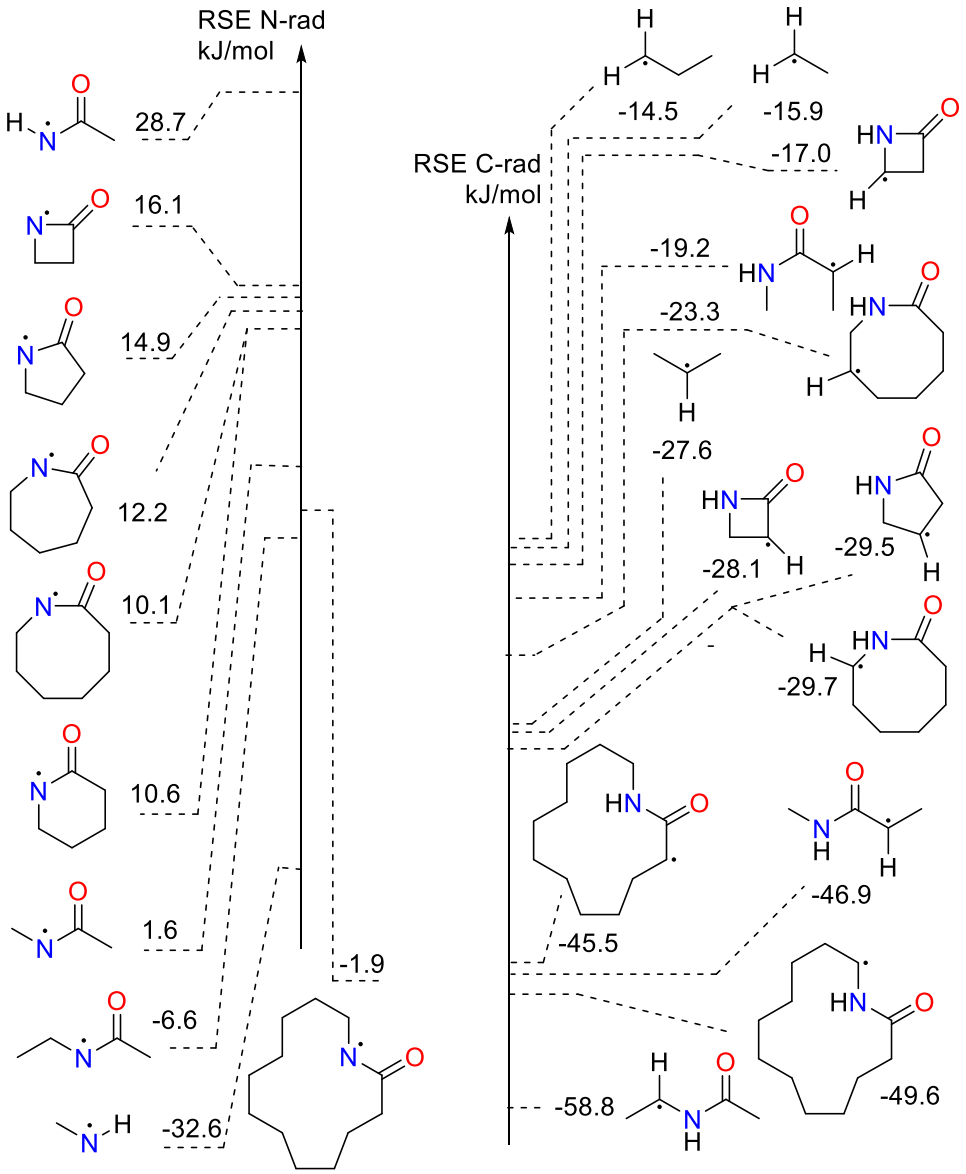

Figure 8. RSE values for selected *N*-centered radicals and *C*-centered radicals in selected heterocyclic and acyclic systems.

7. CONCLUSIONS

This doctoral thesis presents extensive research of the mechanism of the HLF reaction. Contribution to the fundamental understating of the HLF reaction was given through the three articles discussed herewith.

The EPR measurements constitute the first detection of *N*- and *C*-centered radical intermediates generated from *N*-bromo amines and they constitute the first known detection of traces of the HLF reaction while propagating. Our LFP measurements constitute the first successful detection of nitrogen centered radical and its rearranged carbon radical counterpart from *N*-halo amines in the context of the HLF reaction.

Using NMR, LFP and EPR spectroscopy in combination with DFT calculations, the reaction profile of the HLF reaction was monitored and all significant intermediate radicals and products were identified. Results show that there is no thermodynamic preference for the formation of C_6-functionalized product over C_5-functionalized product, and that the observed regioselectivity was due to the major product being a kinetic product. An alternative hypothesis is that the observed regioselectivity favoring 1,5-HAT products can be attributed to an additional rearrangement reaction exclusive to the C_6 radical. Through another 1,5-HAT step, the C_6 radical is transformed into the most stable C_2 radical. The existence of C_2 radical is experimentally proven not only through EPR spectroscopy but also via synthetic reactions and side products formed, notably imine and aldehyde. NMR analysis of the product mixtures revealed formation of four distinct products. It was established that these four products were parent amine, imine and C_6 and C_5 chlorinated products. The parent amine and imine are disproportionation product of a self-reaction, and it was hypothesized that this is the reason that many chemists in their synthetic work block the C_2 position.

Kinetic modelling on the HLF reaction provided strong evidence that we have two distinct and well-established radical chain reactions to which Bodenstein approximation along with long-chain approximation and approximation regarding chain-carrier concentrations apply. These two radical chain reactions leading to two distinct products have the steady state concentration of the nitrogen centered radical in common. Furthermore, mathematical expressions were obtained stating that the HLF reaction follows pseudo-first order kinetics with regard to the second step and that, therefore, the rate of the cycle is determined by the second step. This implies that the regioselectivity of the HLF reaction is determined by the second step and that the second step is rate limiting. This was additionally supported by the experimental and computational results from which we deduced that different rate constants imply the large steady-state concentration of the *C*-centered radicals. Additionally, it was proposed that by

adding halogen sources, typically used as chlorinating agents, or other traps may interfere with the XAT step of the propagation cycle, promoting earlier termination of a reaction cycle.

Finally, HLF reaction was shown to be a viable method for late-stage functionalization of laurolactams. It was demonstrated that a laurolactam is transformed into various bicyclic lactams with ring sizes ranging from 4- to 7-membered rings. Amidyl radicals in these constrained lactam rings exhibited higher RSE values, indicating reduced stability. *C*-centered radicals, particularly those adjacent to carbonyl or amine groups, demonstrated enhanced radical stability, with notable exceptions in highly constrained structures like 2-azetidinone. Computational modelling revealed the lowest activation barriers are observed for the 1,5- and 1,6-HAT *exo*-type cyclization reactions with carbonyl moiety outside the smaller ring. It was calculated that 1,4-HAT *endo*-type reactions proceed with a lower barrier when compared to *exo*-type counterparts.

8. LITERATURE

1. Hofmann AW. Zur kenntniss der coniin-gruppe. Ber Dtsch Chem Ges 1885;18:109–131.

2. Ardura D, López R, Sordo TL. Relative gibbs energies in solution through continuum models: effect of the loss of translational degrees of freedom in bimolecular reactions on Gibbs energy barriers. J Phys Chem B 2005;109:23618–23623.

3. Hayyan M, Hashim MA, Al Nashef IM. Superoxide ion: generation and chemical implications. Chem Rev 2016;116:3029–3085.

4. D. McNaught A, Wilkinson A (eds). The IUPAC compendium of chemical terminology: the gold book. 2nd ed. Oxford UK: Blackwell Scientific Publications, 1997.

5. Gomberg M. An instance of trivalent carbon : triphenyl-methyl. J Am Chem Soc 1900;20:757–771.

6. Wieland H. Tetraphenylhydrazin und hexaphenyläthan. (IX.bhandlung über aromatische hydrazine.). Justus Liebigs Ann Chem 1911;381:200–216.

7. Paneth F, Hofeditz W. Über die darstellung von freiem methyl. Ber Dtsch Chem Ges 1929;62:1335–1347.

8. Lewis GN, Lipkin D. Reversible photochemical processes in rigid media: the dissociation of organic molecules into radicals and ions. J Am Chem Soc 1942;64:2801–2808.

9. Lamb RC, Ayers PW, Toney MK. Organic peroxides. II. the mechanism of the thermal decomposition of 6-heptenoyl peroxide in zoluene. the rearrangements of the 5-hexenyl radical. J Am Chem Soc 1963;85:3483–3486.

10. Julia M. Free-radical cyclizations. Acc Chem Res 1971;4:386–392.

11. Wawzonek S, Thelen PJ. Preparation of N-methylgranatanine. J Am Chem Soc 1950;72:2118–2120.

12. Corey EJ, Hertler WR. A Study of the formation of haloamines and cyclic amines by the free radical chain decomposition of N-haloammonium ions (Hofmann-Löffler reaction). J Am Chem Soc 1960;82:1657–1668.

13. Griller D, Ingold KU. Persistent carbon-centered radicals. Acc Chem Res 1976;9:13–19.

14. Baldock RW, Hudson P, Katritzky AR, et al. Stable free radicals. Part I. A new principle governing the stability of organic free radicals. J Chem Soc 1974;1422–1427.

15. Halliwell B. The chemistry of free radicals. Toxicol Ind Health 1993;9:1–21.

16. Asmus K-D. Sulfur-centered free radicals. Methods Enzymol 1990;186:168–180.

17. Bielski BHJ, Richter HW, Chan PC. Some properties of the ascorbate free radical. Ann N Y Acad Sci 1975;258:231–237.

18. Cowley AH, Hnoosh MH. Free radicals involving phosphorus. J Am Chem Soc 1966;88:2595–2587.

19. Marque S, Tordo P. Reactivity of phosphorus centered radicals. In: Majoral J-P (ed) New aspects in phosphorus chemistry. Berlin, Heidelberg: Springer:43–76.

20. Kerr ME, Bender CM, Monti EJ. An introduction to oxygen free radicals. Heart & Lung 1996;25:200–209.

21. Hioe J, Šakić D, Vrček V, et al. The stability of nitrogen-centered radicals. Org Biomol Chem 2015;13:157–169.

22. Chatgilialoglu C, Studer A. Encyclopedia of radicals in chemistry, biology and materials. Chichester, UK: Wiley, 2012.

23. Rice-Evans CA, Diplock AT. Chapter 2 Mechanisms of radical production. Lab Tech Biochem Mol Biol 1991;22:19–50.

24. Hey DH, A.Waters W. Some organic reactions involving the occurence of free radicals in solution. Chem Rev 1937;21:169–208.

25. Wolff ME. Cyclization of N-halogenated amines (The Hofmann-Löffler Reaction). Chem Rev 1963;63:55–64.

26. Kovacic P, Lowery MK, Field KW. Chemistry of N-bromamines and N-chloramines. Chem Rev 1970;70:639–665.

27. Neale RS. Nitrogen radicals as synthesis intermediates. N-halamide rearrangements and additions to unsaturated hydrocarbons. Syn 1971;1971:1–15.

28. Zard SZ. Recent progress in the generation and use of nitrogen-centred radicals. Chem Soc Rev 2008;37:1603.

29. Fallis AG, Brinza IM. Free radical cyclizations involving nitrogen. Tetrahedron 1997;53:17543–17594.

30. Esker JL, Newcomb M. The generation of nitrogen radicals and their cyclizations for the construction of the pyrrolidine nucleus. Adv Heterocycl Chem 1993;58:1–45.

31. Danen WC, Neugebauer FA. Aminyl free radicals. Angew Chem Int Ed Engl 1975;14:783–789.

32. Rice FO, Grelecki CJ. The dimethylamino radical. J Am Chem Soc 1957;79:2679–2680.

33. Roberts JR, Ingold KU. Kinetic applications or electron paramagnetic resonance spectroscopy. X. Reactions of some alkylamino radicals in solution. J Am Chem Soc 1973;95:3228–3235.

34. Booth GH, Norrish RGW. 39. Photochemical studies of some organic nitrogen derivatives. J Chem Soc 1952;188.

35. Bamford CH. 3. A study of the photolysis of organic nitrogen compounds. Part I. Dimethyl- and diethyl-nitrosoamines. J Chem Soc 1939;12.

36. Cowley BR, Waters WA. 240. Some reactions of the dimethylamino radical, ·NMe_2. J Chem Soc 1961;0:1228–1231.

37. Mackay D, Waters WA. Some reactions of dialkylamino radicals. J Chem Soc, C 1966;813.

38. Michejda CJ, Campbell DH. Amphoteric amino radicals. Tetrahedron Lett 1977;18:577–580.

39. Bellas M, Bryce-Smith D, Gilbert A. 1,4-Photoaddition of amines to benzene. Chem Commun (London) 1967;862.

40. Shkunnikova S, Zipse H, Šakić D. Role of substituents in the Hofmann–Löffler–Freytag reaction. A quantum-chemical case study on nicotine synthesis. Org Biomol Chem 2021;19:854–865.

41. Šakić D, Zipse H. Radical Stability as a Guideline in C-H Amination Reactions. Adv Synth Catal 2016;358:3983–3991.

42. Gassman PG, Uneyama K, Hahnfeld JL. A comparison of the heterolytic vs. homolytic cleavage of the nitrogen-chlorine bond. J Am Chem Soc 1977;99:647–648.

43. Newcomb Martin, Burchill MT, Deeb TM. A mechanistic probe study of potential electron-transfer reactions of lithium dialkylamides. J Am Chem Soc 1988;110:6528–6535.

44. Luca El-CD, Giacomelli G, Nieddu G. A simple protocol for efficient N-chlorination of amides and carbamates. Synt Lett 2005;223–226.

45. Ogata Y, Izawa Y, Tomioka H. The photochemical addition of monochloramine to cyclohexene. Tetrahedron 1967;23:1509–1514.

46. Anderson PS, Lundell F, Cias JL, et al. Synthesis of 1,2,3,3a,8,8a-hexahydroindeno[2,1-b]pyrrole. Tetrahedron Lett 1971;12:2787–2790.

47. Stella L, Raynier B, Surzur J-M. Synthesis of 2-methyl-6,7-benzomorphane via radical cyclisation. Tetrahedron Lett 1977;18:2721–2724.

48. Burgess EM, Lavanish JM. Photochemical decomposition of N-nitrosamines. Tetrahedron Lett 1964;5:1221–1226.

49. Newcomb M, Ha C. Lewis acid activated and catalyzed cyclizations of aminyl radicals from *N*-hydroxypyridine-2-thione carbamates. Tetrahedron Lett 1991;32:6493–6496.

50. Barton DHR, Lacher B, Zard SZ. The invention of new radical chain reactions. Tetrahedron 1986;42:2325–2328.

51. Newcomb M, Deeb TM. N-Hydroxypyridine-2-thione carbamates as aminyl and aminium radical precursors. Cyclizations for synthesis of the pyrrolidine nucleus. J Am Chem Soc 1987;109:3163–3165.

52. Newcomb M, Park S-U, Kaplan J, et al. Facile generation of dialkylaminyl radicals from N-hydroxypyridine-2-thione carbamates. Application in kinetic studies of small ring cycloalkylaminyl radical ring openings. Tetrahedron Lett 1985;26:5651–5654.

53. Newcomb M, Esker JL. Facile production and cyclizations of amidyl radicals. Tetrahedron Lett 1991;32:1035–1038.

54. Kim S, Lee TA. Facile generation of alkyl, aminyl, and alkoxy radicals from se-phenyl benzoselenohydroximate derivatives. Synlett 2000;1997:950–952.

55. Bowman WR, Broadhurst MJ, Coghlan DR, et al. Cyclisation of aminyl radicals derived from amino acids. Tetrahedron Lett 1997;38:6301–6304.

56. Bowman WR, Clark DN, Marmon RJ. Generation of aminyl radicals using sulfenamides as synthetic precursors. Tetrahedron 1994;50:1275–1294.

57. Bowman WR, Clark DN, Marmon RJ. Cyclisation of aminyl radicals using sulfenamide precursors. Tetrahedron Lett 1992;33:4993–4994.

58. Kozuch S. Steady state kinetics of any catalytic network: graph theory, the energy Span model, the analogy between catalysis and electrical circuits, and the meaning of “mechanism.” ACS Catal 2015;5:5242–5255.

59. Perez-Benito JF. Some considerations on the fundamentals of chemical kinetics: steady state, quasi-equilibrium, and transition state theory. J Chem Educ 2017;94:1238–1246.

60. Helfferich FG, Helfferich FG. Kinetics of multistep reactions. 2nd ed. Amsterdam ; Boston: Elsevier, 2004.

61. Löffler K, Freytag C. Über eine neue bildungsweise von N -alkylierten pyrrolidinen. Ber Dtsch Chem Ges 1909;42:3427–3431.

62. Hübner H, Lellmann E. Ueber einen dijodpropylalkohol und einen monojodallylalkohol. Ber Dtsch Chem Ges 1880;13:460–461.

63. Löffler K, Kober S. Über die bildung des i-Nicotins aus N-methyl-p-pyridyl-butylamin (dihydrometanicotin). Ber Dtsch Chem Ges 1909;42:3431–3438.

64. de Armas P, Carrau R, Concepción JI, et al. Synthesis of 1,4-epimine compounds. Iodosobenzene diacetate, an efficient reagent for neutral nitrogen radical generation. Tetrahedron Lett 1985;26:2493–2496.

65. Carrau R, Hernández R, Suárez E, et al. Intramolecular functionalization of N-cyanamide radicals: synthesis of 1,4-and 1,5-N-cyanoepimino compounds. J Chem Soc 1987;937–943.

66. Hernández R, Medina MC, Salazar JA, et al. Intramolecular functionalization of amides leading to lactams. Tetrahedron Lett 1987;28:2533–2536.

67. De Armas P, Francisco CG, Hernández R, et al. Steroidal N-nitroamines. Part 4. Intramolecular functionalization of N-nitroamine radicals: synthesis of 1,4-nitroimine compounds. J Chem Soc 1988;3255–3265.

68. Dorta RL, Francisco CG, Suárez E. Hypervalent organoiodine reagents in the transannular functionalisation of medium-sized lactams: synthesis of 1-azabicyclo compounds. J Chem Soc 1989;1168–1169.

69. Reddy LR, Reddy BVS, Corey EJ. Efficient method for selective introduction of substituents as C(5) of Isoleucine and other α-amino acids. Org Lett 2006;8:2819–2821.

70. Del Castillo E, Muñiz K. Enantioselective synthesis of Nicotine via an iodine-mediated Hofmann–Löffler Reaction. Org Lett 2019;21:705–708.

71. Fan R, Pu D, Wen F, et al. δ and α SP3 C−H bond oxidation of sulfonamides with PhI(OAc)2/I2 under metal-free conditions. J Org Chem 2007;72:8994–8997.

72. Duhamel T, Martínez MD, Sideri IK, et al. 1,3-Diamine Formation from an Interrupted Hofmann–Löffler Reaction: Iodine Catalyst Turnover through Ritter-Type Amination. ACS Catal 2019;9:7741–7745.

73. Kiyokawa K, Nakamura S, Jou K, et al. Transition-metal-free Intramolecular C–H amination of sulfamate esters and N-alkylsulfamides. Chem Commun 2019;55:11782–11785.

74. Short MA, Shehata MF, Sanders MA, et al. Sulfamides direct radical-mediated chlorination of aliphatic C–H bonds. Chem Sci 2020;11:217–223.

75. Chen K, Richter JM, Baran PS. 1,3-diol synthesis via controlled, radical-mediated C−H functionalization. J Am Chem Soc 2008;130:7247–7249.

76. Zhang H, Muñiz K. Selective piperidine synthesis exploiting Iodine-catalyzed Csp3-H amination under visible light. ACS Catal 2017;7:4122–4125.

77. Short MA, Blackburn JM, Roizen JL. Sulfamate esters guide selective radical-mediated chlorination of aliphatic C−H Bonds. Angew Chem Int Ed 2018;57:296–299.

78. Becker P, Duhamel T, Stein CJ, et al. Cooperative light-activated iodine and photoredox catalysis for the amination of Csp3 −H bonds. Angew Chem Int Ed 2017;56:8004–8008.

79. Del Castillo E, Martínez MD, Bosnidou AE, et al. Multiple halogenation of aliphatic C−H bonds within the Hofmann–Löffler manifold. Chemistry A European J 2018;24:17225–17229.

80. Minisci F. Free-radical additions to olefins in the presence of redox systems. Acc Chem Res 1975;8:165–171.

81. Wawzonek S, Nelson MF, Thelen PJ. Preparation of quinuclidines. J Am Chem Soc 1951;73:2806–2808.

82. Zubčić G, You J, Zott FL, et al. Regioselective rearrangement of nitrogen- and carbon-centered radical intermediates in the Hofmann–Löffler–Freytag reaction. J Phys Chem A 2024;128:2574–2583.

83. Edwards OE, Paskovich DH, Reddoch AH. Radical intermediates in chloramine and N-chloroimide reactions. Can J Chem 1973;51:978–980.

84. Forshult S. Trapping as nitroxide radicals of the radicals formed in some reactions of N-bromosuccinimide, N-bromotetramethylsuccinimide, N-chlorosuccinimide and N-bromophthalimide. Acta Chem Scand 1969;23:708–709.

85. Danen WC, Kensler TT. Electron spin resonance study of dialkylamino free radicals in solution. J Am Chem Soc 1970;92:5235–5237.

86. Hadley SG, Volman DH. Photochemical formation of free radicals from aliphatic amines as studied by electron spin resonance. J Am Chem Soc 1967;89:1053–1055.

87. Danen WC, Rickard RC. Nitrogen-centered free radicals, IV. Electron spin resonance study of transient dialkylaminium radical cations. J Am Chem Soc 2002;94:3254–3256.

88. Sutcliffe R, Ingold KU. Kinetic applications of electron paramagnetic resonance spectroscopy. 40. Intramolecular reactions of some N-alkylcarboxamidyl radicals. J Am Chem Soc 1982;104:6071–6075.

89. Danen WC, Gellert RW. Nitrogen-centered free radicals. V. Electron spin resonance evidence for a .pi. electronic ground state of transient amido free radicals. J Am Chem Soc 1972;94:6853–6854.

90. Nelsen SF, Landis RT, Kiehle LH, et al. N-tert-butylanilino radicals. J Am Chem Soc 1972;94:1610–1614.

91. Bridger RF. Reactions of N-phenyl-2-naphthylamino radicals. J Am Chem Soc 1972;94:3124–3132.

92. Musa OM, Horner JH, Shahin H, et al. A kinetic scale for dialkylaminyl radical reactions. J Am Chem Soc 1996;118:3862–3868.

93. Horner JH, Musa OM, Bouvier A, et al. Absolute kinetics of amidyl radical reactions. J Am Chem Soc 1998;120:7738–7748.

94. Le Tadic-Biadatti M-H, Callier-Dublanchet A-C, Horner JH, et al. Absolute rate constants for iminyl radical reactions. J Org Chem 1997;62:559–563.

95. Zubčić G, Pavić K, You J, et al. Light-induced rearrangement from macrocyclic to bicyclic lactam: A case study of *N* -chlorinated laurolactam. Acta Pharm 2025;74:725–737.

96. Zubčić G, Friganović T, Andrijanić L, et al. Mechanistic insights into the propagation cycle of the Hofmann–Löffler–Freytag reaction. Halogen vs hydrogen atom transfer. The J Org Chem.

97. Wu X, Zhang X, Ji X, et al. Visible-light-induced cascade arylazidation of activated alkenes with trimethylsilyl azide. Org Lett 2023;25:5162–5167.

98. Coleman GH, Goheen GE. Preparation of Pyrrolidines. J Am Chem Soc 1938;60:730–730.

99. Carloni P, Eberson L, Greci L, et al. New insights on N-tert-butyl-α-phenylnitrone (PBN) as a spin trap. Part 1. Reaction between PBN and N-chlorobenzotriazole. J Chem Soc 1996;1297–1305.

100. Buettner GR. Spin Trapping: ESR parameters of spin adducts. Free Radic Biol Med 1987;3:259–303.

101. Short MA, Blackburn JM, Roizen JL. Modifying positional selectivity in C–H functionalization reactions with nitrogen-centered radicals: generalizable approaches to 1,6-hydrogen-atom transfer processes. Synlett 2020;31:102–116.

102. Šakić, D. DSakicLab/visualEPR, 2023. https://github.com/DSakicLab/visualEPR (accessed 2024-10-30).

103. Wang W-S, Li S-F, Su K. Nonlinear stability of Runge–Kutta methods for neutral delay differential equations. J Comput Appl Math 2008;214:175–185.

104. Zennaro M. Asymptotic stability analysis of Runge-Kutta methods for nonlinear systems of delay differential equations. Numer Math 1997;77:549–563.

9. CURRICULUM VITAE

Gabrijel Zubčić was born on April 21, 1990 in Zagreb, where he completed his primary and secondary education. After passing the state matriculation exam, he enrolled in the course of Applied Chemistry at the Faculty of Chemical Engineering and Technology at the University of Zagreb, Croatia. In the third year of the undergraduate study, he was among the 10% of the most successful students and received a STEM scholarship. In his graduate studies, he enrolled the course Applied Organic Chemistry. The diploma thesis entitled "Stereoselective arylation of diaryl ketimine catalyzed by chiral Brønsted acids" was produced in the Laboratory for Biomimetic Chemistry of the Institute of Organic Chemistry and Biochemistry, Ruđer Bošković, Zagreb Croatia, under the mentorship of Prof. Matija Gredičak and Prof. Irena Škorić. In 2021, he got a position at the Faculty of Pharmacy and Biochemistry as a doctoral student on the project "Light-driven functionalization of non-reactive positions using oxidative amination" funded by Croatian Science Foundation Installation Grant UIP-2020-02-4867 and led by Assoc. prof. Davor Šakić as principal investigator. During his work at the Faculty, he assisted the laboratory exercises of Analytical Chemistry I and Analytical Chemistry II courses. He participated in various scientific conferences/gatherings in the form of poster presentations and lectures, participated in a science festival and numerous workshops/educations, co-authored a professional paper and held a workshop entitled "Fundamentals of quantum chemical calculations". He participated in the "International School of Quantum Chemistry of Excited States" (QCES2024) at Babeș-Bolyai University in Cluj-Napoca, Romania. He published 5 scientific papers (4 original scientific papers and one review paper). All of the papers are included in the Web of Science Core Collection database. He is a member of the Croatian Chemical Society and the Croatian Society of Chemical Engineers and Technologists. Paper titled “Mechanistic insights into the propagation cycle of the Hofmann–Löffler–Freytag reaction. Halogen vs hydrogen atom transfer” was published as part of The Journal of Organic Chemistry special issue “Physical Organic Chemistry: Never Out of Style”.

List of scientific papers (WoSCC):

1. **Zubčić G**, Friganović T, Andrijanić L, et al. Mechanistic insights into the propagation cycle of the Hofmann–Löffler–Freytag reaction. Halogen vs hydrogen atom transfer. J Org Chem 2025; DOI: 10.1021/acs.joc.4c02997
2. **Zubčić G**, You J, Zott FL, et al. Regioselective rearrangement of nitrogen- and carbon-centered radical intermediates in the Hofmann–Löffler–Freytag reaction. J Phys Chem A 2024; 128, 2574–2583; DOI: 10.1021/acs.jpca.3c07892
3. **Zubčić G**, Pavić K, You J, et al. Light-induced rearrangement from macrocyclic to bicyclic lactam: A case study of N -chlorinated laurolactam. Acta Pharm 2025; 74, 725–737; DOI: 10.2478/acph-2024-0035
4. **Zubčić G**, Shkunnikova S, Šakić D, et al. Renaissance of the Hofmann-Löffler-Freytag Reaction – Development of C–H Functionalisation Strategies Based on Green Chemistry Principles. Chem Ind 2022; 71, 359–373; DOI: 10.15255/KUI.2021.070
5. Toma M, **Zubčić G**, Lapić J, et al. Ferrocenoyl-adenines: substituent effects on regioselective acylation. Beilstein J Org Chem 2022; 18, 1270–1277; DOI: 10.3762/bjoc.18.133

Basic documentation card

University of Zagreb
Faculty of Pharmacy and Biochemistry
Department of analytical chemistry
A. Kovačića 1, 10000 Zagreb, Croatia

Doctoral thesis

STABILITY AND REARRANGEMENTS OF *N*-CENTERED RADICALS RELEVANT FOR BIOACTIVE COMPOUNDS SYNTHESES

Gabrijel Zubčić

SUMMARY

The main goal of this doctoral thesis was to investigate the rearrangement reactions in which nitrogen centered radicals participate. Specific goals of this thesis were to investigate nitrogen centered radicals in the context of the Hofmann–Löffler-Freytag (HLF) reaction, namely, to explain the regioselectivity, investigate the propagation cycle, determine the rate limiting step, utilize the reaction for the generation of pharmaceutically relevant compounds, and compute stabilities of nitrogen centered radical. In this thesis, *N*-chloro derivatives as radical precursors were synthesized using existing methods, and new method was developed for the synthesis of *N*-bromo derivatives. A methodology was developed for the *in-situ* generation and trapping of nitrogen centered radicals and its carbon counterparts using the phenylbutylnitrone (PBN) spin trap and subsequent investigation of the resulting adducts *via* electron paramagnetic resonance (EPR) spectroscopy. Laser flash photolysis (LFP) method was used to directly detect the transient species generated after laser excitation. Nuclear magnetic resonance (NMR) methods were employed in order to analyze complex product mixtures. Quantum-chemical methodology was developed and employed to obtain a quantitative description of the thermodynamic and kinetic properties of the HLF reaction. Additionally, kinetic modelling was done. Using LFP, NMR, and EPR spectroscopy, in combination with density functional theory (DFT) calculations and kinetic modelling, the HLF reaction profile was monitored and all significant intermediate radicals and products were identified in this light-induced radical generation and subsequent chain reaction. It was observed that the major regioselective product of the HLF reaction is kinetically controlled in the hydrogen atom transfer (HAT) step, when different radical stabilities of intermediates are present. Thermodynamic preference for the formation of one product over the other is lost due to the second step of the cycle being highly exothermic, and both C-Cl functionalized product having similar energies. When both radical intermediates have similar stability, the observed regioselectivity can be attributed to a rearrangement reaction exclusive to the C_6-radical where it rearranges to a more stable C_2-radical. When positions are non-equal, NMR analysis of the product mixture revealed the presence of four major products. These four products are amine, imine, C_6- and C_5-chlorinated products. Amine and imine are products of a "self-reaction" of nitrogen radicals (termination) and is the probable reason why many synthetic chemists block the C_2-position in their synthetic works and why the HLF reaction proceeds only in certain solvents in high yields. Kinetic modelling of the HLF reaction showed that its kinetics are pseudo first order with respect to the second step. Thus, it is proposed that the rate limiting step of the HLF reaction is the halogen atom transfer (XAT) step. Additionally, it was proposed that by adding halogen sources, typically used as chlorinating agents the propagation cycle can be terminated. Finally, it was demonstrated that the HLF reaction is a viable method for late-stage functionalization (LSF) in the synthesis of pharmaceuticals. We used HLF reaction as a route for preparing bicyclic rings from *N*-chlorinated macrocyclic lactams. Interplay of different experimental and theoretical techniques have provided a deeper insight into the fundamental aspects of the HLF reaction, and results will be used for better utilization in future synthesis.

The thesis is deposited in the Central Library of the University of Zagreb Faculty of Pharmacy and Biochemistry.

Thesis contains: 95 pages, 8 figures, 2 tables, 28 schemes and 104 references. The original was written in English.
Keywords: Nitrogen-centered radicals, chain reaction, Hofmann–Löffler-Freytag (HLF) reaction, regioselectivity, rate-limiting step, self-reaction
Mentors: **Davor Šakić**, **PhD**, *Associate Professor, University of Zagreb Faculty of Pharmacy and Biochemistry*
Valerije Vrček, **PhD**, *Full Professor, University of Zagreb Faculty of Pharmacy and Biochemistry*
Reviewers: **Kristina Pavić**, **PhD**, *Assistant Professor, University of Zagreb Faculty of Pharmacy and Biochemistry*
Tin Weitner, **PhD**, *Associate professor, University of Zagreb Faculty of Pharmacy and Biochemistry*
Irena Škorić, **PhD,** *Full Professor, University of Zagreb Faculty of Chemical Engineering and Technology*
The thesis was accepted: 19th May 2025.

Temeljna dokumentacijska kartica

Sveučilište u Zagrebu **Doktorski rad**
Farmaceutsko-biokemijski fakultet
Zavod za analitičku kemiju
A. Kovačića 1, 10000 Zagreb, Hrvatska

STABILNOST I PREGRAĐIVANJE *N*-RADIKALA RELEVANTNIH ZA SINTEZE BIOAKTIVNIH SPOJEVA

Gabrijel Zubčić

SAŽETAK

Glavni cilj ovog doktorskog rada bio je istražiti reakcije pregradnje u kojima sudjeluju dušikovi radikali. Specifični ciljevi ovog rada bili su istražiti dušikove radikale u kontekstu Hofmann–Löffler-Freytagove (HLF) reakcije, tj. iznijeti hipotezu koja bi objasnila regioselektivnost, istražiti ciklus propagacije, odrediti korak koji određuje ukupnu brzinu, iskoristiti reakciju za stvaranje farmaceutski relevantnih spojeva i izračunati stabilnost radikala s dušikovim središtem. Sintetizirani su radikalski prekursori, pri čemu su korištene postojeće metode za sintezu *N*-kloro derivata i razvijene nove metode za sintezu *N*-bromo derivata. Razvijena je metoda za *in situ* generiranje i hvatanje dušikovih radikala i njihovih ugljikovih analoga korištenjem fenilbutilnitronske (PBN) spinske stupice i detekciju nastalih adukata putem elektronske paramagnetske rezonancije (EPR). Razvijena je metoda laserske pulsne fotolize (LPF) za izravnu detekciju radikalskih vrsta koje nastaju nakon laserske ekscitacije. Za analizu smjese produkata korištene su metode nuklearne magnetske rezonancije (NMR). Kvantno-kemijska metodologija razvijena je kako bi se dobio kvantitativni opis termodinamičkih i kinetičkih parametara HLF reakcije. Korištenjem NMR spektroskopije, laserske pulsne fotolize LPF i EPR spektroskopije u kombinaciji s izračunima teorije funkcionala gustoće (DFT) i kinetičkim modeliranjem, praćen je profil HLF reakcije i identificirani su svi značajni radikalski intermedijeri i produkti HLF reakcije. Opaženo je da je glavni regioselektivni produkt HLF reakcije kinetički kontroliran u koraku prijenosa atoma vodika (HAT), kada su prisutni radikalski međuprodukti različitih stabilnosti. Termodinamička sklonost za stvaranje jednog produkta u odnosu na drugi gubi se u nastavku propagacijskog ciklusa, zbog toga što je drugi korak ciklusa vrlo egzoterman, te C-Cl funkcionalizirani produkti imaju sličnu energiju. Kada oba radikalna međuprodukta imaju sličnu stabilnost, uočena regioselektivnost može se pripisati reakciji pregradnje vezanoj isključivo uz C_6 radikal. NMR analiza utvrdila je nastanak četiri glavna produkta -amin, imin, C_6 i C_5 klorirani produkti. Amin i imin su produkti "samo-reakcije" dušikovih radikala (terminacija), pa se na temelju toga pretpostavlja da je to razlog zašto mnogi kemičari blokiraju C_2 poziciju u sintetskim protokolima i zašto se HLF reakcija odvija samo u određenim otapalima s visokim prinosima. Kinetičko modeliranje HLF reakcije pokazalo je da je njezina kinetika pseudo prvog reda u odnosu na drugi reakcijski korak. Stoga se predlaže da je najsporiji stupanj HLF reakcije prijenos atoma halogena (XAT). Dodatno, predloženo je da se dodavanjem izvora halogena, koji se obično koriste kao sredstva za kloriranje, propagacijski ciklus može prekinuti. Konačno, pokazano je da se HLF reakcija može upotrijebiti za funkcionalizaciju u kasnoj fazi (LSF) u sintezi farmaceutika. Upotrijebili smo HLF rekaciju za sintezu bicikličkih prstenova iz N-kloriranih makrocikličkih laktama. Međudjelovanje različitih eksperimentalnih i teorijskih tehnika omogućilo je dublji uvid u temeljne aspekte HLF reakcije, a rezultati će se koristiti za bolju upotrebu u budućim sintezama.

Rad je pohranjen u Centralnoj knjižnici Sveučilišta u Zagrebu Farmaceutsko-biokemijskog fakulteta.

Rad sadrži:	95 stranica, 8 slika, 2 tablice, 28 shema i 104 literaturna navoda. Izvornik je na engleskom jeziku.
Ključne riječi:	Dušikovi radikali, lančana reakcija, Hofmann–Löffler-Freytag (HLF) reakcija, regioselektivnost, korak koji određuje brzinu reakcije, samoreakcija
Mentori:	**Dr. sc. Davor Šakić**, *izvanredni profesor Sveučilišta u Zagrebu Farmaceutsko-biokemijskog fakulteta*. **Dr. sc. Valerije Vrček**, *redoviti profesor u trajnom zvanju Sveučilišta u Zagrebu Farmaceutsko-biokemijskog fakulteta*.
Ocjenjivači:	**Dr. sc. Kristina Pavić**, *docent Sveučilišta u Zagrebu Farmaceutsko-biokemijskog fakulteta.* **Dr. sc. Tin Weitner**, *izvanredni profesor Sveučilišta u Zagrebu Farmaceutsko-biokemijskog fakulteta.* **Dr. sc. Irena Škorić**, *redoviti profesor u trajnom zvanju Sveučilišta u Zagrebu Fakulteta kemijskog inženjerstva i tehnologije*

Rad prihvaćen: 19. svibnja 2025.